CANADIAN THESES ON MICROFICHE

THÈSES CANADIENNES SUR MICROFICHE

National Library of Canada
Collections Development Branch

Canadian Theses on
Microfiche Service

Ottawa, Canada
K1A 0N4

Bibliothèque nationale du Canada
Direction du développement des collections

Service des thèses canadiennes
sur microfiche

NOTICE

The quality of this microfiche is heavily dependent upon the quality of the original thesis submitted for microfilming. Every effort has been made to ensure the highest quality of reproduction possible.

If pages are missing, contact the university which granted the degree.

Some pages may have indistinct print especially if the original pages were typed with a poor typewriter ribbon or if the university sent us an inferior photocopy.

Previously copyrighted materials (journal articles, published tests, etc.) are not filmed.

Reproduction in full or in part of this film is governed by the Canadian Copyright Act, R.S.C. 1970, c. C-30. Please read the authorization forms which accompany this thesis.

AVIS

La qualité de cette microfiche dépend grandement de la qualité de la thèse soumise au microfilmage. Nous avons tout fait pour assurer une qualité supérieure de reproduction.

S'il manque des pages, veuillez communiquer avec l'université qui a conféré le grade.

La qualité d'impression de certaines pages peut laisser à désirer, surtout si les pages originales ont été dactylographiées à l'aide d'un ruban usé ou si l'université nous a fait parvenir une photocopie de qualité inférieure.

Les documents qui font déjà l'objet d'un droit d'auteur (articles de revue, examens publiés, etc.) ne sont pas microfilmés.

La reproduction, même partielle, de ce microfilm est soumise à la Loi canadienne sur le droit d'auteur, SRC 1970, c. C-30. Veuillez prendre connaissance des formules d'autorisation qui accompagnent cette thèse.

THIS DISSERTATION
HAS BEEN MICROFILMED
EXACTLY AS RECEIVED

LA THÈSE A ÉTÉ
MICROFILMÉE TELLE QUE
NOUS L'AVONS REÇUE

Canada

NL 339 (r. 86/09)

FINITE ELEMENT ANALYSIS OF REINFORCED CONCRETE MEMBERS

by

Chen Yuan Liang

A thesis
presented to the University of Ottawa
in fulfillment of the
thesis requirement for the degree of
Master of Applied Science
in
Civil Engineering

OTTAWA, Ontario, 1985

ABSTRACT

This thesis presents new refinements of a finite element method to perform nonlinear analysis of two dimensional reinforced concrete members under monotonically increasing loads.

Finite element modelling of reinforced concrete structures is complicated by the presence of reinforcing steel, concrete cracking in tension, slip between the reinforcing steel and the concrete and the nonlinear stress-strain behaviour of concrete in compression.

An existing genearal purpose structural analysis program NONSAP-1974 Version was modified to include:

-- Two dimensional continuum elements with nonlinear incremental orthotropic strees-strain relationship, compressive strain softening, tension cracking, tension stiffening and interlock shear transfer;

-- Three dimensional elastic-plastic truss elements;

-- Three dimensional linkage elements to represent steel-concrete interaction.

The numerial algorithmic was incremental load steps with a combined initial stiffness and tangential stiffness formulation within the load step. Concrete cracking was accomplished by unbalanced force redistrubution with the load step.

Finite element calculations were compared with published expremental results for an axially loaded tensile specimen; under reinforced, over reinforced and shear sensitive reinforced concrete beams. The good correlation between the calculated and published results demonstrated the applicability of the presented work.

ACKNOWLEDGEMENTS

The work presented in this thesis was carried out under the supervision of Associate Dean/Professor N.J. Gardner. His intersts in this topic, encouragement and continuous guidance throughout this work is gratefully acknowledged.

The author also wishes to express his sincere appreciation to the following individuals:

To Professor A. G. Razaqpur at Carleton University for his patient help and valuable criticism in this investigation;

To Dr. M. S. Cheung at Public Works, Canada and Dr. M. S. Mirza at McGill University for their encouragement and helpful comments on this thesis work;

To Mr. Pak Lok Sau for his help from various aspects, and to Mr. Hee Chaung Fu and Mr. Angelos Alexandridis for their friendship in the period of the author's study at the University of Ottawa.

The author appreciates the financial support from the Chinese Government and Department of Civil Engineering, the University of Ottawa.

LIST OF FIGURES

NOMENCLATURE

$[B]$	Strain shape function matrix
$[C]^e$	Location matrix for the element
C	Distance from the reinforced end
$[D'], [D]$	Elasticity matrix in local/global system
D_{ijkl}	General function of strains
d	Local bond slip
E, E_s	Elastic/Secant elasticity modulus
E_c, E_{ic}	$E_c = \frac{\sigma_c}{\varepsilon_c}$, $E_{ic} = \frac{\sigma_{ic}}{\varepsilon_{ic}}$
E_o	Initial elasticity modulus of concrete
E_{st}	Elasticity of steel
E_{sh}	Modulus of steel in strain hardening portion
E_i	Tangential modulus in material orthotropic direction i
E_1, E_2	Tangential moduli of elasticity corresponding to the local system 1, 2
G, G_s	Elastic/Secant shear modulus
G'_{12}	Effective shear modulus for the material under plane stress
G_{12}	Shear modulus for the material under plane stress corresponding to material orthotropy, 1, 2
F_{ij}	Elastic response function
F_{ijkl}	General function of stress
f'_t	Direct tensile strength of concrete

f'_c	Compressive strength of concrete
f'_y	Yield strength of steel reinforcement
$[K]^e$, $[K]$	Stiffness matrix (element/global)
K, K_s	Elastic/Secant bulk modulus
K_h	Linkage stiffness in the direction parallel to the reinforcing bar
K_v, K_p	Linkage stiffness in the direction normal to the reinforcing bar
$[I]$	Identity matrix
l	Linkage spacing
m	Number of reinforcing bars in one direction
$[N]$	Displacement shape function matrix
n	Tangential modulus ratio
P_{ij}	Elastic response function
p_i	$p = \frac{\sigma_{ic}}{f'_c}$
q_i	$q = \frac{\varepsilon_{iu}}{\varepsilon_{ic}}$
$\{R\}^e$, $\{R\}$	Applied force vector (element/global)
$\{dR\}$	Incremental applied force vector
dR_h	Incremental shear force transferred at the steel-concrete interface
dR_v	Incremental normal force transferred at the steel-concrete interface
$\{R_{ubl}\}$	Unbalanced nodal force vector
$[T]$	Transformation matrix
U^e, U	Strain energy (element/global)
$\{u\}$	Displacement vector
u, v, w	Displacement components in the global system,

	x, y, z
u	Nominal bond stress
V^e, V	Potential energy of loads
W	Strain energy density function
x, y, z	Cartesion coordinates in global system
1, 2, 3	Cartesion coordinates in material orthotropic system or local system
α	Stress ratio
α'	Incremental stress ratio
β_i	Shear retention factor for cracked concrete corresponding to the direction i
$\{\delta\}^e$, $\{\delta\}$	Nodal displacement vector (element/global)
$\{d\delta\}^e$, $\{d\delta\}$	Incremental nodal displacement vector (element/global)
$\{\delta^*\}$	Virtual nodal displacement vector
$\epsilon_{ij}\epsilon_{kl}, \epsilon_{mn}$	Strain tensor
$d\epsilon_{ij}$, $d\epsilon_{kl}$	Incremental strain tensor
$\{\epsilon\}$	Strain vector
ϵ_x , ϵ_y , γ_{xy}	Strain components in the global system, x, y
ϵ_1 , ϵ_2 , γ_{12}	Strain components in the local system, 1, 2
$\{d\epsilon\}$	Incremental strain vector
$d\epsilon_x, d\epsilon_y, d\gamma_{xy}$	Incremental strain components in the global system, x, y
$d\epsilon_1, d\epsilon_2, d\gamma_{12}$	Incremental strain components in the local system, 1, 2
$\{\epsilon^*\}$	Virtual strain vector
ϵ_{it}	Tensile strain corresponding to the maximum tensile stress, σ_{it} , in direction i
ϵ_{itu}	Strain at which the cracked concrete completely releases the tensile stress in direction i

ε_c	Strain corresponding to the uniaxial compressive strength f'_c
ε_{ic}	Strain corresponding to the maximum compressive stress, σ_{ic}, in direction i
ε_{icu}	Maximum compressive strain in material orthotropic direction i at which concrete crushs
ε_{iu}	Equivalent uniaxial strain in the direction i
ε_s	Strain of reinforcing steel
$d\varepsilon_s$	Incremental strain of steel
θ	Countclockwise angle from the global system, x, y, to the local system, 1, 2
ν , ν_s	Elastic/Secant Poisson's ratio
ν_{12} , ν_{21}	Poisson's ratio corresponding to the local system, 1, 2
ν	Effective Poisson's ratio of concrete under biaxial stresses
Π_p^e , Π_p	Total potential energy (element/global)
σ_{ij},σ_{kl},σ_{mn}	Stress tensor
$d\sigma_{ij}$, $d\sigma_{kl}$	Incremental stress tensor
$\{\sigma\}$	Stress vector
σ_x, σ_y, τ_{xy}	Stress components in the global system, x, y
σ_1, σ_2, τ_{12}	Stress components in the local system, 1, 2
$\{d\sigma\}$	Incremental stress vector
$d\sigma_x$, $d\sigma_y$, $d\tau_{xy}$	Incremental stress components in the global system, x, y
$d\sigma_1$, $d\sigma_2$, $d\tau_{12}$	Incremental stress components in the local system, 1, 2
σ_{it}	Maximum tensile stress of concrete in the direction i
σ_{ic}	Maximum compressive stress of concrete in the direction i
σ_{icu}	Compressive stress at which the failed concrete

	crushs in direction i
σ_{ir}	Released tensile stress of the cracked concrete in material orthotropic direction i
$d\sigma_{ir}$	Incremental released stress vector of the cracked concrete
$\{\sigma_{cr}\}$	Releasing stress vector of the cracking concrete
σ_{icr}	Releasing stress of the cracking concrete in material orthotropic direction i
σ'_i	Compressive stress of failed concrete in material orthotropic direction i
$d\sigma'_i$	Incremental compressive stress of failed concrete in material orthotropic direction i
σ_s	Stress of reinforcing steel
$d\sigma_s$	Incremental stress of steel
ϕ	Diameter of reinforcing bar
Ω	Complementary energy density function
$[\ ]^t$	Transpose of a matrix
$[\ ]^{-1}$	Inverse of a matrix
Σ	Summation sign
$\int$	Integration sign

CONVERSION FACTORS

The following is a list of the conversion factors for all imperial units (English System) used throughout this thesis to the International System of Units (SI).

1 in.	= 0.0254 meter = 25.4 mm
1 $in.^2$	= 0.00064516 m^2 = 645.16 mm^2
1 lb. (1 pound force)	= 4.4482 N
1 kip (1000 lbs. force)	= 4448.2 N = 4.4482 kN
1 psi (1 pound-force/$in.^2$)	= 6895 Pascal = 0.006895 MPa
1 ksi (1 kip/$in.^2$)	= 6895000.0 Pascal = 6.895 MPa
1 lb-in.	= 0.112985 Newton-meter
1 kip-in.	= 112.985 N-m = 0.112985 kN-m

TABLE OF CONTENTS

Chapter I

INTRODUCTION

1.1 AN OUTLINE OF THE FINITE ELEMENT METHOD

The finite element method initially evolved from the stiffness matrix methods for the linear elastic analysis of framed structures where the beams and columns could easily be considered as discrete elements. By using a computer, the matrices involved can quickly be computed and the corresponding large number of simultaneous algebraic equations can easily be solved. However, difficulties of the analysis of continua such as continuous solids, slabs or shells encouraged the development of matrix methods with various types of imaginary discrete elements to approximate the nature of continuous systems.

In the finite element method, the continuum is idealized as an assembly of discrete sub-structures connected only at a limited number of points, known as nodes. All loads are always represented by nodal forces which are the basic knowns of the problem. The displacements of these nodal points become the basic unknowns similar to the conventional structural stiffness method. A function is chosen to

define uniquely the state of displacement within each element in terms of its nodal displacements. Using compatibility of the displacements at the appropriate nodes and along the element boundary, the behaviour of the whole system can be defined in terms of these unknown nodal displacements. Using equilibrium, the nodal displacements can be determined and by back-substitution, the displacement at any point within the elements and hence the internal strains and stresses can be found.

With the rapid development of digital computers and the successful application of the finite element method to linear elastic continuum analysis, the finite element method has now been widely accepted as a powerful technique for structural analysis. Recently, a number of finite element program packages using various elements and material models have become available for nonlinear structural analysis and for the evaluation of stresses and deformations with different degrees of success.

1.2 INTERESTS OF REINFORCED CONCRETE STRUCTURE ANALYSIS

In the past few decades, considerable interest has developed concerning the response of reinforced concrete members and structural systems to applied loads. These studies had the objective of accurate prediction of different

aspects of the structural behaviour of reinforced concrete structures such as deformations, internal stresses in concrete and steel, and cracking patterns through the working and ultimate load ranges up to failure.

However, the development of an analytical model for reinforced concrete structures is complicated by the following factors: nonhomogeneity of the composite materials and concrete itself; nonlinearity of the stress-strain relationships of concrete and the reinforcing steel; the behaviour of the interaction between concrete and the reinforcing steel; the time-dependant concrete creep and shrinkage; changes in geometry of the structure due to progressive cracking under sustained loads; the complexity and lack of precise information on postfailure concrete behaviour which is particularly important to the ultimate analysis because concrete exhibits cracking at relatively low tensile stress level (postfailure is defined in this thesis as the material behaviour after a specimen or an element reaches its maximum load carrying capacity). Because of these complexities, early analytical studies of reinforced concrete members and structures were based either on simplifying assumptions, such as linear elastic material behaviour, or on an empirical approach, using the results from large numbers of experimental tests.

Experimental and field studies on various structures have indicated that many of these structures are loaded beyond the range of linear elastic behaviour. Obviously, linear elastic modelling is not sufficient for complete analysis of reinforced concrete structures. Modern experimental equipment makes it possible to obtain valuable insight into the behaviour of test specimens and even prototype structures. However, tests on structures are very expensive and time consuming because a large number of models must be tested if variations of important parameters are to be investigated. Furthermore, only experimental approaches on structural systems are not sufficient for adequate evaluation of safety with respect to the limit state. Faced with the wide range of sizes and types of reinforced concrete structures, it is impractical to design them based on experimental work alone. Because of complexity of these structures and the nature of the material involved, it has therefore become advantageous to develop more sophisticated analysis procedures.

The advent of modern analytic models and large digital computers now provide the powerful tools to develop analytical approaches which can replace many of the experimental tests and give highly sophisticated understanding. The finite element method has shown outstanding advantages in the analysis of reinforced concrete structures.

1.3 REVIEW OF PREVIOUS WORK

Ngo and Scordelis (1967) were the first to demonstrate the application of the finite element method to reinforced concrete structures. The concrete-steel interaction was idealized by the springs of zero length having a constant stiffness. These authors examined linear elastic analysis on simple reinforced concrete beams with predefined crack patterns.

Nilson (1968) expanded the technique further by adding nonlinear material and a nonlinear bond-slip relationship in an incremental loading procedure. In these early studies, cracking of the concrete was modelled by the separation of the nodes. Thus, propagation of cracks in the structure was constrained, with cracks developing only along the inter-element boundaries. Moreover, nodal separation amounted to a continuous change in the structural topology, and to nodal connectivity of the finite element mesh. This resulted in serious computational inefficiencies in the computer implementation of the procedure.

Rashid (1968) incorporated the cracking of concrete and nonlinear material behaviour in the analytical model by altering the material property matrices (or elasticity matrices) of individual elements.

Ngo, Franklin and Scordelis (1970) formulated a more refined model of a reinforced concrete beam which introduced aggregate interlock linkages along predicted diagonal tension crack of various lengths. Beams with and without stirrups were analyzed.

Franklin (1970) developed an analytical model which accounted automatically for cracking within finite elements and redistribution of the unbalanced stresses into the system. This allowed the analysis to be carried out in one computer run without stopping the solution. Incremental loading with iteration within each load increment was used to account for cracking and material nonlinearity.

The group at McGill University under Mirza et al. has done a series of studies on the finite element application to reinforced concrete members. Houde (1973) derived a quantitative relationship describing the bond stress-displacement phenomena at the steel-concrete interface and shear-transfer behaviour of postfailure concrete elements. Khouzam (1976) incorporated the stress-displacement relationship for cracked concrete shear transfer into a nonlinear finite element program. Hanna (1983) developed a concrete material model which was based on endochronic theory.

A group at the University of California at Berkeley under Scordelis et al. is quite active in the application of the finite element methods in structural analysis. A number of computer programs have been developed, covering nonlinear material, nonlinear geometry, static and dynamic loads, time-dependant reinforced concrete structure analysis. (Ngo and Scordelis, 1967; Scordelis, 1972, 1978; Nilson, 1968; Lin, 1973; Lin and Scordelis, 1975; Kang, 1977; Greunen, 1979; Chan, 1982)

Powerful multipurpose program packages are now available such as ADINA (Bathe and Ramaswamy, 1979), NONSAP-C (Adham at el, 1975) which simulated concrete behaviour with classical nonlinear elasticity-based models. Programs using other material models have been developed, such as elastic-plastic models (Lin, 1973; Chen and Chen, 1975), a plastic-fracturing model (Bazant and Shieh, 1980), endochronic models (Bazant et al., 1976; Hanna, 1983) and a model based on fracture mechanics approaches (Bazant and Cedolin, 1980).

It is well recognized that the finite element method can provide a valuable technique for nonlinear analysis of reinforced concrete members and structural systems. Some models have given quite good correlation between the computed values and the experimental results. But there is

still room left for developing more sophisticated material models. In particular, a general agreement on how to represent the structural response, to model concrete postfailure behaviour and to idealize the interactions at the steel-concrete interface is needed.

1.4 OBJECTIVE AND SCOPE

The emphasis of this thesis is on the application of the finite element method to reinforced concrete planar members under monotonically increasing loads. The major theoretical aspects of the present investigation are:

(1) to survey various concrete stress-strain relationships and failure criteria. The nonlinear orthotropic model is chosen for concrete material in this study. A finite element initial stiffness formulation with tangential stiffness formulation, coupled with a time step integration scheme, is developed to analyze the concrete material behaviour throughout the inelastic and ultimate ranges. Within a time step, an incremental load procedure with an iterative approach to obtain an equilibrium position of a structure for each load increment is adopted to trace the nonlinear behaviour of such a structure.

(2) to examine postfailure concrete models. The smeared cracking approach is used in the present study. The model chosen includes tension stiffening, postfailure concrete shear transfer, concrete strain softening under high compressive stress. An efficient numerical analysis procedure is developed for cracking simulation.

(3) to evaluate the available bond stress-slip relationships to model the interaction at the steel-concrete interface. One is incorporated into an analytical model for the analysis of the bond-dowel behaviour.

In summary, the objective of the program work in this study is to extend an existing general purpose program NONSAP-1974 Version (Bathe et al., 1974a; 1974b) to model reinforced concrete members under monotonically increasing loads.

The available NONSAP program contained 3D truss elements, 2D isoparametric elements, 3D thick solid elements and 3D thick shell elements. The nonlinearities in NONSAP covered large displacements, large strains, and nonlinear material behaviour. The material descriptions available for truss elements were limited to linear and nonlinear elastic; while the 2D elements were limited to isotropic linear elastic, orthotropic linear elastic, Mooney-Rivlin material,

elastic-plastic, variable tangent moduli and curve description for isotropic model. Furthermore, NONSAP did both static and dynamic analysis for structural systems.

The NONSAP extensions considered were:

(1) bilinear elastoplastic stress-strain relationship for 3D truss elements to model the reinforcement,

(2) 3D linkage spring elements with a nonlinear bond-slip relationship for simulation of the steel-concrete interaction,

(3) nonlinear orthotropic material description for 2D isoparametric element to represent concrete behaviour under biaxial stresses,

(4) concrete tension cracking and unbalanced force redistribution,

(5) aggregate interlock shear transfer along tension cracks,

(6) concrete strain softening in compression,

(7) a combined approach of the initial stiffness method and the tangential stiffness method for numerical iterative solution for nonlinear analysis.

Several numerical examples are presented to demonstrate the validity and applicability of the present analytical method. The examples can be classified into three cat-

egories. The first category is an axially loaded tensile specimen in which ultimate stage is controlled by crack propagation. The second category is a simple beam without stirrups in which ultimate behaviour is governed by concrete shear capacity. The third category are three simple beams and a continuous beam in which ultimate stages are determined either by the reinforcing steel yielding or by concrete compression. The examples are compared with theoretical, and experimental results and with available analytical results by other researchers.

It is hoped that this study can expand NONSAP element types and material descriptions to nonlinear analysis of 2D (even 3D in future studies) reinforced concrete structures. It is further hoped that the investigation in the present study will be of some value in the stress and deformation analysis of structures.

Chapter II

CONSTITUTIVE MODELS OF CONCRETE UNDER MULTIAXIAL STRESSES

2.1 GENERAL REMARKS

Concrete is a complex heterogeneous material exhibiting phenomena such as inelasticity, cracking, time dependency. Since the mathematical modelling of concrete properties is such a complicated problem, it is usually endeavored to find models which represent the dominant behaviour of the material in the way that the overall response of actual structures can be modelled analytically. For several decades, improved experimental techniques have offered a better understanding of concrete behaviour and models based on experimental statistics have been presented.

As follows, the topics concerning concrete modelling are investigated in the present study:

(1) Nonlinearity of concrete stress-strain relationship,

(2) Concrete failure criteria,

(3) Concrete postfailure behaviour.

2.2 NONLINEARITY OF CONCRETE STRESS-STRAIN RELATIONSHIP

2.2.1 General

From experimental investigation it has been established that concrete behaves nonlinearly under applied loads. FIG.2.1 shows typical stress-strain curves by which the strain in concrete of different strength is plotted against the stress in the uniaxial loading tests. It is also recognized that under a multiaxial stress state the behaviour of concrete is significantly different from that observed under uniaxial stress. One of the most comprehensive and dependable studies under biaxial stress conditions was published by Kupfer et al. (1973), whose results are presented here to illustrate the behaviour of concrete under biaxial stresses. In FIG.2.2 to FIG.2.4, the stress-strain curves for specimens tested at different constant principal stress ratios are shown. Nine ratios, which cover the whole range of compression-compression, compression-tension and tension-tension, were used. It can be seen that the stiffness of the concrete in a principal direction increases in the presence of compression in the other principal direction. This increase in stiffness has been ascribed to the confinement of potential microcracks because of the biaxial stress state.

The pronounced nonlinear behaviour of concrete has brought about an intensive research effort in the past few years, proposing a large number of constitutive models. No agreement on a constitutive relationship for the inelastic response under one, two or three dimensional stress states even for short time loading has been reached. Most analytic models attempt to derive constitutive relationship for one, two or three dimensional stress states in terms of one or more values obtained from a simple uniaxial test or a triaxial cell test. In many cases, everything is related in terms of one measured property, the uniaxial compressive strength of the concrete f'_c . In other cases,where measured uniaxial stress-strain data are available for the material, one or more additional factors such as the initial tangent modulus of elasticity E_o, the tensile strength f'_t , the strain at compression strength ε_c or Poisson's ratio ν may be considered. It is important to note that even this simple uniaxial curve for a given concrete specimen is subject to considerable variations depending on environmental conditions, rates and methods of loading.

The highlights of these constitutive models for short time loading will be discussed using the following broad categorization:

(1) Nonlinear elasticity-based theory,

(2) Plasticity-based theory,

(3) Endochronic theory.

2.2.2 Nonlinear elasticity-based theory

In general, there are two different approaches in the formulation of the nonlinear elasticity-based models. The first approach describes the material behaviour in a secant stress-strain formulation and the second uses piecewise linear step incremental techniques.

(1) Total material descriptions in the form of secant stress-strain formulation

(a) Cauchy type

The current state of stress, σ_{ij}, is expressed uniquely as a function of the current state of strain, ε_{kl}, that is:

$$\sigma_{ij} = P_{ij}(\varepsilon_{kl}) \qquad (2.1)$$

where the P_{ij} is the elastic response function.

(b) Green (hyperelastic) type

This type of modelling is based on the assumption of existence of a strain energy density function $W(\varepsilon_{ij})$ or a complementary energy density function $\Omega(\sigma_{ij})$ such that:

$$\sigma_{ij} = \frac{\partial W}{\partial \varepsilon_{ij}} = D_{ijkl}(\varepsilon_{mn})\,\varepsilon_{kl} \qquad (2.2)$$

$$\varepsilon_{ij} = \frac{\partial \Omega}{\partial \sigma_{ij}} = F_{ijkl}\,(\sigma_{mn})\,\sigma_{kl}$$

in which $W = \int_{o}^{\varepsilon_{ij}} \sigma_{ij}\, d\varepsilon_{ij}$ and $\Omega = \int_{o}^{\sigma_{ij}} \varepsilon_{ij}\, d\sigma_{ij}$

are functions of the current components of the strain and stress tensors; and D_{ijkl} and F_{ijkl} are general functions of their indicated either stress or strain tensors.

The behaviour of total material descriptions including both Cauchy type and Green type is reversible and path independent, and thus their applications are restricted primarily to monotonic or proportional loading regimes. Despite these shortcomings, the secant type of formulation has been utilized in describing the nonlinear behaviour of concrete material.

In general, most of isotropic secant constitutive models for concrete have been formulated basically as a simple extension of isotropic linear elastic stress-strain relationships. For these isotropic nonlinear elastic models, the two constant elastic moduli (E and ν , or K and G) are replaced by secant moduli (E_s and ν_s , or K_s and G_s),

in which, E, E_s = the elastic/secant elasticity modulus,

ν, ν_s = the elastic/secant Poisson's ratio,

K, K_s = the elastic/secant bulk modulus,

G, G_s = the elastic/secant shear modulus.

They are assumed to be the functions of the stress and/or strain invariants.

Examples using total material descriptions are:

(1a) Total stress-strain models based on decoupled secant moduli K_s and G_s (Cedolin et al., 1977; Kotsovos and Newman, 1978; Kupfer and Gerstle 1973; and Murray, 1979),

(1b) Total stress-strain models based on coupled secant moduli K_s and G_s (Kotsovos and Newman, 1978),

(1c) Total stress-strain models based on decoupled secant moduli E_s and ν_s considering the softening behaviour (Ottosen, 1979),

(1d) Total stress-strain models based on general Cauchy type of formulation (Bazant and Tsubaki, 1980).

In the early application of the finite element method to concrete problems, simplified forms of total material descriptions were generally utilized, basically as a simple extension of linear elastic theory. These simplified secant models are attractive from programming and computer economy points of view. Considering existing experimental evidence and its limitation on the procedure of applied loads, total material descriptions are not likely to be widely acceptable for practical purposes.

(2) Incremental material descriptions in the form of tangential stress-strain models

In contrast, incremental material descriptions do not have the shortcoming of reversibility and path independency. The most prominent models of this category are the differential (hypoelastic) formulation. That is:

$$d\sigma_{ij} = F_{ij}\left(d\varepsilon_{kl} , \sigma_{mn} \right) \qquad (2.3)$$

where $d\sigma_{ij}$ = incremental stress tensor,

$d\varepsilon_{kl}$ = incremental strain tensor,

F_{ij} = elastic response function.

These tangential laws provide a more realistic representation of the material behaviour than the total material descriptions in the form of secant formulations, and in fact, incremental models comprise the Cauchy and Green models as special limiting cases.

Various incremental constitutive relationships have been developed and utilized for modelling the behaviour of concrete. Examples are:

(2a) Incremental stress-strain models based on modification of isotropic linear elastic formulations (Kupfer et al., 1969,1973; Bathe and Ramasway, 1979; and Gerstle, 1981),

(2b) Incremental multiaxial orthotropic models (Liu et al.,1972; Kupfer and Gerstle, 1973; Tasuji et al., 1978; Elwi and Murray, 1979; and Chan, 1982),

(2c) Hypoelastic models (Coon and Evans, 1972).

Incremental stress-strain description is a more general form of the material constitutive relationship. The main body of the early incremental finite element analyses was conducted with simplified forms of hypoelasticity. In the most simplified form, the biaxial or triaxial stress and strain state are projected onto an one-dimensional 'equivalent uniaxial curve', resulting in a stress- or strain-dependant modulus of elasticity. A more refined model is based on the decoupling of volumetric and deviatoric stress and strain increments and on the assumption of nonlinear bulk and shear moduli. More sophisticated incremental models assume an orthotropic constitutive relationship with the principal stress directions coinciding with the directions of orthotropy.

In the hypoelastical model based on the classical theory of hypoelasticity, the resulting constitutive equations contain many material constants which are difficult to relate directly to experimental results. Furthermore, the material elasticity matrix is not always symmetric.

Generally, nonlinear elasticity-based models are at present most widely used in various finite element programs for reinforced concrete structure analysis for their simplicity. They provide a reasonable representation of the overall concrete behaviour, but some of them do not give good representation near the ultimate loads.

2.2.3 Plasticity-based theory

Plasticity-based models, originally developed for metals, have been extended to include concrete in recent years. Two approaches have been proposed to characterize concrete stress-strain relationships.

(1) Classical plasticity-based models

(1a) Elastic-perfectly plastic models (Lin, 1973; and Cervenka et al., 1971),

(1b) Elastic-strain hardening plastic models (Chen and Chen, 1975; Epstein et al., 1977; Murray et al., 1979; and Buyukozturk, 1977).

Plasticity-based models are based on the micromechanism of plastic slip in crystals which is defined by the strain increment at constant stress without change in elastic modulus. The plastic slip mechanism accounts only for part of the inelastic behaviour of concrete.

In elastic-perfectly plastic models, the material behaviour before failure is assumed to be linear or nonlinear elastic until a combined multiaxial stress state reaches the failure surface. Once it yields, the flow theory of plasticity is introduced. The postfailure behaviour is governed by the constitutive relationship of the failed material. The formulation of the incremental plastic stress-strain relationship is based on the definition of the condition of yielding at which the plastic flow begins and on the failure condition at which material failure begins.

Elastic-strain hardening plastic models are a generalization of the elastic-perfectly plastic models. In these models, an initial discontinuity surface defined as the limiting surface for the elastic behaviour is located at a certain distance from the failure surface. When the material stress reaches the elastic limit surface, a new discontinuity surface called the loading surface is developed. This new surface replaces the initial discontinuity surface. Unloading and reloading of the material within this subsequent loading surface results in elastic behaviour, and no additional irrecoverable deformation will occur until this new surface is reached. Further discontinuity and additional irrecoverable plastic deformation will result if loading is continued beyond this surface. Final collapse of the material is defined when the failure surface is reached and

material failure occurs, depending on the nature of the stress state.

Classical plasticity models usually cannot represent the nonlinear behaviour of concrete adequately, especially in multiaxial compression with a large value of the stress ratio and at high stress levels. They account, in principle, for the dependance of deformations of the stress path, but unloading and reloading are elastic, and a reasonable description of cyclic behaviour has not been obtained.

(2) Plastic-fracturing models (Bazant et al., 1979)

A more significant contribution, in addition to plastic slip, to the inelastic behaviour of concrete, results from microcracking which is accompanied by a decrease of elastic moduli. This component of inelastic behaviour is considered in the plastic-fracturing models (Bazant et al., 1979).

Plastic-fracturing models represent an extension of classical incremental plasticity which adheres to the use of loading surfaces and the flow rule based on these surfaces, and introduce, in addition to plastic strain increments,

the cracking stress relaxations due to microcracking. This theory uses a cracking loading surface in strain space to compute the cracking stress decrements caused by given strain increments. Nonlinear behaviour upon unloading and reloading is accounted for by introducing a jump-kinematic hardening rule, according to which the instantaneous center of the (plastic and cracking) loading surface jumps to a new location whenever a load reversal takes place. The plastic-fracturing theory has been shown to be capable of representing a very broad range of inelastic phenomena. These are: strain-softening, inelastic dilatancy due to shear and internal friction, hysteretic loops during cyclic loads, etc. However, a large number of functions and parameters are obtained by a nonstandard, optional fitting technique, and this model gives a non-symmetric stiffness matrix which demands much more computer time.

2.2.4 Endochronic theory

The endochronic theory is an extension of the endochronic theory of viscoplasticity, in which inelastic strains are not obtained from a loading surface but directly from the evolution of a measure of irreversible damage, referred to as intrinsic time, which increases whenever deformation takes place (Bazant et al., 1976).

It is capable of representing unloading irreversibilities, the salient feature of inelastic behaviour without the use of any inequalities (unloading criteria). This makes the endochronic theory extremely effective for cyclic loading. All inelastic strains tied to one time-like variable makes it easy to control the stiffening of the material by changing the rate of growth of the intrinsic time. However, even for loading, it cannot be reduced to an incrementally linear form. Nevertheless, in the vicinity of specified loading direction the endochronic theory can be linearized, i.e., brought into an incrementally linear form. The tangential moduli of linearized form are not constant and depend on the chosen direction in the vicinity of which the behaviour is linearized.

The endochronic approach can not use an incremental procedure, therefore it is quite costly in computing time. Furthermore, like plastic-fracturing model, a large number of functions and parameters are required which can only be obtained by a quite nonstandard, optional fitting technique.

2.2.5 The model in the present study

The analytical model chosen in this study to represent the concrete stress-strain relationship under biaxial

stress states before failure is the incremental nonlinear orthotropic model used by Chan (1982). The model will be discussed in detail as follows.

In the present model, the incremental stress-strain relationship is formulated assuming that the principal axes of material orthotropy coincide with the principal stress directions (i.e., principal axes of current state of stress). The tangential moduli E_1 and E_2 in the principal directions of orthotropy are obtained from the corresponding stress-strain relationship in the current principal stress directions, 1 and 2.

Under plane stress state, the incremental constitutive relationship in the directions 1 and 2 for an orthotropic material can be written as:

$$\begin{Bmatrix} d\varepsilon_1 \\ d\varepsilon_2 \\ d\gamma_{12} \end{Bmatrix} = \begin{bmatrix} E_1^{-1} & -\nu_{12}E_2^{-1} & 0 \\ -\nu_{21}E_1^{-1} & E_2^{-1} & 0 \\ 0 & 0 & G_{12}^{-1} \end{bmatrix} \begin{Bmatrix} d\sigma_1 \\ d\sigma_2 \\ d\tau_{12} \end{Bmatrix} \qquad (2.4)$$

where $d\varepsilon_1$, $d\varepsilon_2$, $d\gamma_{12}$ = incremental strain components in the material orthotropic directions, 1, 2

$d\sigma_1, d\sigma_2, d\tau_{12}$ = incremental stress components in 1, 2

ν_{12}, ν_{21} = Poisson's ratio in material orthotropy 1, 2

G_{12} = shear modulus in material orthotropy 1, 2

Using symmetry,

$$\nu_{12} E_1 = \nu_{21} E_2 \qquad (2.5)$$

For simplicity, it is usually assumed that:

$$\nu^2 = \nu_{12} \nu_{21} \qquad (2.6)$$

where ν = the effective Poisson's ratio for the concrete.

Based on these assumptions, EQ. 2.4 can be rewritten as:

$$\begin{Bmatrix} d\varepsilon_1 \\ d\varepsilon_2 \\ d\gamma_{12} \end{Bmatrix} = \begin{bmatrix} E_1 & -\nu(\sqrt{E_1 E_2})^{-1} & 0 \\ & E_2^{-1} & 0 \\ \text{SYMM.} & & G_{12}^{-1} \end{bmatrix} \begin{Bmatrix} d\sigma_1 \\ d\sigma_2 \\ d\tau_{12} \end{Bmatrix} \qquad (2.7)$$

Inverting EQ. 2.7 gives :

$$\begin{Bmatrix} d\sigma_1 \\ d\sigma_2 \\ d\tau_{12} \end{Bmatrix} = \frac{1}{1-\nu^2} \begin{bmatrix} E_1 & \nu\sqrt{E_1 E_2} & 0 \\ & E_2 & 0 \\ \text{SYMM.} & & (1-\nu^2)G_{12} \end{bmatrix} \begin{Bmatrix} d\varepsilon_1 \\ d\varepsilon_2 \\ d\gamma_{12} \end{Bmatrix} \qquad (2.8)$$

The orthotropic form of the incremental relationship implies that there is no coupling between the normal stress increments and the shear stress increments in the principal stress direction. The proper definition of the shear behaviour presents a main difficulty in this case owing to the lack of available experimental evidence. Therefore, it is assumed that the shear modulus G_{12} remains invariant with respect to the rotation of coordinate axes (Darwin et al., 1977; and Elwi and Murray, 1979). Hence:

$$G'_{12} = \frac{1}{4(1-\nu^2)} \left(E_1 + E_2 - 2\nu\sqrt{E_1 E_2} \right) \qquad (2.9)$$

where G'_{12} = the effective shear modulus for the concrete.

EQ. 2.8 can be rearranged to:

$$\begin{Bmatrix} d\sigma_1 \\ d\sigma_2 \\ d\tau_{12} \end{Bmatrix} = \begin{bmatrix} E_1 & 0 & 0 \\ & E_2 & 0 \\ \text{SYMM.} & & G'_{12} \end{bmatrix} \begin{Bmatrix} d\varepsilon_{1u} \\ d\varepsilon_{2u} \\ d\gamma_{12} \end{Bmatrix} \qquad (2.10)$$

where the increments of equivalent uniaxial strains, $d\varepsilon_{1u}$ and $d\varepsilon_{2u}$, are defined as:

$$\begin{aligned} d\varepsilon_{1u} &= \frac{1}{1-\nu^2} d\varepsilon_1 + \frac{\nu\sqrt{E_2}}{(1-\nu^2)\sqrt{E_1}} d\varepsilon_2 \\ d\varepsilon_{2u} &= \frac{\nu\sqrt{E_1}}{(1-\nu^2)\sqrt{E_2}} d\varepsilon_1 + \frac{1}{1-\nu^2} d\varepsilon_2 \end{aligned} \qquad (2.11)$$

Substituting $d\varepsilon_1 = \frac{d\sigma_1}{E_1} - \nu_{12}\frac{d\sigma_2}{E2}$ and $d\varepsilon_2 = \frac{d\sigma_2}{E_2} - \nu_{21}\frac{d\sigma_1}{E_1}$, EQ. 2.11 can be rewritten as:

$$\begin{aligned} d\varepsilon_{1u} &= \frac{d\varepsilon_1}{1 - \nu_{12}\alpha' n} \\ d\varepsilon_{2u} &= \frac{d\varepsilon_2}{1 - \nu_{21}\alpha' n} \end{aligned} \qquad (2.12)$$

where $\alpha' = \frac{d\sigma_1}{d\sigma_2}$, biaxial incremental stress ratio,

$$n = \frac{E_2}{E_1}, \text{ tangential modulus ratio.}$$

EQ. 2.10 suggests a set of uniaxial stress-strain relationships in which stress σ_i is related to the equivalent uniaxial incremental strains, $d\varepsilon_{1_u}$ and $d\varepsilon_{2_u}$. E_1 and E_2 include the effects of confinement but not of Poisson's ratio ν, which is removed through the use of the equivalent uniaxial strains.

Computationally, the increment of the equivalent uniaxial strain $d\varepsilon_{iu}$ is:

$$d\varepsilon_{iu} = \frac{d\sigma_i}{E_i} \tag{2.13}$$

And the total equivalent uniaxial strain ε_{iu} is then obtained by summation along the deformation path:

$$\varepsilon_{iu} = \Sigma d\varepsilon_{iu} = \Sigma \frac{d\sigma_i}{E_i} \tag{2.14}$$

EQ. 2.14 characterizes concrete as a path dependent material.

In the compressive portion before reaching the maximum compressive strength stage, Saenz (1964) suggested an uniaxial stress-strain curve:

$$\sigma = \frac{E_o \varepsilon}{1 + \left(\frac{E_o}{E_c} - 2\right)\frac{\varepsilon}{\varepsilon_c} + \left(\frac{\varepsilon}{\varepsilon_c}\right)^2} \qquad (2.15)$$

where $E_c = \frac{\sigma_c}{\varepsilon_c}$

σ, ε = uniaxial stress and strain, respectively,

σ_c, ε_c = the uniaxial maximum compressive stress and the corresponding strain, respectively.

Darwin and Pecknold (1977) proposed the use of an equivalent uniaxial stress-strain curve for the biaxial stress state:

$$\sigma_i = \frac{E_o \varepsilon_{iu}}{1 + \left(\frac{Eo}{E_{ic}} - 2\right)\left(\frac{\varepsilon_{iu}}{\varepsilon_{ic}}\right) + \left(\frac{\varepsilon_{iu}}{\varepsilon_{ic}}\right)^2} \quad \text{for } |\sigma_i| \leq |\sigma_{ic}| \qquad (2.16)$$

where $E_{ic} = \frac{\sigma_{ic}}{\varepsilon_{ic}}$

σ_{ic}, ε_{ic} = maximum compressive stress and corresponding strain in principal stress direction i.

In the tensile portion, the relationship is linear:

$$\sigma_i = E_o \varepsilon_{iu} \qquad \text{for } \sigma_i \leq \sigma_{it} \qquad (2.17)$$

where σ_{it} = maximum tensile stress of concrete in principal stress direction i.

By differentiating EQ. 2.16 with respect to ε_{iu}, the modulus of elasticity E_i in the compressive portion can be obtained:

$$E_i = \frac{\partial \sigma_i}{\partial \varepsilon_{iu}} = \frac{E_o(1 - q_i^2)}{(1 + (\frac{E_o}{E_{ic}} - 2)\, q_i + q_i^2)^2} \qquad (2.18)$$

for $|\sigma_i| \leq |\sigma_{ic}|$

where $q_i = \frac{\varepsilon_{iu}}{\varepsilon_{ic}}$

Differentiating EQ. 2.17 with respect to ε_{iu} gives the tensile elasticity modulus:

$$E_i = E_o \qquad \text{for } \sigma_i \leq \sigma_{it} \qquad (2.19)$$

A typical equivalent uniaxial stress-strain curve for a biaxial stress state is shown in FIG.2.5. The point of maximum compressive stress and corresponding strain under biaxial loading is discussed in the following section.

2.3 FAILURE CRITERIA OF CONCRETE

2.3.1 General

Concrete failure is defined in this section as the maximum load carrying capacity of a concrete specimen or a concrete element. The biaxial failure envelope of concrete obtained by Kupfer et al. (1973) is shown in FIG.2.6.

The main observed characteristics of the concrete failure behaviour under biaxial stress states can be summarized as follows:

(1) Various failure modes of concrete under different combinations of biaxial loading can be illustrated by FIG.2.7. Failure of concrete occurs by tensile splitting with the cracked surface orthogonal to the direction of the maximum tensile stress or strain. Experimental observations from different sources all indicate that the maximum tensile deformation measured by the maximum tensile strain component is a dominant parameter in predicting brittle cracking of concrete (Wu, 1974). It is assumed that the plane of cracking in concrete is normal to the direction of the maximum tensile strain component. However, a general strain criterion for failure of concrete is still incomplete. So far, most of the existing failure criteria for concrete are expressed in stress space only.

(2) As can be seen from the results obtained by Kupfer et al. (1973) in FIG.2.6, the maximum compressive stress increases under a biaxial compression state. A maximum stress increase of approximately 25% is achieved at a stress ratio of $\frac{\sigma_1}{\sigma_2} = 0.5$ and of about 16% at an equal biaxial compression state of $\frac{\sigma_1}{\sigma_2} = 1.0$. Under a biaxial compression-tension state the maximum compressive stress decreases

almost linearly as the applied tensile stress is increased. Under a biaxial tension state, the maximum tensile stress is almost the same as that of uniaxial tensile strength.

(3) It is clear from FIG.2.2 that the concrete strain corresponding to the maximum stress is dependent on the current stress ratio, $\alpha = \frac{\sigma_1}{\sigma_2}$. For a biaxial compression state, the strain corresponding to the maximum stress is higher than that under the uniaxial compression state. In a biaxial compression-tension state, the magnitudes at the concrete failure of both the principal compressive stress, the corresponding strain and the maximum tensile stress, the corresponding strain decrease as the tensile stress increases. Under a biaxial tension state, there is no significant change in the maximum principal tensile strain, compared with that under the uniaxial tension state.

2.3.2 Review of concrete failure criteria

The accurate prediction of concrete failure at different states is complicated as it depends not only on the physical and mechanical properties of the aggregate and cement paste, but also on the nature of loading. The concrete material shows a great variety of values of load carrying capacities when subjected to different conditions. Using failure envelopes based on experimental statistics seems

to be the only way to model the maximum stress characteristics of concrete for practical applications.

For the past few decades, a large amount of research has been done on the mechanical properties of concrete under multiaxial loading. Considerable experimental data are now available regarding the multiaxial concrete failure envelopes and a large number of models have been presented in the literature. These can be divided into three approaches:

(1) Isotropy-based theory,

(2) Crack friction theory,

(3) Fracture mechanics-based theory.

In the first category, it is accepted as a general approach that concrete is a homogeneous, elastic, isotropic and continuous body; the effect of loading time and rate on concrete failure is negligible; the sample is loaded for the first time, and hence there is no 'material memory' nor load case history; the behaviour at fracture is independent of the loading sequence. In what follows, a brief review of some of the commonly used failure criteria for concrete based on material isotropy is given.

(1) One-parameter models (Chen et al., 1982)

(1a) maximum tensile stress criterion.

(1b) maximum tensile strain criterion.

(1c) Tresca criterion

(1d) von Mises criterion

(2) Two-parameter models

(2a) Mohr-Coulomb criterion (Chen et al., 1982)

(2b) Drucker-Prager criterion (1952)

(2c) Kupfer et al. criterion (1973)

(3) Three-parameter models

(3a) Bresler-Pister criterion (1958)

(3b) Gardner criterion (1969)

(3c) Argyris et al. criterion (1974)

(4) Four-parameter models

(4a) Ottosen criterion (1977)

(4b) Hsieh et al. criterion (1979)

(4c) Mohr-Coulomb criterion with a maximum tensile strength cutoff (Cowan, 1953)

(5) Five-parameter models

(5a) Willam and Warnke criterion (1974)

(6) Dual criterion expressed in terms of stresses as well as strains

(6a) Wu criterion (1974)

In fact, the progressive damage in concrete leads certainly to oriented anisotropies near the ultimate failure region. In the second category, crack friction theory has been proposed recently by Bazant et al. (1980) to account for the effect of these oriented anisotropies on the failure condition. This theory is based on internal friction, but differs from the classical Mohr-Coulomb friction theory. In crack friction theory, friction is considered on one particular plane, the crack plane, rather than as isotropic frictional behaviour as in the Mohr-Coulomb criterion. It is further assumed that the crack plane can have any orientation, which contrasts with the Mohr-Coulomb friction theory for which the frictional slip plane can have only one orientation as determined by the limiting stress. However, the crack friction theory is not presently available for general use.

In recent years, the area of fracture mechanics concepts applied to formulate stress toughness and energy criteria of concrete for material failure has been considered (Bazant and Cedolin, 1980). However failure models in this category are still under development. Further study and experimental work are needed before this concept can be adopted in practical applications.

2.3.3 The model in the present study

In the present study, an isotropy-based failure envelope is used to find the concrete maximum stress and the corresponding strain. The biaxial maximum stress envelope is divided into four different regions as shown in FIG.2.8, depending on the biaxial stress ratio $\alpha = \frac{\sigma_1}{\sigma_2}$. Compressive stresses are negative with tensile stresses positive, and the principal directions are chosen in such a way that $\sigma_1 \geq \sigma_2$ algebraically.

The four regions of the maximum stress envelope are summarized as follows.

1. Biaxial compression, σ_1 = compression, σ_2 = compression. Part 1: $0.0 \leq \alpha \leq 1.0$

$$\sigma_{2c} = \frac{1+3.65\alpha}{(1+\alpha)^2} f'_c \qquad (2.20)$$

$$\sigma_{1c} = \alpha \sigma_{2c}$$

$$\varepsilon_{2c} = \varepsilon_c (-2 + 3p_2)$$

$$\varepsilon_{1c} = \varepsilon_c (0.35p_1 + 2.25p_1^2 - 1.60p_1^3) \qquad (2.21)$$

where $p_1 = \frac{\sigma_{1c}}{f'_c}$ and $p_2 = \frac{\sigma_{2c}}{f'_c}$

EQ. 2.20 is based on the Kupfer et al. (1973) biaxial maximum stress envelope, while EQ. 2.21 is proposed by Darwin et al. (1977). Concrete is assumed to behave as strain softening in compression when calculated strain is beyond the strain corresponding the maximum compressive stress and crushing over a specified ultimate strain (strain softening is defined in this thesis as a further increase in strain causes a decrease in stress). The strain softening behaviour of concrete will be discussed in detail in the sub-section 2.4.3.

2. Tension-compression , σ_1 = tension, σ_2 = compression. Part 2: $-0.17 \leq \alpha < 0.0$

$$\sigma_{2c} = \frac{1 + 3.28\alpha}{(1 + \alpha)^2} f'_c \qquad (2.22)$$

$$\sigma_{1t} = \alpha \sigma_{2c}$$

$$\varepsilon_{2c} = \varepsilon_c (4.42 - 8.38p_2 + 7.54p_2^2 - 2.58p_2^3) \qquad (2.23)$$

$$\varepsilon_{1t} = \frac{\sigma_{1t}}{E_o}$$

where $p_2 \geq 0.65$

EQ. 2.22 is proposed by Darwin et al. (1977), while EQ. 2.23 is given by Rajagopal (1976). The concrete failure in this region is assumed to occur due to strain softening in the compression direction.

3. tension-compression . σ_1 = tension, σ_2 = compression. Part 3: $-\infty < \alpha < -0.17$

$$\sigma_{2c} = 0.65 f'_c$$
$$\sigma_{1t} = f'_t \qquad (2.24)$$

$$\varepsilon_{2c} = \varepsilon_c (4.42 - 8.38 p_2 + 7.54 p_2^2 - 2.58 p_2^3) \qquad (2.25)$$

$$\varepsilon_{1t} = \frac{\sigma_{1t}}{E_o}$$

where $p_2 < 0.65$,

Failure is assumed to be caused by cracking of concrete in direction 1 and strain softening in direction 2.

4. Biaxial tension, σ_1 = tension, σ_2 = tension. Part 4: $1.0 \leq \alpha < \infty$

$$\sigma_{1t} = \sigma_{2t} = f'_t \qquad (2.26)$$

$$\varepsilon_{1t} = \varepsilon_{2t} = \frac{f'_t}{E_o} \qquad (2.27)$$

For biaxial tension, the uniaxial tensile strength, f'_t, is chosen as the tension cut-off point. If calculated tensile stress reaches f'_t, concrete cracking is assumed to occur.

Five material properties of concrete are needed to identify the material. These are (1) uniaxial initial tangent modulus, E_o ; (2) uniaxial compressive strength, f_c' ; (3)strain corresponding to uniaxial compressive strength, ε_c ; (4) uniaxial tensile strength, f_t' ; (5) Poisson's ratio, ν . All these values can be obtained from uniaxial load tests on concrete.

2.4 CONCRETE POSTFAILURE BEHAVIOUR

2.4.1 General

In the nonlinear finite element method applied to reinforced concrete structures, modelling of postfailure behaviour of concrete is one of the extremely important aspects which is little understood due to its complicated nature. The following behaviour characteristics are normally considered in postfailure concrete modelling.

(1) Tension stiffening

When the concrete principal tensile stress in concrete reaches the maximum tensile stress, tensile splitting occurs and primary cracks form at finite intervals along the reinforced concrete member. The total load is transferred across the cracks by the reinforcement, but the concrete between cracks is still capable of carrying stresses because of the bond between reinforcement and concrete. FIG.2.9

shows a typical stress distribution in the concrete and steel in an axially loaded tensile specimen. The concrete stress is zero at the crack, but it would not be zero if it is averaged over the length of the element. As the load increases and the average tensile strain perpendicular to the cracks increases, more cracks form and the tension carried by the concrete decreases.

(2) Strain softening

When the principal compressive stress in concrete reaches the maximum compressive stress, concrete strain softening occurs as its compressive stress decreases with an increase in compressive strain. This will result in unloading in the concrete until it crushes at the ultimate compressive strain.

(3) Shear transfer

The cracked surfaces are normally rough and irregular and capable of transferring shear forces by the phenomenon known as 'aggregate interlock' or 'shear friction'. As the crack width increases, the concrete contact area on the two sides of the crack decreases and the shear force transferred by the aggregate interlock mechanism decreases. Furthermore, the movement of the cracked pieces of concrete parallel to the crack causes the reinforcement crossing the crack to transfer the shear force by the dowel action. Due

to lack of dependable data, dowel action will not be considered in this study.

2.4.2 Tension stiffening

There are basically two methods to incorporate the tension stiffening effect. The first approach is to estimate, on the assumption of unloading in the concrete, the remaining average tensile stress in the concrete, which is called concrete referred method (Scanlon, 1971, FIG.2.10a; Lin and Scordelis, 1973, FIG.2.10b). Because of averaging, the steel stress at the crack is always underestimated while the concrete stress is overestimated (not actually equal to zero at the crack). Furthermore, concrete referred method does not consider the influence reinforcement direction and location to the concrete crack. The second approach is to ignore the concrete tensile stress perpendicular to the crack after concrete cracking and use an increased stiffness for the reinforcement, which is generally termed the steel referred method (Gilbert et al., 1978, FIG.2.10c). This method gives actual concrete stress in the crack (equal to zero) and takes into account of reinforcement direction and location to the crack, but the steel stress calculated in the reinforcement is exaggerated.

The first method is more popular than the second one and is also used in this study for its simplicity.

In order to model the tension stiffening effect, the normal tensile stress perpendicular to the cracked plane should be released gradually after cracking takes place, and this can be accomplished by using the simplified bilinear tensile stress-strain relationship for concrete as shown in FIG.2.11. The released tensile stress, σ_{ir} , at strain ε_{iu} perpendicular to the crack can be written as

$$\sigma_{ir} = \frac{\varepsilon_{iu} - \varepsilon_{itu}}{\varepsilon_{it} - \varepsilon_{itu}} \sigma_{it}, \qquad (2.28)$$

where ε_{it} = the cracking strain in direction i,

ε_{itu} = the strain at which the cracked concrete completely releases the tensile stress.

At this stage, no general agreement can be reached on the concrete strain at which the cracked concrete completely releases the tensile stress. Lin and Scordelis recommended ε_{itu} as $5\,\varepsilon_{it}$ (1975), Gilbert and Warner used ε_{itu} as $10\,\varepsilon_{it}$ (1977), while Hughes, Chapman and Hanna employed ε_{itu} as $20\,\varepsilon_{it}$ to $30\,\varepsilon_{it}$ (Hughes and Chapman, 1966; Hanna, 1983). In the present study, ε_{itu} is chosen as $10\,\varepsilon_{it}$ (Gilbert and Warner, 1977). A discussion on this aspect will be given in Section 6.2.

For the strains $(\varepsilon_{ir})_a$ and $(\varepsilon_{ir})_b$ at the two points, a and b, shown in FIG.2.11, the released stresses $(\sigma_{ir})_a$ and $(\sigma_{ir})_b$ are given by:

$$(\sigma_{ir})_a = \frac{(\varepsilon_{iu})_a - \varepsilon_{itu}}{(\varepsilon_{it}) - \varepsilon_{itu}} \sigma_{it}$$
$$(\sigma_{ir})_b = \frac{(\varepsilon_{iu})_b - \varepsilon_{itu}}{(\varepsilon_{it}) - \varepsilon_{itu}} \sigma_{it} \quad (2.29)$$

The increment of released stress, $d\sigma_{ir}$, can be expressed in terms of strain increment $d\varepsilon_{iu}$ perpendicular to the crack as:

$$d\sigma_{ir} = \frac{(\varepsilon_{iu})_b - (\varepsilon_{iu})_a}{\varepsilon_{it} - \varepsilon_{itu}} \sigma_{it} = \frac{d\varepsilon_{iu}}{\varepsilon_{it} - \varepsilon_{itu}} \sigma_{it} \quad (2.30)$$

where $d\varepsilon_{iu} = (\varepsilon_{iu})_b - (\varepsilon_{iu})_a$

2.4.3 Strain softening in compression

The existence of the falling branch of the concrete stress-strain curve beyond the maximum compressive stress of concrete has long been established. In the present study, a linear unloading curve based on the envelope curve obtained from uniaxial cyclic load tests of Karsan and Jirsa (1969) as shown in FIG.2.12 is used.

As calculated concrete stress reaches the maximum compressive stress, the magnitude of the concrete compressive stress decreases with an increase in the magnitude of the compressive strain, leading to a negative tangent modulus. The following procedure is adopted in the present study to avoid possible numerical problems caused by negative elasticity modulus: when a calculated principal stress σ_i reaches the value of the maximum compressive stress σ_{ic}, concrete strain softening is assumed to occur. The stress drops to σ_i' and the elastic moduli in both directions are set to zero for the any subsequent stiffness assembly, which is geometrically shown in FIG.2.12. The constitutive relationship after failure becomes:

$$d\sigma_i = 0 \; d\varepsilon_{iu} \tag{2.31}$$

At a strain $|\varepsilon_{iu}| < |\varepsilon_{icu}|$, the stress σ_i' in the concrete is:

$$\sigma_i' = \sigma_{ic} + \frac{\sigma_{icu} - \sigma_{ic}}{\varepsilon_{icu} - \varepsilon_{ic}} \left(\varepsilon_{iu} - \varepsilon_{ic} \right) \tag{2.32}$$

where σ_{icu}, ε_{icu} = the stress and the corresponding strain at which the failed concrete crushs.

In this study, σ_{icu} is chosen as $0.2f_c'$, while ε_{icu} as $4\varepsilon_{ic}$.

Referring to FIG.2.12 and using the similar procedure for the incremental stress $d\sigma'_i$ in the concrete strain softening portion, it gives:

$$d\sigma'_i = - \frac{\sigma_{icu} - \sigma_{ic}}{\varepsilon_{icu} - \varepsilon_{ic}} d\varepsilon_{iu} \qquad (2.33)$$

where $d\varepsilon_{iu} = (\varepsilon_{iu})_b - (\varepsilon_{iu})_a$.

2.4.4 Shear transfer

In order to model the shear transfer behaviour for the postfailure concrete, a usual method is to modify the concrete constitutive relationship by making the shear modulus of the cracked concrete equal to a fraction of the uncracked concrete shear modulus, i.e., to modify the uncracked shear modulus, G, by a factor β which can be considered to be a constant or a function of the tensile strain normal to the crack.

It is noted that using a constant value for the shear retention factor, which usually equals 0.4-0.6, does not take into account the dependence of the shear retention factor on the magnitude of the strain perpendicular to the crack and on the relative movement of the cracked pieces of concrete parallel to the crack.

For simplicity, the shear retention factor in this study is chosen from Al-Mahaidi et al. (1979) model. It can expressed as:

$$\beta_i = \frac{0.4}{\frac{\varepsilon_{iu}}{\varepsilon_{it}}} \qquad \text{for } \varepsilon_{iu} > \varepsilon_{it}$$

$$\beta_i = 1.0 \qquad \text{for } \varepsilon_{iu} \leq \varepsilon_{it} \qquad (2.24)$$

Chapter III

MODELS OF REINFORCEMENT AND INTERACTION OF STEEL AND CONCRETE

3.1 GENERAL REMARKS

Reinforced concrete is a composite material consisting of concrete and reinforcing steel. Modelling reinforcing steel and simulating the behaviour at the steel-concrete interface are the important aspects in nonlinear analysis of the finite element method applied to reinforced concrete structures.

Material modelling for reinforcing steel usually can be represented by bilinear or trilinear stress-strain relationship.

The steel-concrete interface mechanical property is a complicated due to the bond between the two different materials. The bond is now recognized as a combination of chemical adhesion, friction and interlocking between the deformed reinforcing bar lugs and the surrounding concrete. Strictly speaking, the bond is a complicated three dimensional problem even in planar structural situations, and it

is difficult to model mathematically and also difficult to verify by experimental work. However, an intensive investigation on this matter has been done by a number of researchers for years and quite a lot of valuable experimental data are available in the literature. Several mathematical models have been presented and some finite element programs have achieved success by applying these models in the reinforced concrete structure analysis.

Modelling of the reinforcement and representation of the bond are discussed in this chapter.

3.2 MODELLING OF REINFORCING STEEL

3.2.1 Material modelling

Typical stress-strain curves for steel reinforcing bars, loaded monotonically in tension, are illustrated in FIG.3.1.

For applications to the situation where the response is purely elastic, incremental steel stress, $d\sigma_s$, can be determined by the linear elastic relationship:

$$d\sigma_s = E_{st}\, d\varepsilon_s \qquad \text{for } \sigma_s < f_y' \qquad (3.1)$$

where $d\varepsilon_s$ = the incremental steel strain,

E_{st} = the elasticity modulus of steel,

f_y' = the steel yield strength.

For applications requiring consideration of plastic deformation, it is common to idealize the behaviour into a bilinear, trilinear or complete steel stress-strain curve as shown in FIG.3.2. In this study, a bilinear curve is used with the possibility of using strain hardening after yielding. FIG.3.3 gives the bilinear relationship, where E_{sh} is the modulus of steel in strain hardening portion. The steel stress-strain relationship in this portion can be expressed as:

$$d\sigma_s = E_{sh}\, d\sigma_s \qquad \text{for } \sigma_s \geq f_y' \qquad (3.2)$$

3.2.2 Element modelling

In modelling the reinforcement by the finite element method, there are basically three approaches. These are:

(1) Distributed approach (FIG.3.4a).

The steel is assumed to be distributed over the concrete element, with a particular orientation angle θ. A composite steel-concrete constitutive relationship is used in this case. Perfect bond must be assigned between the concrete and steel.

(2) Embedded approach (FIG.3.4b)

It may be used in connection with higher order isoparametric concrete elements. The reinforcing bar is considered to be an axial member so built into the isoparametric element that its displacements are consistent with those of the element. To derive such a relationship, perfect bond should also be assumed.

(3) Discrete approach (FIG.3.4c)

This method uses bar elements or beam elements. In planar cases, the bar element, in which only axial force is considered, may be assumed to be pin-connected with two degrees of freedom at each nodal point; while beam element, which is assumed to be capable of resisting axial force, shear and bending, is assigned to have three degrees of freedom at each beam element end. The reinforcement bar elements are easily superimposed on a structural system model. A significaht advantage of this method, in addition to its simplicity, is that it can account for bond-slip behaviour between the reinforcement and the surrounding concrete. This approach has been most widely used.

The discrete approach is chosen in this study in which the 3D pin-connected bar element models the reinforcement including flexural steel and web steel as shown in FIG.3.5.

3.3 BOND BEHAVIOUR MODELLING

3.3.1 Bond stress-slip relationship

Various representations have been suggested to simulate the bond stress-slip relationship based on experimental results. The bond stress is defined here as the unit shear force acting parallel to the reinforcing steel axis at the steel-concrete interface.

Nilson (1968) evaluated Bresler and Bertero's (1968) experimental results and derived a tentative local bond stress-slip relationship with a third-order polynomial:

$$u = 3.606*10^{6}d - 5.356*10^{9}d^{2} + 1.986*10^{12}d^{3} \quad (3.3)$$

where u = the nominal bond stress in psi,

d = the local bond slip in inches.

In another paper, Nilson (1972) suggested the following simplified expression representing the bond stress-slip relationship:

$$u = 3100\ (1.43C + 1.5)\ d\ f'_c \quad (3.4)$$

$$\text{with}\quad u \leq (1.43C + 1.5)\ f'_c$$

where u and d are defined in EQ. 3.3,

C = the distance from the reinforcement end in inches,

f'_c = concrete compressive strength in psi.

EQ. 3.4 indicated that the bond stress-slip relationship is a function of the reinforcement end distance.

Houde (1972) and Mirza and Houde (1979) undertook an experimental program to derive a general bond stress-slip relationship which included the effect of load level, the type of tests, the quality of the concrete and the bar size. The bond stress at the steel-concrete interface is seen to reach a maximum value at a slip about 0.0012" (0.03048 mm). Before the peak value is reached, the relationship can be expressed with the fourth-order polynomial:

$$u = 1.95*10^{6}d - 2.35*10^{9}d^{2} + 1.39*10^{12}d^{3} - 3.3*10^{14}d^{4} \quad (3.5)$$

where u and d are defined in EQ. 3.3.

In metric system, EQ. 3.5 can be rewritten as:

$$u = 5.29*10^{2}d - 2.51*10^{4}d^{2} + 5.85*10^{5}d^{3} - 5.47*10^{6}d^{4} \quad (3.5a)$$

where u = the nominal bond stress in MPa,
d = the local bond slip in mm.

This relationship is plotted in FIG.3.6 and the comparison with the other models is shown in FIG.3.7.

Because of successful use of Houde's model by other investigators (Houde, 1972; Khouzam, 1977; Hanna, 1983),

it is used in the present study. Since the maximum value of EQ. 3.5 is 0.00125" (0.03175 mm), this extreme is chosen as the maximum slip. In this investigation, the method determining the bond stress in the bond failure portion is by balancing residual forces at the steel-concrete interface. A discussion on this matter is given in sub-section 5.2.2.

3.3.2 Linkage spring element

In the finite element analysis applied to reinforced concrete structures, modelling the bond between reinforcing steel and the surrounding concrete, first carried out by Ngo and Scordelis (1968), is commonly simulated by a spring of zero length with a constant or nonconstant spring modulus. The modelling of the bond-dowel phenomenon can be represented by multidirectional springs with zero length as shown in the FIG.3.8.

For a 2D problem, the linkage element consists of two orthogonal springs which connect and transmit shear force between nodes i and j, normal force between nodes m and n. The constitutive relationship for the element can be represented as:

$$\begin{Bmatrix} dR_h \\ dR_v \end{Bmatrix} = \begin{bmatrix} K_h & 0 \\ 0 & K_v \end{bmatrix} \begin{Bmatrix} dd_h \\ dd_v \end{Bmatrix} \qquad (3.6)$$

where dR_h =the incremental shear force transferred at the steel-concrete interface,

dR_v = the incremental normal force transferred at the steel-concrete interface,

K_h = spring stiffness representing the interface shear force transfer,

K_v = spring stiffness representing the interface normal force transfer,

dd_h = the incremental local slip at the interface,

dd_v = the incremental local split at the interface

The value of K_h can be derived from the measured bond stress-slip relationship. Differentiating EQ. 3.5 with respect to slip d , the nonconstant spring stiffness for the shear transfer can be determined:

$$K_h = \frac{du}{dd} A = (1.95*10^6 - 4.07*10^9 d + 3.17*10^{12} d^2 - 1.32*10^{15} d^3) m\pi\phi l \quad (3.7)$$

where u and d are defined in EQ. 3.3,

$A = m\pi\phi l$, the tributary surface area,

m = the number of reinforcing bars,

ϕ = the diameter of reinforcing bars,

l = the linkage element spacing.

In metric system, EQ. 3.7 can be rewritten as:

$$K_h = (5.29*10^2 - 5.02*10^4 d + 1.75*10^6 d^2 - 2.19*10^7 d^3) m\pi\phi l \quad (3.7a)$$

where = the nominal bond stress in MPa

= the local bond slip in mm.

The value of K_v relates to force transfer by dowel action. A comprehensive analytical model for dowel stiffness K_v in an analysis procedure has not been produced yet.

In two extreme cases, K_v may be assigned either an arbitrary small value if dowel action is not to be considered, or a arbitrary large value if a rigid connection in the interface normal direction is assumed. Following Nilson (1969) and other investigators' assumption, the relationship of steel and surrounding concrete is supposed essentially to be rigidly connected perpendicular to the slip, and K_v is represented by an arbitrary large value in this investigation. A discussion concerning the dowel effect will be given in section 6.2.

3.3.3 Formation of the element stiffness matrix

In order to generalize the utilization of the stiffness matrix, a three dimensional linkage element with three degrees of freedom at each node is developed in the present study.

Referring to FIG.3.8, the formation of the linkage spring element stiffness in the global coordinate system is worked out by simple transformation.

As for 2D problems, the relationship between the bond-dowel forces and corresponding displacements can be written in matrix form as follows:

$$\begin{Bmatrix} F_{1h} \\ F_{1v} \\ F_{2h} \\ F_{2v} \end{Bmatrix} = \begin{bmatrix} K_h & 0 & -K_h & 0 \\ 0 & K_v & 0 & -K_v \\ -K_h & 0 & K_h & 0 \\ 0 & -K_v & 0 & K_v \end{bmatrix} \begin{Bmatrix} \delta_1 \\ \delta_2 \\ \delta_3 \\ \delta_4 \end{Bmatrix} \qquad (3.8)$$

where F_{1h} , F_{2h} = the transferred forces along the reinforcement longitudinal direction at nodal point 1 and 2, respectively,

F_{1v} , F_{2v} = the transferred forces normal to reinforcement longitudinal direction at nodal point 1 and 2, respectively,

K_h , K_v = the linkage spring stiffnesses along and normal to reinforcement longitudinal direction, respectively.

δ_1 , δ_3 = the displacements along the reinforcement longitudinal direction at nodal point 1 and 2, respectively,

δ_2 , δ_4 = the displacements normal to the reinforcement longitudinal direction at nodal point 1 and 2, respectively,

To transform the element stiffness matrix $[K]^e_{12}$ from the local coordinate system, 1 and 2, to $[K]^e_{xy}$, in the global coordinate system, x and y, the following transformation is applied:

$$[K]^e_{xy} = [T]^t [K]^e_{12} [T]$$

$$[T] = \begin{bmatrix} c & s & 0 & 0 \\ -s & c & 0 & 0 \\ 0 & 0 & c & s \\ 0 & 0 & -s & c \end{bmatrix} \qquad (3.10)$$

Hence, $[K]^e_{xy}$ can be represented as:

$$[K]^e_{xy} = \begin{bmatrix} K_h c^2+K_v s^2 & K_h sc-K_v sc & -K_h c^2-K_v s^2 & -K_h sc+K_v sc \\ K_h sc-K_v sc & K_h s^2+K_v c^2 & -K_h sc+K_v sc & -K_h s^2-K_v c^2 \\ -K_h c^2-K_v s^2 & -K_h sc+K_v sc & K_h c^2+K_v s^2 & K_h sc-K_v sc \\ -K_h sc+K_v sc & -K_h s^2-K_v c^2 & K_h sc-K_v sc & K_h s^2+K_v c^2 \end{bmatrix} \qquad (3.11)$$

in which, $c = \cos\theta$, $s = \sin\theta$,

θ = the counterclockwise angle between the global system, x, y, and the local system, 1, 2.

In respect to 3D problems, the relationship between the bond-dowel forces and corresponding to displacements can be written in matrix form as follows:

$$\begin{Bmatrix} F_{1h} \\ F_{1v} \\ F_{1p} \\ F_{2h} \\ F_{2v} \\ F_{2p} \end{Bmatrix} = \begin{bmatrix} K_h & 0 & 0 & -K_h & 0 & 0 \\ 0 & K_v & 0 & 0 & -K_v & 0 \\ 0 & 0 & K_p & 0 & 0 & -K_p \\ -K_h & 0 & 0 & K_h & 0 & 0 \\ 0 & -K_v & 0 & 0 & K_v & 0 \\ 0 & 0 & -K_p & 0 & 0 & K_p \end{bmatrix} \begin{Bmatrix} \delta_1 \\ \delta_2 \\ \delta_3 \\ \delta_4 \\ \delta_5 \\ \delta_6 \end{Bmatrix} \quad (3.12)$$

where F_{1h}, F_{2h} = the transferred forces along the reinforcement longitudinal direction at nodal point 1 and 2, respectively,

F_{1v}, F_{2v} = the transferred forces in one of normal to the reinforcement longitudinal direction at nodal point 1 and 2, respectively,

F_{1p}, F_{2p} = the transferred forces in the other of normal to reinforcement longitudinal direction at nodal point 1 and 2, respectively,

K_h = the linkage spring stiffness along the reinforcement longitudinal direction,

K_v, K_p = the linkage spring stiffnesses in one of two directions normal to the reinforcement longitudinal direction, respectively,

δ_1, δ_4 = the displacements along the reinforcement longitudinal direction at nodal point 1 and 2, respectively,

δ_2, δ_5 = the displacements in one of the directions which are normal to the reinforcement longitudinal direction at nodal point 1 and 2, respectively,

δ_3 , δ_6 = the displacements in the other one of two directions which are normal to the reinforcement longitudinal direction at nodal point 1 and 2, respectively.

To transform the element stiffness matrix $[K]^e_{123}$ from the local coordinate system, 1, 2 and 3, to $[K]^e_{xyz}$, in the global coordinate system, x, y and z, the following transformation is applied:

$$[K]^e_{xyz} = [T]^t [K]^e_{123} [T]$$

$$\text{where } [T] = \begin{bmatrix} [t] & 0 \\ 0 & [t] \end{bmatrix} \qquad (3.13)$$

$$[t] = \begin{bmatrix} C_x & C_y & C_z \\ \dfrac{-C_y}{\sqrt{C_x^2 + C_y^2}} & \dfrac{C_x}{\sqrt{C_x^2 + C_y^2}} & 0 \\ \dfrac{-C_x C_y}{\sqrt{C_x^2 + C_y^2}} & \dfrac{-C_y C_z}{\sqrt{C_x^2 + C_y^2}} & \sqrt{C_x^2 + C_y^2} \end{bmatrix} \qquad (3.14)$$

$$\text{where } C_x = \frac{L_{ix}}{L_i} \quad , \quad C_y = \frac{L_{iy}}{L_i} \quad , \quad C_z = \frac{L_{iz}}{L_i} \quad ,$$

$$L_i = \sqrt{L_{ix}^2 + L_{iy}^2 + L_{iz}^2}$$

$$L_{ix} = x_j - x_i, \quad L_{iy} = y_j - y_i, \quad L_{iz} = z_j - z_i.$$

Therefore, the element stiffness matrix $[K]^e_{xyz}$ in the global coordinate system, x, y and z, can be obtained in the following form:

$$
[K]^{e}_{xyz} =
\begin{array}{|c|c|c|c|c|c|}
\hline
\begin{array}{l} K_h c_x^2 \\ +K_p \dfrac{c_y^2}{c_x^2 + c_y^2} \\ +K_v \dfrac{c_x^2 c_y^2}{c_x^2 + c_y^2} \end{array} &
\begin{array}{l} K_h c_x c_y \\ -K_p \dfrac{c_x c_y}{c_x^2 + c_y^2} \\ +K_v \dfrac{c_x c_y c_z^2}{c_x^2 + c_y^2} \end{array} &
\begin{array}{l} K_h c_x c_z \\ \\ -K_v c_x c_z \end{array} &
\begin{array}{l} -K_h c_x^2 \\ -K_p \dfrac{c_y^2}{c_x^2 + c_y^2} \\ -K_v \dfrac{c_x^2 c_z^2}{c_x^2 + c_y^2} \end{array} &
\begin{array}{l} -K_h c_x c_y \\ +K_p \dfrac{c_x c_y}{c_x^2 + c_y^2} \\ -K_v \dfrac{c_x c_y c_z^2}{c_x^2 + c_y^2} \end{array} &
\begin{array}{l} -K_h c_x c_z \\ \\ +K_v c_x c_z \end{array} \\
\hline
 & \begin{array}{l} K_h c_y^2 \\ +K_p \dfrac{c_x^2}{c_x^2 + c_y^2} \\ +K_v \dfrac{c_x^2 c_z^2}{c_x^2 + c_y^2} \end{array} &
\begin{array}{l} K_h c_y c_z \\ \\ -K_v c_y c_z \end{array} &
\begin{array}{l} -K_h c_x c_y \\ +K_p \dfrac{c_x c_y}{c_x^2 + c_y^2} \\ -K_v \dfrac{c_x c_y c_z^2}{c_x^2 + c_y^2} \end{array} &
\begin{array}{l} -K_h c_y^2 \\ -K_p \dfrac{c_x^2}{c_x^2 + c_y^2} \\ -K_v \dfrac{c_y^2 c_z^2}{c_x^2 + c_y^2} \end{array} &
\begin{array}{l} -K_h c_y c_z \\ \\ +K_v c_y c_z \end{array} \\
\hline
 & &
\begin{array}{l} K_h c_z^2 \\ +K_v (c_x^2 + c_y^2) \end{array} &
\begin{array}{l} -K_h c_x c_z \\ +K_v c_x c_z \end{array} &
\begin{array}{l} -K_h c_y c_z \\ +K_v c_y c_z \end{array} &
\begin{array}{l} -K_h c_z^2 \\ -K_v (c_x^2 + c_y^2) \end{array} \\
\hline
 & & &
\begin{array}{l} K_h c_x \\ +K_p \dfrac{c_y^2}{c_x^2 + c_y^2} \\ +K_v \dfrac{c_x^2 c_z^2}{c_x^2 + c_y^2} \end{array} &
\begin{array}{l} K_h c_x c_y \\ -K_p \dfrac{c_x c_y}{c_x^2 + c_y^2} \\ +K_v \dfrac{c_x c_y c_z^2}{c_x^2 + c_y^2} \end{array} &
\begin{array}{l} K_h c_x c_z \\ \\ -K_v c_x c_z \end{array} \\
\hline
 & & & &
\begin{array}{l} K_h c_y^2 \\ +K_p \dfrac{c_x^2}{c_x^2 + c_y^2} \\ +K_v \dfrac{c_y^2 c_z^2}{c_x^2 + c_y^2} \end{array} &
\begin{array}{l} K_h c_y c_z \\ \\ -K_v c_y c_z \end{array} \\
\hline
 & & & & &
\begin{array}{l} K_h c_z^2 \\ +K_v (c_x^2 + c_y^2) \end{array} \\
\hline
\end{array}
$$

SYMM.

(3.15)

Chapter IV

FINITE ELEMENT APPLICATION IN RC STRUCTURE STRESS ANALYSIS

4.1 GENERAL REMARKS

The computer program used in this analysis is a modified, extended NONSAP--1974 Version (Bathe et al., 1974a; 1974b), written in Fortran IV language, and it is operable on the AMDAHL V8/470 computer at the University of Ottawa.

The thrust of this research program is to construct a realistic analytical model to simulate the behaviour of reinforced concrete structures. In its present form, the program only concerns static, material and geometric nonlinear analysis for planar reinforced concrete structures under monotonically increasing loads. Concrete is modelled in the planar 4-noded to 8-noded isoparametric element group, while reinforcing steel (including flexural and web steel) is assigned in the bar element group and steel-concrete interaction is simulated by the separated linkage spring elements. It can be noted, however, that the program is written in such a way that not many modifications are

needed to include dynamic problems or three dimensional structural problems.

In the view point of computer programing, the problems are focused in this chapter on five aspects of concrete elements which are as follows:

(1) Mathematical formulation,

(2) Numerical solution process for nonlinear analysis,

(3) Cracking model,

(4) Cracking modes,

(5) Cracking propagation.

All these are discussed at length in the following.

4.2 MATHEMATICAL FORMULATION

For a structural system, the total potential energy, Π_p, can be represented by the sum of the element energy, Π_p^e, i.e.,

$$\Pi_p = \sum_e \Pi_p^e = \sum_e U^e + \sum_e V^e \qquad (4.1)$$

where U^e = the element strain energy:

$$U^e = \int_{Vol} \frac{1}{2} \{\varepsilon\}^t \{\sigma\} \, dVol$$

$$= \frac{1}{2}\int_{vol}\{\varepsilon\}^t [D]\ \{\varepsilon\}\ dVol$$

$$= \frac{1}{2}\int_{vol}(\{\delta\}^e)^t [B]^t [D][B]\{\delta\}\ dVol$$

$$= \frac{1}{2}\ (\{\delta\}^e)^t [K]^e \{\delta\}^e \qquad (4.2)$$

V^e = the element potential energy due to the applied loads:

$$V^e = -\ (\{\delta\}^e)^t \{R\}^e \qquad (4.3)$$

in which, $\{\sigma\} = [D]\{\varepsilon\}$ (4.4), [D] = the elasticity matrix

$\{\varepsilon\} = [B]\{\delta\}^e$ (4.5), [B] the strain shape function matrix

$[K]^e = \int_{vol}[B]^t [D][B]dVol$ (4.6), $[K]^e$ the element stiffness matrix

$\{R\}^e$ = the applied loads in the element.

Introducing $[C]^e$ matrix, which determines the element location in the overall system when the element matrix in the local system is being transferred to the global system, it yields:

$$\Pi_p = \frac{1}{2}\ \{\delta\}^t [K]\{\delta\} - \{\delta\}^t \{R\} \qquad (4.7)$$

where $$[K] = \sum_e ([C]^e)^t [K]^e [C]^e \qquad (4.8)$$

$$\{\delta\} = \sum_e [C]^e \{\delta\}^e \qquad (4.9)$$

$$\{R\} = \sum_e ([C]^e)^t \{R\}^e \qquad (4.10)$$

Since the principle of the minimum potential energy suggests that, for a prescribed set of displacements and strains, the equilibrium conditions are satisfied when the total potential energy is at its minimum, differentiating EQ. 4.7 with respect to each of the nodal displacements, in turn and setting the result equal to zero, a set of simultaneous equations can be obtained:

$$\begin{Bmatrix} \frac{\partial \Pi_p}{\partial \delta_1} \\ \frac{\partial \Pi_p}{\partial \delta_2} \\ \vdots \\ \frac{\partial \Pi_p}{\partial \delta_n} \end{Bmatrix} = \begin{Bmatrix} 0 \\ 0 \\ \vdots \\ 0 \end{Bmatrix} \qquad (4.11a)$$

in which n is the total number of degrees of freedom of the discrete system. They can be rewritten as:

$$[K]\{\delta\} = \{R\} \qquad (4.11)$$

Similarly, in the case of incremental loading, EQ. 4.11 gives:

$$[K]\ \{d\delta\} = \{dR\} \tag{4.12}$$

EQ. 4.11 and EQ. 4.12 are the governing equations of the finite element method.

The basic calculation procedures to this approach for plane stress problems are illustrated as follows.

(1) Construct the element strain shape matrix

Considering an isoparametric element with n nodal points,

$$\begin{Bmatrix} d\varepsilon_x \\ d\varepsilon_y \\ d\gamma_{xy} \end{Bmatrix} = \begin{bmatrix} \dfrac{\partial du}{\partial x} \\ \dfrac{\partial dv}{\partial y} \\ \dfrac{\partial du}{\partial y} + \dfrac{\partial dv}{\partial x} \end{bmatrix} = [B] \begin{Bmatrix} d\delta_1 \\ \vdots \\ d\delta_n \end{Bmatrix} \quad d\delta_i = \begin{Bmatrix} d\delta_{ix} \\ d\delta_{iy} \end{Bmatrix}$$

$$[B] = \begin{bmatrix} \dfrac{\partial N_1}{\partial x} & 0 & \dfrac{\partial N_2}{\partial x} & 0 & \cdots & \dfrac{\partial N_n}{\partial x} & 0 \\ 0 & \dfrac{\partial N_1}{\partial y} & 0 & \dfrac{\partial N_2}{\partial y} & \cdots & 0 & \dfrac{\partial N_n}{\partial y} \\ \dfrac{\partial N_1}{\partial y} & \dfrac{\partial N_1}{\partial x} & \dfrac{\partial N_2}{\partial y} & \dfrac{\partial N_2}{\partial x} & \cdots & \dfrac{\partial N_n}{\partial y} & \dfrac{\partial N_n}{\partial x} \end{bmatrix} \tag{4.13}$$

where $\begin{Bmatrix} du \\ dv \end{Bmatrix} = [N]\{d\delta\}^e = [IN_1 \cdots IN_i \cdots IN_n]\{d\delta\}^e$

[N] = the element displacement shape function matrix.

(2) Construct the element elasticity matrix [D'] in the local coordinate system, 1, 2,

$$\begin{Bmatrix} d\sigma_1 \\ d\sigma_2 \\ d\tau_{12} \end{Bmatrix} = [D'] \begin{Bmatrix} d\varepsilon_1 \\ d\varepsilon_2 \\ d\gamma_{12} \end{Bmatrix}; \quad \begin{Bmatrix} d\,\varepsilon_1 \\ d\,\varepsilon_2 \\ d\,\gamma_{12} \end{Bmatrix} = \begin{bmatrix} \cos^2\theta & \sin^2\theta & \sin\theta\cos\theta \\ \sin^2\theta & \cos^2\theta & -\sin\theta\cos\theta \\ -2\sin\theta\cos\theta & 2\sin\theta\cos\theta & \cos^2\theta - \sin^2\theta \end{bmatrix} \begin{Bmatrix} d\,\varepsilon_x \\ d\,\varepsilon_y \\ d\,\gamma_{xy} \end{Bmatrix}$$

$$[D'] = \frac{1}{1-\nu^2} \begin{bmatrix} E_1 & \nu\sqrt{E_1 E_2} & 0 \\ & E_2 & 0 \\ \text{SYMM.} & & (1-\nu^2)G'_{12} \end{bmatrix} \qquad (4.14)$$

(3) Transfer [D'] in the local coordinate system, 1,2, to [D] in the global coordinate system, x,y,

$$[D] = [T]^t [D'][T] \qquad (4.15)$$

where transformation matrix [T] is given by:

$$[T] = \begin{bmatrix} \cos^2\theta & \sin^2\theta & \sin\theta\cos\theta \\ \sin^2\theta & \cos^2\theta & -\sin\theta\cos\theta \\ -2\sin\theta\cos\theta & 2\sin\theta\cos\theta & \cos^2\theta - \sin^2\theta \end{bmatrix} \qquad (4.16)$$

in which, θ is the counterclockwise angle between the global coordinates, x, y, and the local coordinates, 1, 2, that coincide with material orthotropy principal axes.

(4) Carry out the matrix multiplication $[B]^t [D][B]$ and then apply numerical integration over the

element area

$$[K]^e = \int_{vol}[B]^t[D][B]dVol \qquad (4.17)$$

(5) Construct the system stiffness matrix [K]

$$[K] = \sum_e ([C]^e)^t[K]^e[C]^e \qquad (4.18)$$

(6) Solve simultaneous algebraic equations

$$\{d\delta\} = [K]^{-1}\{dR\} \qquad (4.19)$$

(7) Calculate the element strains and the element stresses.

4.3 NUMERICAL SOLUTION PROCESS FOR NONLINEAR ANALYSIS

In general, the use of finite element methods for structural applications results in a system of simultaneous equations as EQ. 4.11 or EQ. 4.12. For simplicity in this section, the matrix [K] , and vectors {δ}, {R} are reduced to the scalar equivalents, K and δ, R. Therefore, EQ. 4.11 can be rewritten in the form:

$$K\delta = R \qquad (4.20)$$

in which δ is the vector of the basic unknowns referring to nodal displacements, R is the vector of applied loads and K is the assembled stiffness matrix.

If the coefficients of the matrix K depend on the unknowns δ or their derivatives, the problem clearly becomes nonlinear. In this case, a step-by-step procedure, an iterative procedure, or a combination of the two must be adopted. Many options remain open for the numerical sequence to be followed. Some of the most generally applicable methods available are discussed in the following:

(1) step-by-step method

In this approach, the load R is divided into a number of small increments, ΔR, and the displacement response, δ, is obtained by the summation of its increment, $\Delta\delta$. This can be represented as:

$$K(\delta_r)\,\Delta\delta_r = \Delta R_r$$
$$\delta_{r+1} = \delta_r + \Delta\delta_r \qquad (4.21)$$

where r is the r^{th} load step.

An improved solution can be found when the residuals, R_r^u, from the previous step are added to the current load increment, ΔR_r, for the solution of δ_{r+1}. The computational procedure is:

$$K(\delta_r)\,\Delta\delta_r = \Delta R_r + R_r^u$$
$$\delta_{r+1} = \delta_r + \Delta\delta_r \qquad (4.22)$$

The two methods for a single variable are geometrically shown in FIG.4.1a and FIG.4.1b. Neither method guarantees convergence. The solutions tend to drift away from the true path unless ΔR is chosen to be very small. Therefore, the step-by-step method is rarely adopted for nonlinear analysis.

(2) iterative method

(2a) direct iteration

By this method successive solutions are performed. In each of them, the previous solution for the unknown δ_r is used to predict the current values of the coefficient matrix. The iterative process yields the $(r+1)^{th}$ approximation being:

$$\delta_{r+1} = [K(\delta_r)]^{-1} R \qquad (4.23)$$

If the process is convergent, the ture solution can be approached as r tends to infinity.

For practical purposes, the iterative process is deemed to have converged when some measure (usually a norm of the nodal unknowns) of the change in the unknowns δ between successive iterations has become tolerably small. The process is illustrated diagrammatically as a single variable in FIG.4.2a. The assumed dependence of K on δ is a basic problem function which must be presented before solution can commence. A disadvantage of the direct iteration method is that convergence of the solution scheme is not guaranteed and cannot be predicted at the initial solution stage.

(2b) The Newton-Raphson method

During any step of an iterative process of solution, EQ.4.20 will not be satisfied unless convergence has occurred. A system of residual forces can be assumed to exist , so that:

$$\Psi = K\delta - R \neq 0 \qquad (4.24)$$

These residual forces Ψ can be interpreted as a measure of the departure of EQ.4.20 from equilibrium. Since K is a function of δ and possibly its derivatives, then at any step of the iterative process, $\Psi = \Psi(\delta)$.

If the true solution exists at $\delta_r + \Delta\delta_r$, then

the Newton-Raphson approximation for the general term of the residual force vector, $\Psi(\delta_r)$, can be written in an improved solution using curtailed Taylor expression as:

$$\Psi(\delta_{r+1}) = \Psi(\delta_r) + \left(\frac{d\Psi}{d\delta}\right)_r \Delta\delta_r \qquad (4.25)$$

with $\delta_{r+1} = \delta_r + \Delta\delta_r$

$$\left(\frac{d\Psi}{d\delta}\right)_r = \frac{d\,[K(\delta_r)\,\delta - R]}{d\delta} = J(\delta_r) \qquad (4.26)$$

The improved value of δ_{r+1} can then be obtained by computing:

$$\Delta\delta_r = -(J(\delta_r))^{-1}\,\Psi(\delta_r) = -\left[\frac{dK(\delta_r)}{d\delta}\right]^{-1}\Psi(\delta_r) \qquad (4.27)$$

This allows the correction to the vector of unknowns δ to be obtained from the residual force vector for any iteration. Again an iterative approach must be followed with the vector of unknowns being corrected at each stage according to EQ.4.27 until convergence of the process is deemed to have occurred. The technique is illustrated schematically in FIG.4.2b in a single variable situation. Solutions to the nonlinear problem will be achieved when the residual forces Ψ become tolerably small.

(2c) the tangential stiffness method

In any nonlinear case, in which the stiffness depends on the degrees of displacement in some manner, K is equal to the local gradient of the force/displacement relationship of the structure at any point and is termed the tangential stiffness. The analysis of such problems must proceed in an incremental manner since the solution at any stage may not only depend on the current displacements of the structure but also on the previous loading history. Consequently, the problem can be linearized over any increment of load and therefore the matrix, K , containing the nonlinear terms, can be discarded from EQ. 4.25 and EQ. 4. 26. With this modification, the solution process is identical to that described in the previous Newton-Raphson method which is sometimes termed a generalized Newton-Raphson method.

The solution algorithm is illustrated in FIG.4.2c. Solution is commenced from a trial value δ_r of the unknowns. The tangential stiffness, $K(\delta)$, corresponding to this displacement state is then determined and the residual forces calculated according to EQ. 4.24. The correction, $\Delta\delta_r$, to the trial value is computed according to the linearized form of EQ. 4.27 which is:

$$\Delta\delta_r = [K(\delta_r)]^{-1} \psi(\delta_r) \qquad (4.28)$$

An improved approximation to the unknowns is then obtained being $\delta_{r+1} = \delta_r + \Delta\delta_r$. This iterative process then

would continue until the solution converges the nonlinear solution as indicated by the condition that $\Psi(\delta_r) = K(\delta_r)\,\delta_r - R$ is within the tolerance.

(2d) the initial stiffness method

In the methods previously described, the complete reduction and solution of the full set of simultaneous equations describing the discrete structure are essential for each iteration. For the method of direct iteration the equation solution indicated by EQ.4.23 is necessary, while the Newton-Raphson technique and tangential stiffness method requires the equation solution indicated by EQ.4.27. If the tangential stiffness matrix in EQ.4.27 is replaced, at all steps of the computation, by the stiffness corresponding to the initial trial value of δ_o, a complete factorisation, or reduction, of the assembled equations can be avoided. In this case, a complete equation solution needs only be performed for the first iteration and subsequent approximations to the nonlinear solution performed, via the expression:

$$\Delta\delta_r = [K(\delta_o)]^{-1}\,\Psi(\delta_r) \qquad (4.28)$$

Since the same stiffness matrix $K(\delta_o)$ is employed at each stage, the reduced equations can be stored in their reduced or factored form and a second or subsequent solution merely necessitates the reduction of the right-hand side

($\Psi(\delta_r)$) terms, together with a back substitution. This has an immediate advantage of significantly reducing computing time per iteration, but reduces the convergent rate as can be seen from FIG.4.2d where the scheme is schematically illustrated.

In NONSAP-1974 Version (Bathe et al., 1974a; 1974b), the initial stiffness method was used whereby a new tangent stiffness matrix could be formed in each loading step only, and during iteration the stiffness always remained unchanged. The convergence tolerations in the iteration is the ratio of the Euclidian norms of incremental displacements and total displacements. Therefore the solution path in the analysis of a system with path dependent material properties can only be determined by sufficiently small steps for solution accuracy.

In this study, a combined initial stiffness method with the tangential stiffness method is used by which the stiffness can be changed at selected iterative intervals within each loading step. The solution algorithm is illustrated in FIG.4.3. The convergence tolerance in the iteration is from both the ratio of the Euclidian norms of incremental displacements and total displacements and the ratio of Euclidian norms of residual forces and incremental loads.

These procedures are worked out for the elements before material failures. The postfailure concrete element modelling and calculation procedures are discussed in the following sections.

4.4 CRACKING MODEL

Basically, three different cracking models have been used to represent concrete cracking in finite element analytical models. These are :

(1) Smeared cracking approach (FIG.4.4)

It gives automatic generation of cracks without the redefinition of the finite element topology, which corresponds to an averaging procedure of local discontinuities. This allows an equivalent continuum treatment with localized material anisotropy. It simplifies the solution algorithms substantially and fits well into the approximate nature of the finite element method with C_o-continuity of displacement and bounded non-singular strain and stress fields. However, it tends to diffuse the cracking system and loses accuracy of the prediction in the strain and stress field around the crack tip.

(2) Discrete cracking approach (FIG.4.5)

This approach is normally followed by disconnecting displacement at nodal points for adjoining elements in a finite mesh. It represents a more rational method of modelling cracks. In the early studies of the finite element method application to reinforced concrete structures, this approach was often used by the investigators (Ngo ang Scordelis, 1967; Nilson, 1968). The main problem in the approach is that the techniques of redefinition of element nodes are extremely complex and time-consuming. However, if detained local behaviour at the crack tip area is of interest, this method exhibits a particular useness.

(3) Fracture mechanics approach

In the context of fracture mechanics, the approach to cracking is characterized by use of the stress intensity factor or the energy release rate. Main efforts are concentrated on the stress field surrounding a crack tip. During cracking, it is now generaly agreed that for cracks of sufficient length the approach gives a more reasonable representation. However, this requires the mesh changes with each crack increment, and usually discrete crack modelling is the only way. Alternately, a model that captures the essence of fracture mechanics and the simplicity of the smeared crack approach has been proposed by Bazant and Cedolin (1979). For the specific problems in which fracture mechanics is the appropriate tool, a cracking model based on fracture mechanics may be necessary.

Because of its simplicity, the smeared cracking approach is most widely accepted in general finite element programs for the reinforced concrete structure analysis and is used in the present study.

4.5 CRACKING MODES

The 4-noded to 8-noded isoparametric elements are introduced for the concrete elements. Each integration point only stands for partial element material behaviour during Gauss numerical integration in finding the element stiffness matrix. Due to this characteristic, this program checks concrete failing modes and imposes cracking at one integration point after another, if cracking occurs.

To simulate the behaviour of reinforced concrete structures, six different crack modes for an integration point of a concrete element are assumed as far as the concrete analytical model is concerned. Referring to FIG.4.6, there are:

(1) uncracked concrete,
(2) one 'crack',
(3) first 'crack' closed,
(4) first 'crack' closed, second 'crack' open,
    or alternatively first 'crack' open
    and second 'crack' closed,
(5) both 'cracks' closed,

(6) both 'cracks' open.

The concrete in an element is assumed to have partially cracked when the principle tensile stresses of concrete at any integration point of the element reach the failure envelope region of Part 3 or Part 4 in FIG.2.8. Once this first crack appears, the crack is fixed normally to the maximum principle stress direction in the current and further analysis as shown in FIG.4.6. The appropriate stress-strain relationship coinciding the axis of orthotropy normal to the crack can be expressed by zero elasticity modulus for that integration point of the element. For example, cracking along the crack normal to θ angle between the global coordinate axis x and the local coordinate axis 1 in the counterclockwise manner induces EQ. 4.14 to be:

$$[D'] = \begin{bmatrix} 0 & 0 & 0 \\ & \frac{E_2}{1-\nu^2} & 0 \\ \text{SYMM.} & & \beta_1 G \end{bmatrix} \qquad (4.29)$$

where β_1 = the shear modulus retention factor in local coordinate axis 1, as given in sub-section 2.4.4,

G = the shear modulus for the isotropic linear elastic concrete material, i.e.

$$G = \frac{E_o}{2(1+\nu)} \; . \qquad (4.30)$$

The cracked concrete is assumed to behave as an anisotropic material under uniaxial loading perpendicular to the crack. The stress parallel to the crack can be determined as:

$$d\sigma_2 = \frac{E_o}{1-\nu^2}\, d\varepsilon_{2u} \qquad (4.31)$$

The second crack appears if $\sigma_2 \geq \sigma_{2t}$, and new formed crack is in the direction orthogonal to the existed one. No distinction will be made in the material stiffness of uncracked concrete in an element, in which all cracks, are closed (FIG.4.6 cases(1), (3) and (5)). Material stiffness will be the same for the concrete having only one crack, and one crack open and the other closed (Fig 4.6 cases (2) and (4)). The concrete having two cracks open is assumed to transfer shear force only. In that case, the element stiffness matrix in the local coordinate system, 1 and 2, corresponding to two crack directions, is written as:

$$[D'] = \begin{bmatrix} 0 & 0 & 0 \\ & 0 & 0 \\ \text{SYMM.} & & \beta_1\beta_2 G \end{bmatrix} \qquad (4.32)$$

where β_1, β_2 can be obtained from EQ. 2.33 concerning local coordinates, 1 and 2, respectively.

In this investigation, the computer program modifies the structure stuffness automatically when cracking occurs.

4.6 CRACKING PROPAGATION

To restore equilibrium when any cracking occurs, unbalanced forces due to cracking in new formed element are applied at its nodal points common with the adjacent elements and the remaining uncracked portion of that new formed element, and redistributed during the next iteration but at the same load level. FIG.4.7 shows restraint of unbalanced nodal forces when Element A is cracking at Integration Point a so as to distribute its tensile stress into the surrounding concrete elements and the remaining uncracked portion of Element A.

The virtal energy principal suggests:

$$([\delta^*]^e)^t \{R_{ubl}\}^e = \int_{vol} \{\varepsilon^*\}^t \{\sigma_{cr}\} dVol \qquad (4.33)$$

where $\{\delta^*\}$ = the virtal element displacement vector,

$\{\varepsilon^*\}$ = the virtal strain vector,

$\{\sigma_{cr}\}$ = the releasing stress vector due to concrete cracking.

The unbalanced nodal forces, $\{R_{ubl}\}$, can be obtained as follows:

$$\{R_{ubl}\} = \int_{vol} [B]^t \{\sigma_{cr}\} dVol \qquad (4.34)$$

In the global coordinate system, $\{\sigma_{cr}\}$ can be expressed as:

$$\{\sigma_{cr}\} = \begin{Bmatrix} \sigma_x \\ \sigma_y \\ \tau_{xy} \end{Bmatrix}_{cr} = \begin{bmatrix} \cos^2\theta & \sin^2\theta \\ \sin^2\theta & \cos^2\theta \\ \sin\theta\cos\theta & -\sin\theta\cos\theta \end{bmatrix} \begin{Bmatrix} \sigma_{1cr} \\ \sigma_{2cr} \end{Bmatrix} \qquad (4.35)$$

in which, σ_{1cr} and σ_{2cr} are releasing stress σ_{icr} in the local coordinate system, 1 and 2, respectively.

$$\begin{aligned} \sigma_{1cr} &= \sigma_1 - \sigma_{1r} && \text{for } \sigma_1 > \sigma_{1t} \\ \sigma_{2cr} &= \sigma_2 - \sigma_{2r} && \text{for } \sigma_2 > \sigma_{2t} \end{aligned} \qquad (4.36)$$

where σ_{ir} can be found in sub-section 2.4.2.

The whole these procedures in transferring unbalanced forces are done automatically following checking concrete failure in this program.

The flow charts for the computer program are given in Appendix B.

Chapter V

CASE STUDIES

5.1 GENERAL REMARKS

The stress-strain relationship based on the concrete nonlinear orthotropic material modelling, postfailure behaviour modelling and the bilinear stress-strain relationship modelling elastoplastic reinforcing steel together with the nonlinear bond stress-slip relationship are all incorporated in one finite element program for the nonlinear analysis of planar reinforced concrete members.

To verify the accuracy of the proposed nonlinear finite element models, the following six numerical examples are presented in which the analytical results obtained using the proposed model are compared with the experimental data and the analytical results obtained by other investigators:

(1) an axially loaded tensile specimen tested by Houde in McGill University (Houde, 1973);

(2) a tested series of simply supported reinforced concrete beams at the University of Ottawa (Pilette, 1984):

a beam with web reinforcement, Beam A,

a beam without web reinforcement, Beam B,

an over-reinforced concrete beam, Beam C;

(3) a simple reinforced concrete beam with web reinforcement tested by Burns and Seiss at the University of Illinois (Burns and Seiss, 1962);

(4) a two-span continuous beam, Beam 23100, by Duddeck, et al. at the Technical University of Braunschweig (Duddeck, et al., 1976).

All specimens were divided into a finite number of discrete elements. Concrete is modelled by rectangular plane stress elements, while pin-connected bar elements are chosen for the steel reinforcement, and bond-dowel linkage elements are introduced at the nodes connecting the bar elements and concrete elements.

5.2 AXIALLY LOADED TENSILE SPECIMEN (HOUDE, 1973/MCGILL)

5.2.1 Analytical idealization

The axially loaded tensile specimen selected was the same as the one analyzed by Nilson (1968) and Houde (1973) which was modelled after Broms's experiment specimen T-RC3-1 (Broms, et al., 1965) and Houde's tests #1, #2, #3

(Houde, 1973). The specimen consisted of a concrete prism 33*8.1*3.5 in., axially reinforced with a No.8 bar. The material properties used for the analysis as follows:

Concrete	Compressive strength	f'_c = 4130 psi
	Tensile strength	$f'_t = 7.5\sqrt{f'_c}$ = 482 psi
	Elasticity modulus	$E_o = 57000\sqrt{f'_c}$=3.54*10 psi
	Poisson's ratio	ν = 0.15
	Strain at f'_c	$\varepsilon_c = 2*f'_c/E_o$= 0.002333
Steel	Yield strength	f' = 40000 psi
	Elasticity modulus	E_{st}= 29*10 psi
	No.8 bar diameter	ϕ = 1.0 in.
	No.8 bar steel area	A_s = 1*0.79 = 0.79 $in.^2$

The finite element idealization used to model axially loaded specimen is shown in FIG.5.1. Because of symmetry, only one quarter of the specimen was modelled for the analysis. Idealization of the concrete required 44 isoparametric elements, while the reinforcement was represented by 12 axial bar elements. Twelve linkage elements were used to model the steel-concrete interaction.

The test specimen was subjected to an incremental loading of ten increments equivalent to a stress of 4 ksi in the protruding bar. In this analysis, load increment is tak-

en as a steel stress of 1 ksi at the end of protruding bar in each step (equivalent to a load level of 0.79 kip in the steel bar)

5.2.2 Experimental and analytical responses

(1) Steel displacement vs steel stress (FIG.5.2)

FIG.5.2 shows the steel displacements measured at the free end of the bar with progressive loading. For comparison, the analytical results of Nilson's (1968), Houde's (1973) and experimental data as well as the displacement of a steel bar without concrete encasement, the displacement of a elastically transferred section with perfect bond are also plotted in FIG.5.2.

The results obtained with the proposed model in the present study are similar to those obtained by Nilson (1968) and Houde (1973). The curve shows a better agreement with the experimental data according to the comparison in FIG.5.2. The initial part of the curve is nearly linear and corresponds to the elastically transferred section behaviour. At a stress of 18 ksi at the free end of the steel bar, a primary crack forms as all concrete elements in one row at 13.5 " to 15.0" (in Houde's tests No.1 and No.2, this turn steel stress value was observed as 18 ksi, while Nil-

son's and Houde's analytical results were 24 ksi and 28 ksi, respectively). from the free end face are overstressed and progressively crack. After cracking, displacements are seen to be close to but smaller than the free bar displacements because certain bond linkages remain intact and some force is transferred from the steel bar to the concrete.

A second crack appears in the specimen at the element row of 3.0" to 4.5" from the free end face at a steel stress of 26 ksi. The formation of the second crack is obtained at a distance approximately equal to the member width, 8 in., as observed in the experimental test (Broms, et at., 1965), which could not be found by Houde's analytical model (Houde, 1973).

(2) Steel stress variation (FIG.5.3)

The variation of the steel stress with distance from the center line is presented in FIG.5.3. Up to a stress of 16 ksi at the free end of the steel bar, the steel stress decreases rapidly with distance from the end face in a pattern similar to those observed in tests of specimens with instrumented bar (Houde, 1973).

At a stress of 18 ksi at the free end of the steel bar, the concrete elements in one row at 13.5" to 15.0" from the end face release their tensile stresses and the steel bar had to carry the total applied load; the steel stress in this portion is then equal to the free bar stress.

FIG.5.3 shows the differences of steel stress along longitudinal steel bar direction before the first primary crack forms (at the free steel bar stress of 4, 8, 12, 16 ksi), after the primary crack appears (20, 24 ksi) and the second primary crack forms (28, 32, 36, 40 ksi).

(3) Bond shear force variation (FIG.5.4)

FIG.5.4 shows the bond shear stress variation vs loading with distance from the center line. It can be noted that before primary crack forms (at a steel stress of 8, 16 ksi), these bond shear stresses transfer load smoothly between the steel bar and the surrounding concrete. After the first primary crack appears (a steel stress of 20, 28, 40 ksi), the bond shear stress varies rapidly with distance from the primary crack, and even changes its direction at the primary crack as would be expected. This phenomenon can also be found in FIG.2.9.

At a steel stress of 24 ksi, bond failure commenced. The third linkage element from the center line section (13.5" from the free end face) was broken and consequently the bond forces varies according to balance of the residual forces between steel bars and the concrete in following load steps. From FIG.5.4, it can be noted that bond shear stress at failed linkage part of steel-concrete interface (12.75" to 14.25" form the free end face) decreases with the further axially loading (at a steel stress of 28, 40 ksi). The bond stress-slip relationship seems to have a negative tangential portion after the bond reachs its failure criterion as shown in FIG.3.4 obtained by some investigators, which was not given in Houde's experimental formulae(Houde, 1973). This phenomenon is similar to the concrete strain softening behaviour in compression. However, further investigation is needed to formulate this effect.

(4) Concrete stress distribution (FIG.5.5 and FIG. 5.6)

Distribution of principal concrete stress is given in FIG.5.5 for a steel stress of 16 ksi, before the first primary crack forms. In this analysis, the concrete principal stress at an integration point of an isoparametric element reaching its maximum tensile stress first time is found

at a steel stress of 8 ksi, at the corner of free face and protruding steel bar (concrete element No. 2, integration point No. 2). At the following load steps, concrete crack propagates progressively around the steel bar. This phenomenon is noted as internal concrete cracking, which was modelled as precracked concrete by Houde (1973) in his finite element element analysis. Up to a steel stress of 16 ksi, although internal cracks form around steel bar, the cracked concrete is still able to carry some load due to its tensile stiffening effect, and the steel stress decreases rather smoothly with the distance from the free end face. The load is partially transferred from the steel bar to the surrounding concrete through the steel-concrete interaction, which is similar to the behaviour of elastically transferred section.

When the first primary crack forms at a steel stress of 18 ksi, the concrete stress drops to zero at the location of the crack and the total applied load in this part is carried by steel bar. FIG.5.6 shows the concrete stress distribution and the steel stress variation at a steel stress of 20 ksi in the protruding bar.

5.3 SIMPLE BEAM TEST SERIES, BEAM A, B, C (PILETTE, 1984/OTTAWA)

5.3.1 Test series

As part of the undergraduate reinforced concrete design course at the University of Ottawa, the students have to construct and test to failure a series of reinforced concrete beams which are designed to demonstrate the various aspects of the design codes of the three simply supported beams (FIG.5.7) involved. Beam A was designed to meet the requirements of CAN3 A23.3-M77 with both under-reinforced flexure steel and adequate shear steel; Beam B was similar to Beam A except without shear reinforcement so that would fail in shear; Beam C was designed to be over-reinforced and fail by crushing of the concrete, but had adequate shear steel (Pilette, 1984).

The material properties of these simply supported reinforced concrete beams are listed as follows:

Concrete	Compressive strength	$f_c' = 30.9$ MPa
	Tensile strength	$f_t' = 3.65$ MPa
	Elasticity modulus	$E_o = 5000\sqrt{f_c'} = 27794$ MPa
	Poisson's ratio	$\nu = 0.15$
	Strain at f_c'	$\varepsilon_c = 2*f_c'/E_o = 0.002224$
	Yield strength	$f_y' = 483$ MPa
	Elasticity modulus	$E_{st} = 200000$ MPa

Steel	#20 bar diameter	ϕ = 20 mm
	2#20 steel area	A_s = 2*300 = 600 mm^2
	#30 bar diameter	ϕ = 30 mm
	2#30 steel area	A_s = 2*700 = 1400 mm^2
Stirrups	Yield strength	f'_y = 362 MPa
	Elasticity modulus	E_{st} = 200000 MPa
	No.2 bar diameter	ϕ = 0.25 in. = 6.35 mm
	2*No.2 steel area	A_{st} = 2*32.5 = 65 mm^2

5.3.2 Beam A

A simple reinforced concrete beam, Beam A, was designed to resist full flexure and shear loads up to the ultimate load, as determined by CAN3 A23.3-M77. The main purpose of making this beam was to illustrate a ductile behaviour through the yielding of the tension reinforcement and preventing failure by diagonal tension with adequate web reinforcement. The member as shown in FIG.5.7a consisted of a concrete prism 2750*125*250 mm, main reinforcement with 2#20 bar, and web reinforcement with Imperial No.2 stirrups spaced 100 mm centres.

The finite element idealization used to model this test specimen is shown in FIG.5.8. Due to symmetry of the member and the applied loading, only one half of the speci-

men is needed to be modelled for analysis. Idealization of the concrete required 78 isoparametric elements, while the reinforcement was represented by 78 axial bar elements. Fourteen linkage elements were used to model the steel-concrete interaction.

The test specimen was subjected to an incremental loading of thirteen increments equivalent to a load level of P = 4.5 kN. In this analysis, load increment is taken as P = 2.25 kN in each step.

The analytical results of the proposed model and theoretic, experimental data are given below in Table No.1:

Table No.1 Beam A

PARAMETER	THEORY (CAN3 A23.3)	EXPERIMENT	ANALYSIS (F.E. MODEL)
cracking moment	6.28 kN-m (7.85 kN)	17.8 kN-m (22.25kN)	7.2 kN-m (9.00 kN)
ultimate moment	52.4 kN-m (65.5 kN)	46.3 kN-m (57.0 kN)	45.0 kN-m (56.25kN)
shear capacity	79.52 kN	-----	-----

The load-deflection curve for the center line section of Beam A using the proposed analytical model is compared with the experimental load-deflection curve in FIG.5.9. A good agreement between the analytical and experimental response is obtained.

5.3.3 Beam B

A simple reinforced concrete beam without stirrups, Beam B, was designed to resist full flexure loads up to the ultimate load, but the shear capacity was not provided. The member as shown in FIG.5.7b consisted of a concrete prism 2750*125*255 mm, and main reinforcement with 2#20 bar.

The finite element idealization used to model this beam is shown in FIG.5.10. Due to symmetry of the specimen and the applied loading, only one half of the specimen is needed to be modelled for the analysis. Idealization of the concrete required 78 isoparametric elements, while the reinforcement was represented by 13 axial bar elements. Fourteen linkage elements were used to model the steel-concrete interaction.

The test specimen was subjected to an incremental loading of nine increments equivalent to a load level of P = 4.5 kN. In this analysis, load increment is taken as P = 2.25 kN in each step.

The analytical results of the proposed model, theoretical and experimental data are given below in Table No.2:

Table No.2 Beam B

PARAMETER	THEORY (CAN3 A23.3)	EXPERIMENT	ANALYSIS (F.E. MODEL)
cracking moment	7.10 kN-m (8.88 kN)	16.0 kN-m (20.0 kN)	7.2 kN-m (9.0 kN)
shear capacity	35.8 kN	38.9 kN	40.5 kN
ultimate moment	52.4 kN-m (65.5 kN)	-----	-----

The load-deflection curve for the center line section of Beam B using the proposed analytical model is compared with the experimental load-deflection curve in FIG.5.11. A good agreement between the analytical and experimental response is obtained.

5.3.4 Beam C

An over-reinforced concrete simple beam, Beam C, was designed with main reinforcement in excess of that per-

mitted by CAN3 A23.3-M77. Adequate shear reinforcement was provided, in order that a brittle failure by crushing of the compression concrete would result. This beam was made to illustrate the difference in the normal ductile flexure failure and compression failure of over-reinforced concrete beam. The member as shown in FIG.5.7c consisted of a concrete prism 2750*125*260 mm, main reinforcement with 2#30 bar, and web reinforcement with Imperial No.2 stirrups spaced 50 mm centers.

The finite element idealization used to model the specimen is shown in FIG.5.8. Due to symmetry of the specimen and the applied loading, only one half of the specimen is needed to be modelled for analysis. Idealization of the concrete required 78 isoparametric elements, while the reinforcement was represented by 78 axial bar elements. Fourteen linkage elements were used to model the steel-concrete interaction.

The test specimen was subjected to an incremental loading of sixteen increments equivalent to a load level of P = 4.5 kN. In this analysis, load increment is taken as P = 2.25 kN in each step.

The obtained analytical results using the proposed model, theoretical and experimental data are given below in Table No.3:

Table No.3 Beam C			
PARAMETER	THEORY (CAN3 A23.3)	EXPERIMENT	ANALYSIS (F.E. MODEL)
cracking moment	11.9 kN-m (14.8 kN)	21.4 kN-m (26.8 kN)	9.0 kN-m (11.25 kN)
ultimate moment	62.1 kN-m (77.8 kN)	57.0 kN-m (71.3 kN)	63.0 kN-m (78.75 kN)
shear capacity	132.46 kN	-----	-----

The load-deflection curve for the center line section of Beam C using the proposed analytical model is compared with the experimental load-deflection curve in FIG.5.12. A good agreement between the analytical and experimental response is obtained.

5.4 SIMPLE BEAM J-4 (BURNS AND SEISS, 1962/ILLINOIS)

5.4.1 Analytical idealization

A reinforced concrete simple beam with stirrups, Beam J-4, tested by Burns and Seiss at the University of Illinois (Burns and Seiss, 1962) is chosen in this analysis as shown in FIG.5.13. The member consisted of a concrete prism 3900*200*500 mm, main reinforcement with 2 No.8 bar, and

No.3 web reinforcement spaced 152 mm centers. The material properties used for the analysis are as follows:

Concrete	Compressive strength	f'_c = 33.2 MPa
	Tensile strength	$f'_t = 0.6*\sqrt{f'_c}$ = 3.46 MPa
	Elasticity modulus	$E_o = 5000\sqrt{f'_c}$ = 28809.7 MPa
	Poisson's ratio	ν = 0.15
	Strain at f'_c	$\varepsilon_c = 2*f'_c/E_o$ = 0.002305
Steel	Yield strength	f' = 309.6 MPa
	Elasticity modulus	E_{st} = 186000 MPa
	No.8 bar diameter	ϕ = 25.4 mm
	2*No.8 steel area	A_s = 2*509.68=1019.35mm^2
Stirrups	No.3 bar diameter	ϕ = 9.525 mm
	2*No.3 steel area	A_s = 2*70.97= 141.94 mm^2

The finite element idealization used to model Beam J-4 is shown in FIG.5.14. Because of symmetry, only one half of the specimen was modelled for analysis. Idealization of the concrete required 52 isoparametric elements, while the reinforcement was represented by 59 axial bar elements. Fourteen linkage elements were used to model the steel-concrete interaction.

In this analysis, load increment is taken as 5 kN in each step.

5.4.2 Experimental and analytical responses

This beam was designed to resist full flexure and shear loads up to the ultimate load, as determined by ACI 318 and CAN3 A23.3-M77. The main purpose of analyzing this beam was to illustrate a ductile behaviour through the yielding of the tension reinforcement and preventing failure by diagonal tension with adequate web reinforcement. The comparison of the analytical results, theoretical and experimental data are given below in Table No.4:

Table No.4 Beam J-4

PARAMETER	THEORY (CAN3 A23.3)	EXPERIMENT	ANALYSIS (F.E. MODEL)
cracking moment	25.87 kN-m (28.75 kN)	-----	40.5 kN-m (45.0 kN)
ultimate moment	142.56 kN-m (158.40 kN)	147.6 kN-m (164.0 kN)	153.0 kN-m (170.0 kN)
shear capacity	218.26 kN	-----	-----

The load-deflection response obtained using the proposed analytical model is compared with the experimental load-deflection curve in FIG. 5.15 which also shows the analytical results of Hanna's (1983), Buyukozturk's (1977) and Darwin, Pecknold's (1974). The computed load-deflection curve compares favorably with the experimental load-deflection curve shown in FIG. 5.15.

5.5 CONTINUOUS BEAM 23100 (BUDDECK, ET AL., 1976/BRAUNSCHEWIG)

5.5.1 Analytical idealization

The two-span continuous beam, Beam 23100, tested at the Technical University of Braunschweig (Duddeck, et al., 1976) is chosen in this analysis as shown in FIG.5.16. This continuous beam had double reinforcement with 8 bars (4 mm diameter) which lay with 4 bars at each side. The web reinforcement consisted of 3 mm diameter stirrups spaced 30mm centres. The material properties used for the analysis as follows:

Concrete	Compressive strength	f'_c = 32 MPa
	Tensile strength	$f'_t = 0.6*\sqrt{f'_c}$ = 3.4 MPa
	Elasticity modulus	$E_o = 5000\sqrt{f'_c}$ = 28284 MPa
	Poisson's ratio	ν = 0.15
	Strain at f'_c	$\varepsilon_c = 2*fc'/E_o$ = 0.00226
	Yield strength	f' = 579 MPa

Steel	Elasticity modulus	E_0 = 196000 MPa
	Bar diameter	ϕ = 4.0 mm
	Steel area	A_s = 4*12.57 = 50.27 mm
Stirrups	Bar diameter	ϕ = 3.0 mm
	2 3mm stirrups area	A_s = 2*7.07 = 14.14 mm

The finite element idealization used to model Beam 23100 is shown in FIG.5.17. Because of symmetry, only one span of the specimen is needed to be modelled for analysis. Idealization of the concrete required 75 isoparametric elements, while the reinforcement was represented by 75 axial bar elements. Thirty two linkage elements were used to model the steel-concrete interaction.

In this analysis, load increment is taken as 1.25 kN in each step.

5.5.2 Experimental and analytical responses

This continuous beam was analyzed to illustrate the ductile flexure failure due to the plastic hinge. The analytical results obtained from the proposed model, theoretic and experimental results are given below in Table No.5:

Table No.5 Beam 23100			
PARAMETER	THEORY (CAN3 A23.3)	EXPERIMENT	ANALYSIS (F.E. MODEL)
cracking moment	.302 kN-m (3.82 kN)	.155 kN-m (1.96 kN)	.395 kN-m (5.00 kN)
ultimate moment	2.15 kN-m (27.26kN)	2.55 kN-m (32.3 kN)	2.47 kN-m (31.25kN)
shear capacity	33.54 kN	-----	-----
plastic analysis	51.25 kN	-----	-----

The load-deflection curve for the mid-span section using the proposed analytical model is compared with the experimental load-deflection curve and the analytical results of Hanna (1983) in FIG.5.18. A good agreement between the analytical and experimental response is obtained.

FIG.5.19 presents the analytical and experimental deflection profile for one span of the beam at P = 30.42 kN.

5.6 FINAL REMARKS

From the previous case studies, the proposed model has shown a good approach in analyzing the complicated behaviour of reinforced concrete structural members under monotonically increasing loads. The computer output offers a complete picture of results which are not as easily derived theoretically or experimentally. The cracking loads, ultimate loads, force-displacement curves, load-deflection curves and the stress distributions in different kinds of reinforced concrete members can be easily obtained from a single finite element analysis.

Quantitative and qualitative comparisons between the analytical results and the experimental or theoretical results of these members indicated that:

(1) The computed initial elastic deflection was approximately 5% smaller than the deflection obtained by experimental work. However, a noticeable difference about 20% (in Beam A, B, C) in load-deflection curve in the portion close to ultimate loads was found. This discrepancy might be due to the conforming isoparametric planar element characteristics modelling the concrete which led to a lower bound solution. If a finer concrete element mesh or isoparametric elements with more degrees of freedom was used, or if the

beam elements was chosen instead planar isoparametric elements, the better results in beam load-deflection curves can be expected.

(2) Initial cracking load levels in this analytical model agreed the theoretical results well. It is found that analytical initial cracking value was higher than experimental data in the case of Beam 23100. This may be attribute to that actual concrete around reinforcing steel is weaker than the concrete in other part. This effect was not considered in this study.

(3) The ultimate load obtained by the proposed model in this study showed a good agreement with experimental results. This shows the accuracy and validity of the proposed nonlinear finite element model.

Chapter VI

SUMMARY AND CONCLUSIONS

6.1 SUMMARY

An existing nonlinear finite element program was developed to perform the analysis of planar reinforced members under monotonically increasing loads. The nonlinearity considered in this thesis were concrete stress-strain relationships, concrete failure criteria, concrete postfailure behaviour, yielding of reinforcement and interactions at the steel-concrete interface.

The existing general purpose program NONSAP-1974 Version (Bathe et al., 1974a; 1974b) extensions in this study were: (1) bilinear stress-strain relationship for 3D truss elements to model the reinforcement; (2) 3D linkage spring elements with the nonlinear bond stress-slip relationship for simulation of the steel-concrete interaction; (3) nonlinear orthotropic material description for 2D isoparametric element to represent concrete behaviour under biaxial condition; (4) concrete tention cracking and unbalanced force redistribution; (5) aggregate interlock shear transfer along tension cracks; (6) concrete strain softening

in compression; (7) a combined approach of the initial stiffness method and the tangential stiffness method for numerical iterative solution for nonlinear analysis.

To verify the numerical models in this computer program, six reinforced structural members tested at different institutions are analyzed by the computer program based on the above models. These test specimens are chosen for different members, which are an axially loaded tensile specimen, a singly reinforced simple beam without stirrups, two simple beam with properly designed reinforcement, an over-reinforced simple beam , and a two span continuous beam with double reinforcement. The results are presented and compared with with the available theoretical, experimental results and analytical results obtained by other researchers with a view to demonstrating the applicability and the validity of the present method of the analysis.

6.2 CONCLUSIONS

Based on the investigations carried out in the present study, the following conclusions can be made:

(1) The present method of analysis has been shown to be capable to analyze nonlinear response of reinforced concrete structural members under monotonically increasing loads.

(2) The cracking loads and the ultimate loads show a good agreement with the corresponding experimental results. The stress analysis demonstrates a fair accuracy in both concrete and reinforcement. In this investigation, the analytical results of the force-displacement curve of the axially loaded tensile specimen and the load-deflection curves of the beams are in good agreement.

(3) The gradual release of the tensile stresses in concrete upon cracking improves the analytical predictions of the stress characteristics in reinforced concrete. From this investigation, it is found that the chosen value of the strain at which a complete release of the tensile stress in the cracked concrete takes place is of influence on load deflection curves of the beam specimens. The larger the value, the smaller the deflection of a beam after passing cracking load stage. But its influence on ultimate loads is not so noticeable. In this study, this value was chosen as ten times of the strain corresponding the maximun tensile stress (Gilbert and Warner, 1977) for the analysis in case studies of Chapter five which led to an acceptable results referring load-deflection curves of a set of beam specimens.

(4) The shear retention factor β used to modify the uncracked shear modulus, G, in modelling the postfailure shear behaviour is based on a reasonable assumption. It is

noted in this study that the chosen value of the shear retention factor is not significant to analytical results in case studies, which was obversed by other investigators (Lin, 1973).

(5) The bond stress-slip relationship suggested by Houde (1973) gives satisfactory analytical response in the case studies of the reinforced concrete structural members analyzed in the present study. However, Houde's simulation of the bond failure is obviously unreasonable. In this investigation, the method determining bond stress in bond failure portion used is by balancing residual forces at the steel-concrete interface. The validity of this approach still needs extensive experimental investigation.

(6) Dowel action is not considered in this study, which is treated as perfect bond at the steel-concrete interface in the direction perpendicular to reinforcement longitudinal direction. However, through stress analysis of beams in the present study, it is noted that dowel action does influence the stress direction and accuracy. A valid model with slip-dowel consideration to simulate actions at the steel-concrete interface is required for further analysis.

(7) The cracking modes, cracking models, cracking propagation and numerical solution for the nonlinear analysis improve the analytical predictions of stress field surrounding the cracks, which can be recommended to the future study.

6.3 RECOMMENDATIONS

(1) The constitutive model adopted in this study to represent the behaviour of concrete under a state of biaxial stress could be extended to represent the behaviour of concrete under triaxial stress state. It would be possible to include cyclic loading, dynamic loading if the model could be developed with such consideration. However, experimental studies are needed to be able to check the validity of any proposed model regarding these simulations.

(2) More experimental data on the stress field around the concrete cracks in reinforced members are required. These will enable development of a more accurate model to represent tension stiffening, aggregate interlock mechanism.

(3) Further experimental investigation on bond-dowel model is needed to simulate action at the steel-concrete interface in both the bond stress after bond failure and dowel effect on reinforced concrete beams.

Appendix A

FIGURES

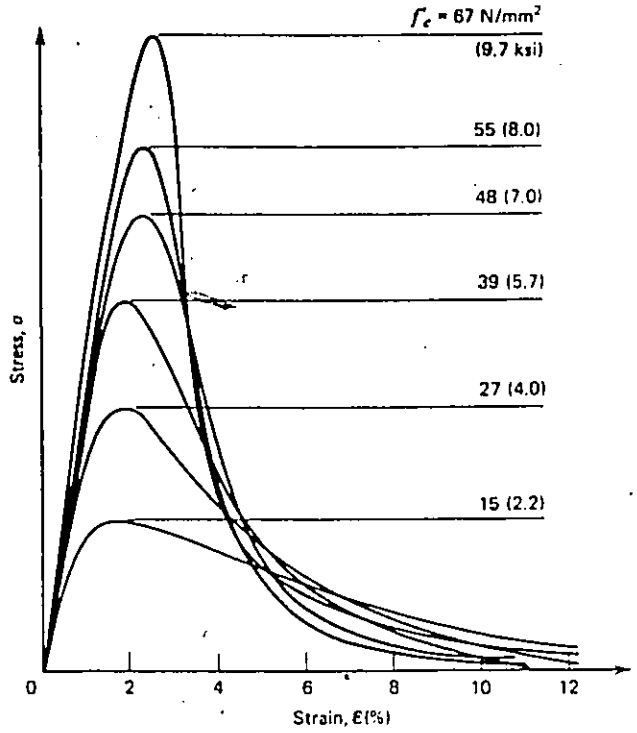

(a) Under Compression (Wischers, 1978)

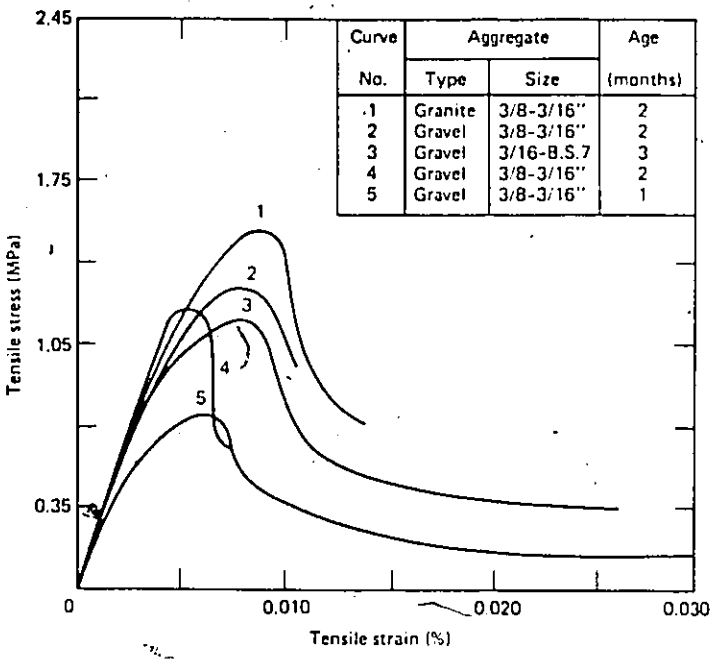

(b) Under Tension (Hughes and Chapman, 1966)

FIG.2.1 Typical Uniaxial Stress-Strain Curves for Concrete

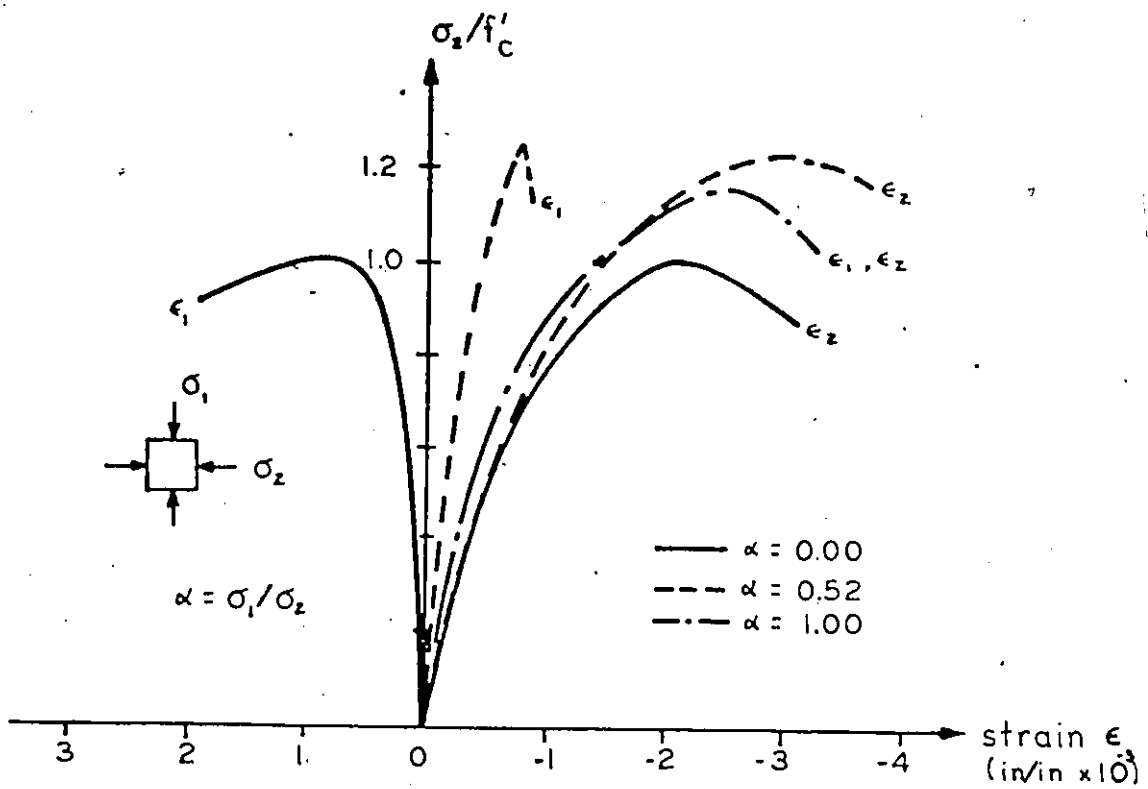

FIG.2.2 Experimental Stress-Strain Curve for Biaxial Compression (Kupfer and Gerstle, 1973)

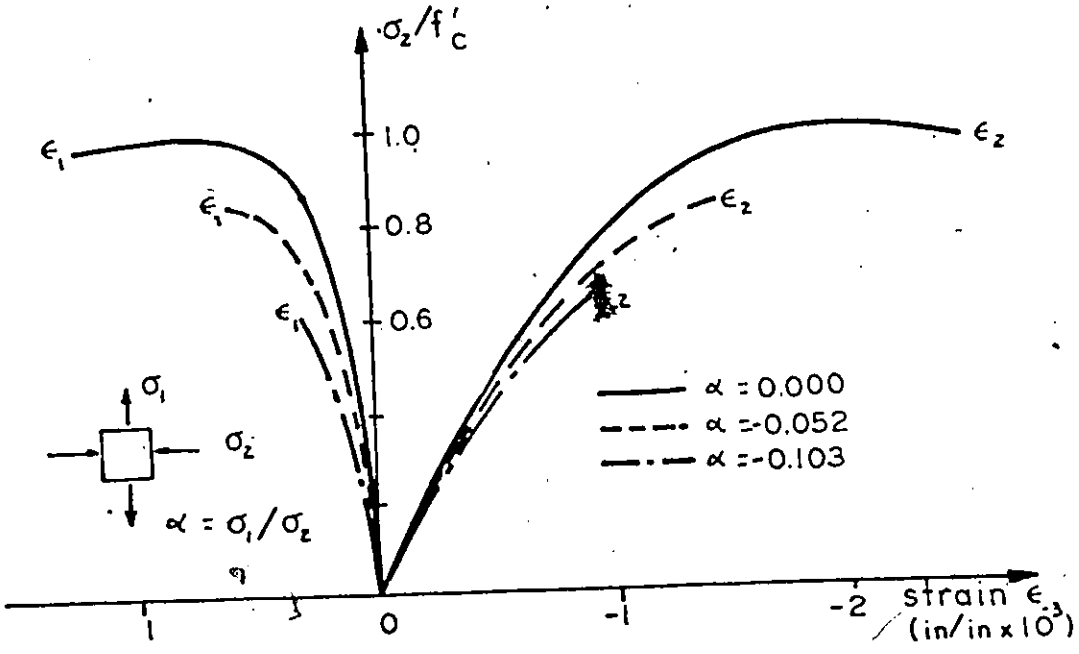

FIG.2.3 Experimental Stress-Strain Curve for Biaxial Tension-Compression (Kupfer and Gerstle, 1973)

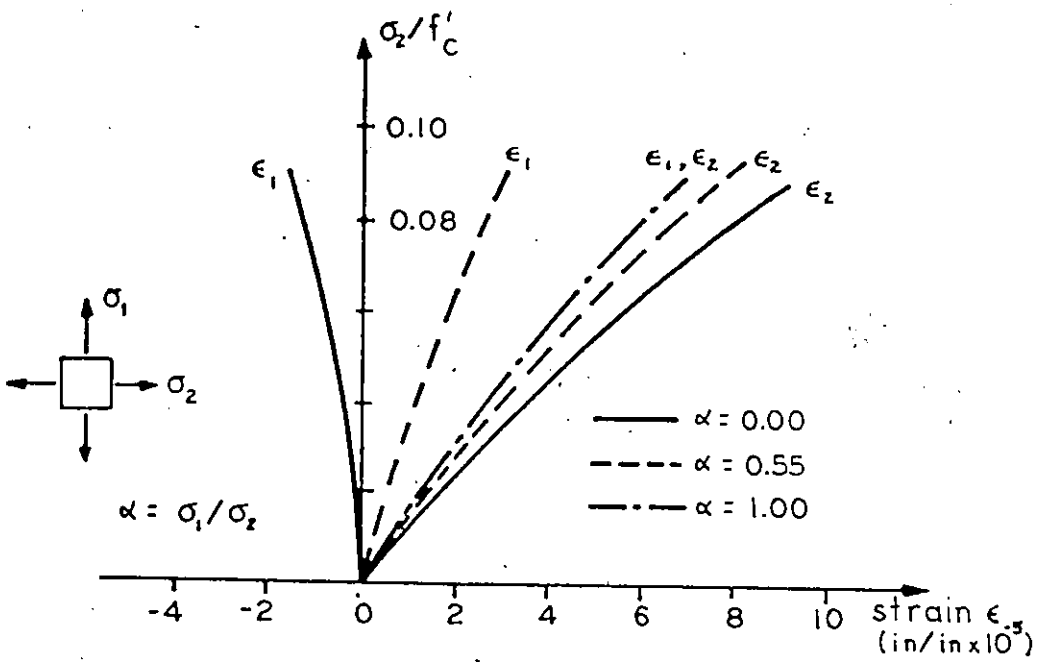

FIG.2.4 Experimental Stress-Strain Curve for Biaxial Tension-Tension (Kupfer and Gerstle, 1973)

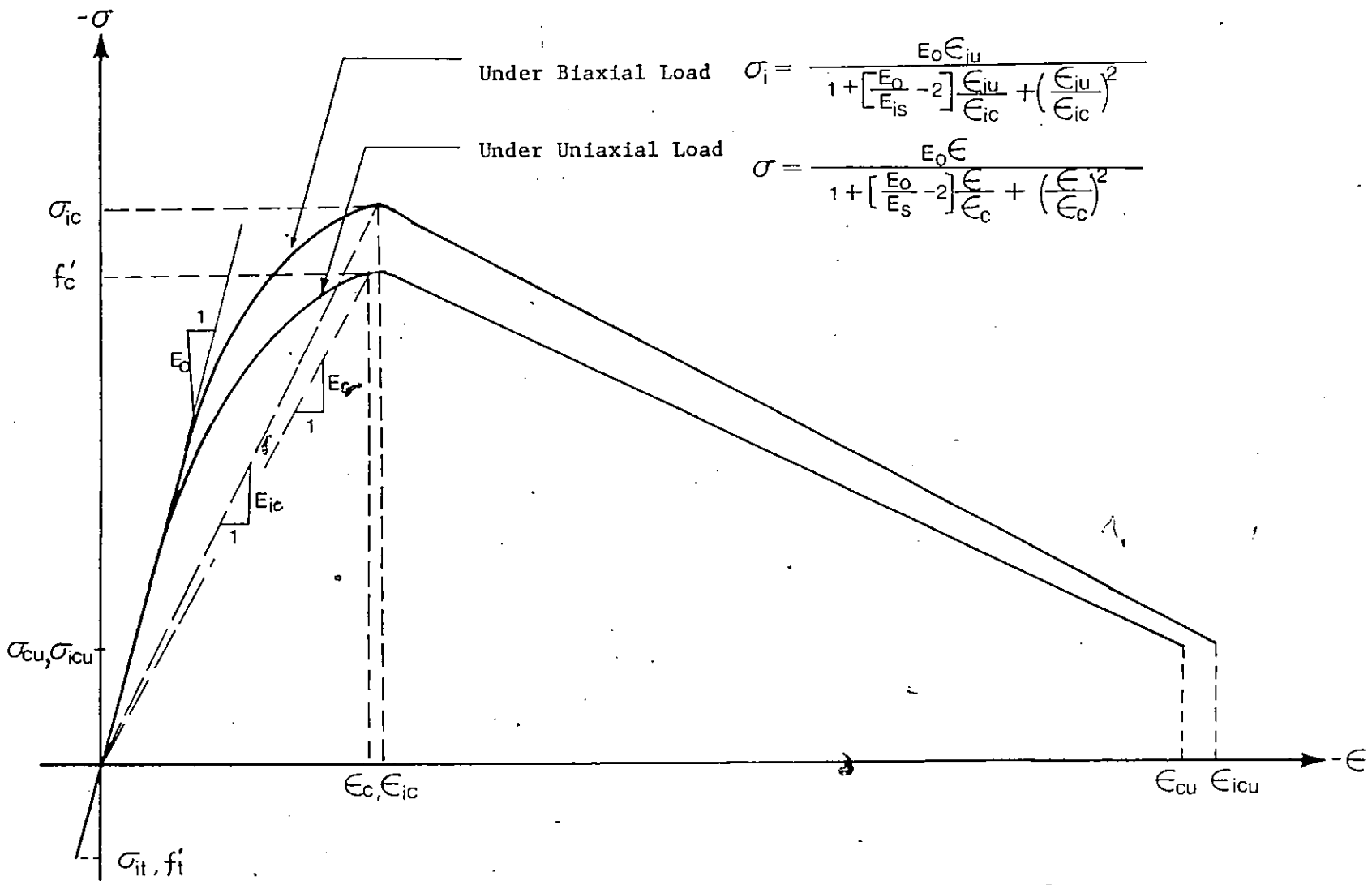

FIG.2.5 Equivalent Uniaxial Stress-Strain Curve for Concrete Modelling Used in the Present Study

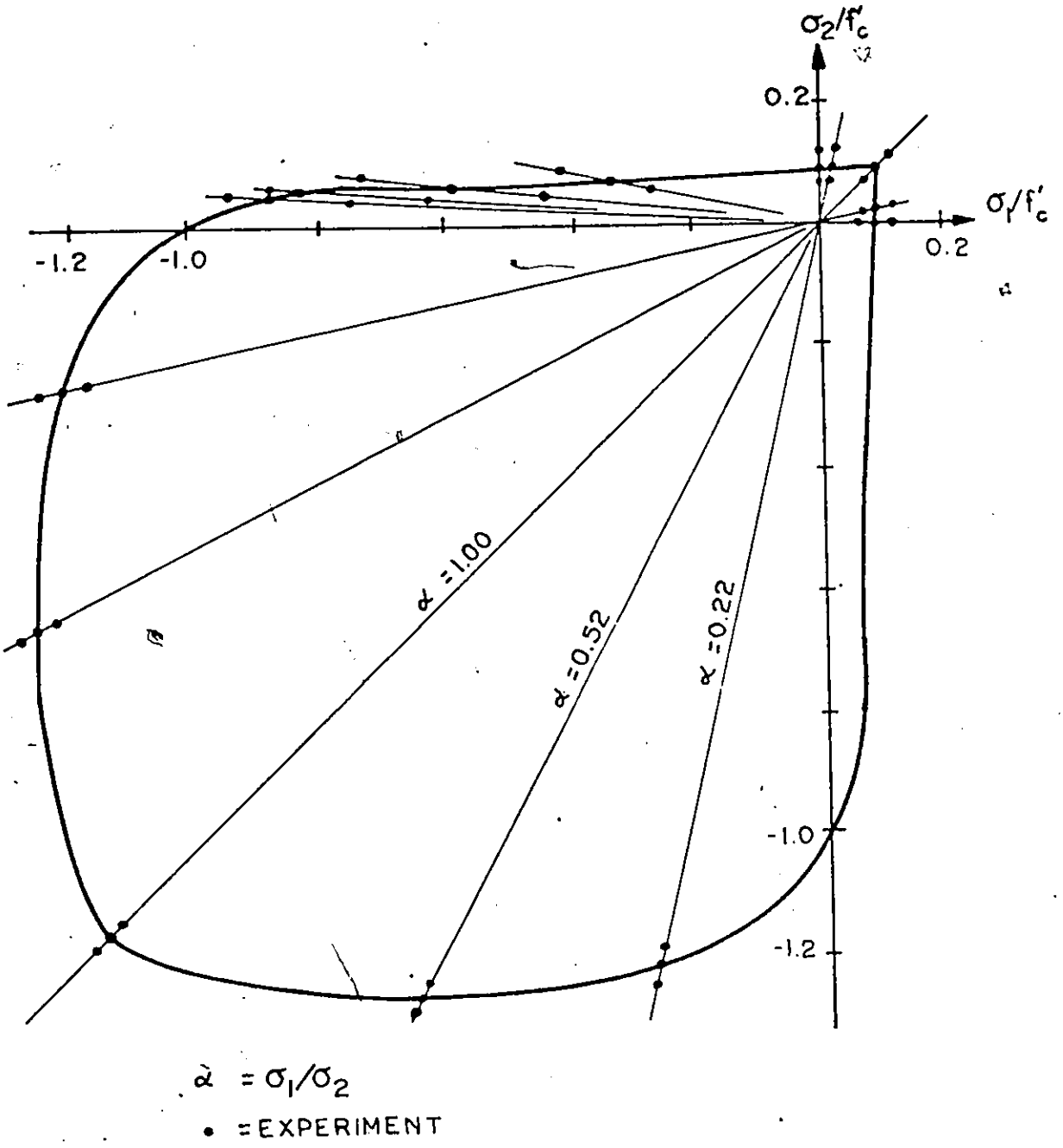

FIG.2.6 Experimental Biaxial Strength Envelope of Plain Concrete (Kupfer and Gerstle, 1973)

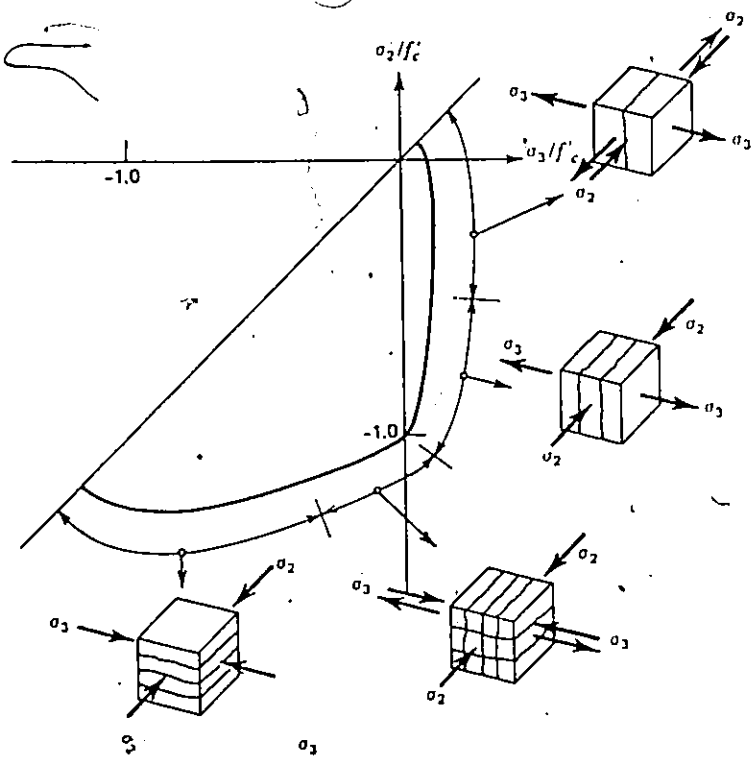

FIG.2.7 Failure Patterns of Biaxial Loaded Concrete (Nelissen, 1972)

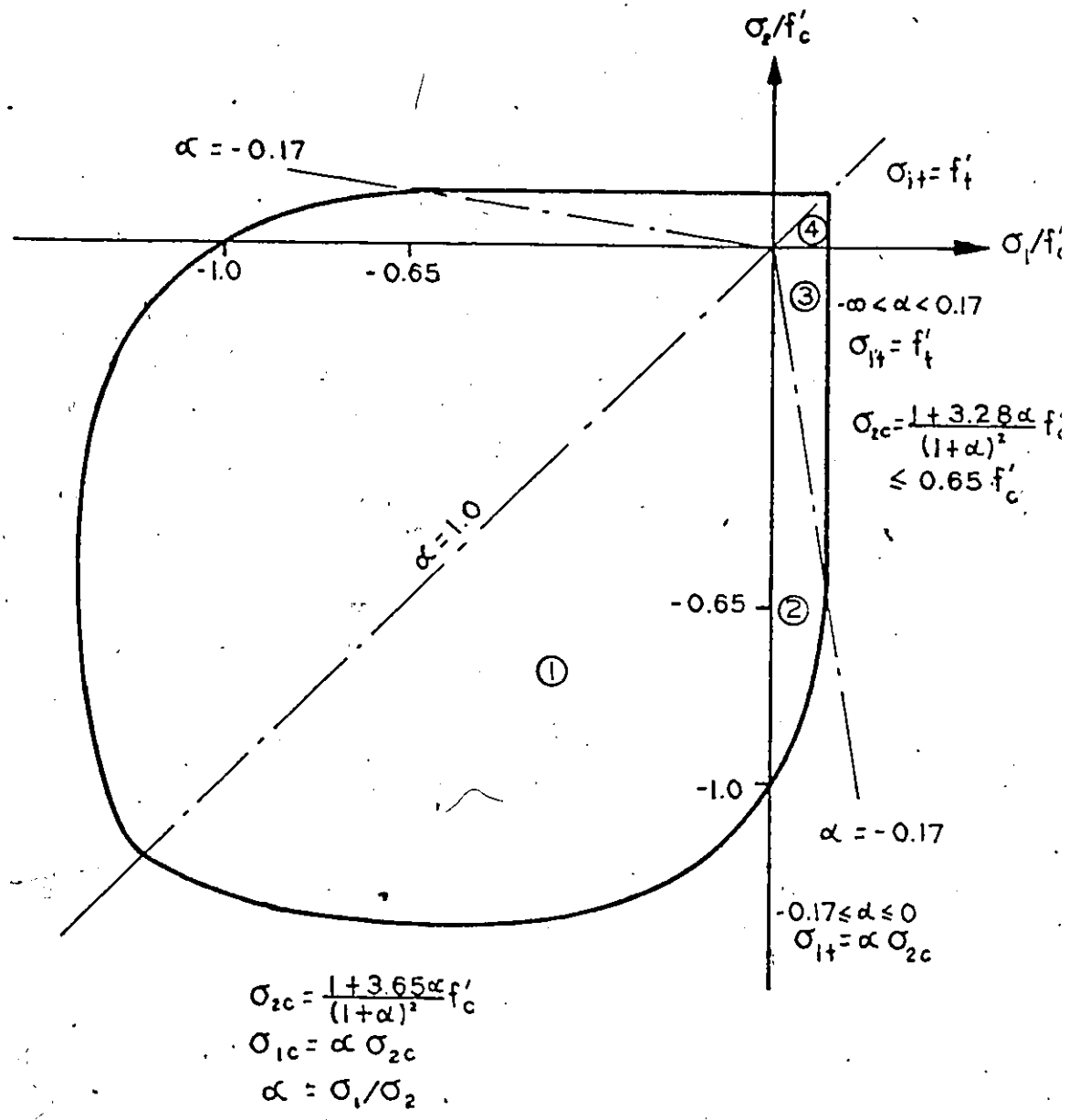

FIG.2.8 Biaxial Strength Envelope Used in the Present Study

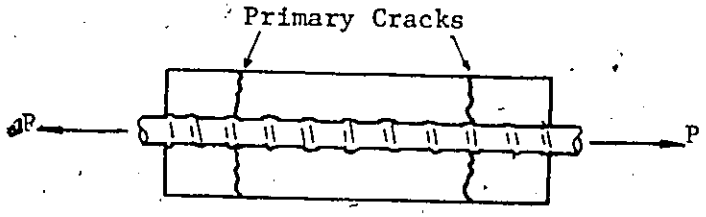

(a) Axially Loaded Tensile Specimen

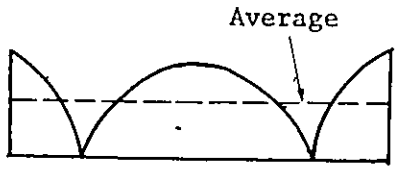

(b) Concrete Stress Distribution

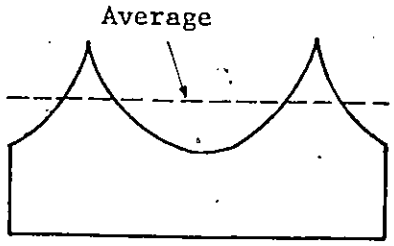

(c) Steel Stress Distribution

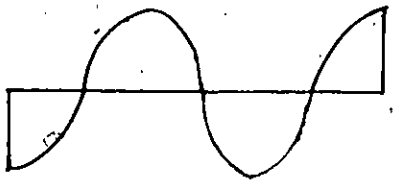

(d) Bond Shear Stress Distribution

FIG.2.9 Stress Distribution in a Cracked Concrete Axially Loaded Tensile Specimen (Lin and Scordelis, 1975)

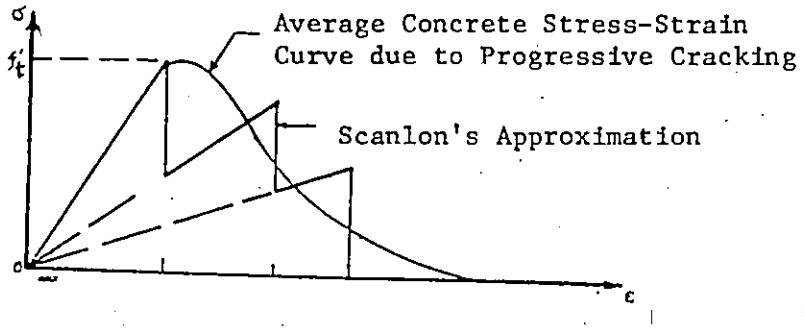

(a) Scanlon's Stepped Approach (Scanlon, 1971)

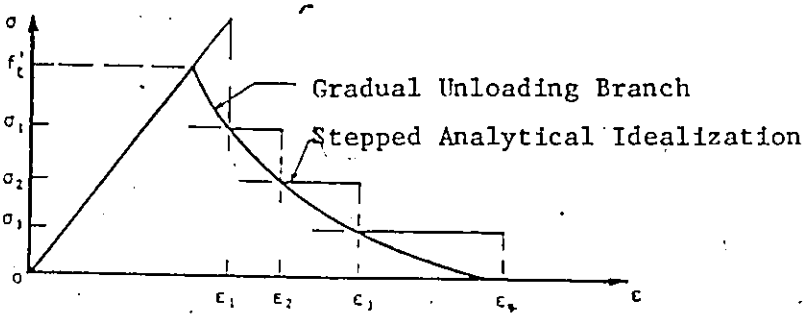

(b) Lin's Gradually Unloading Approach (Lin, 1973)

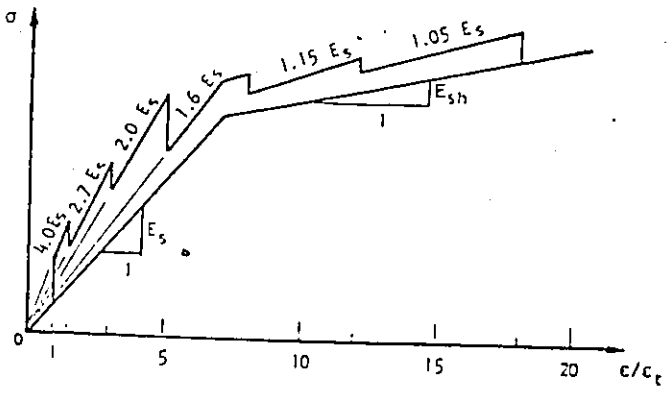

(c) Modified Stress-Strain Diagram for Reinforcing Steel (Gilbert, 1978)

FIG.2.10 Different Tension Stiffening Approaches

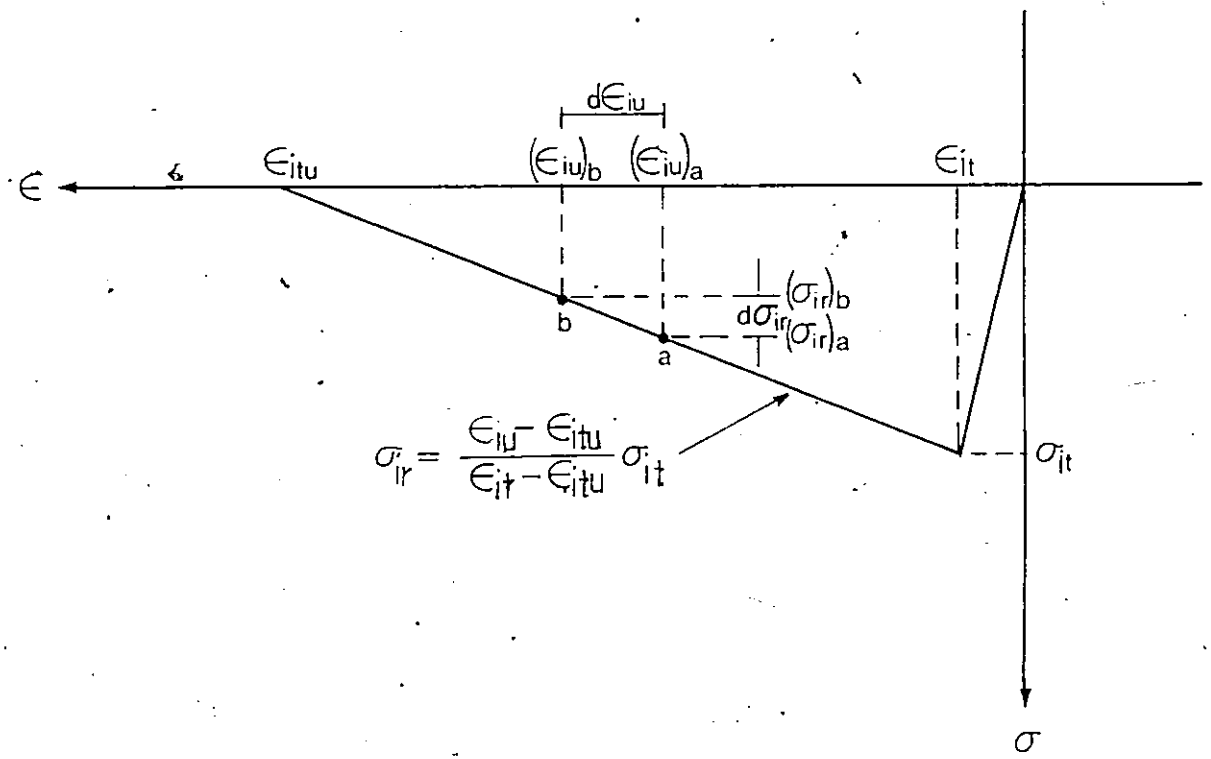

FIG.2.11 Released Tensile Stress after Concrete Cracking

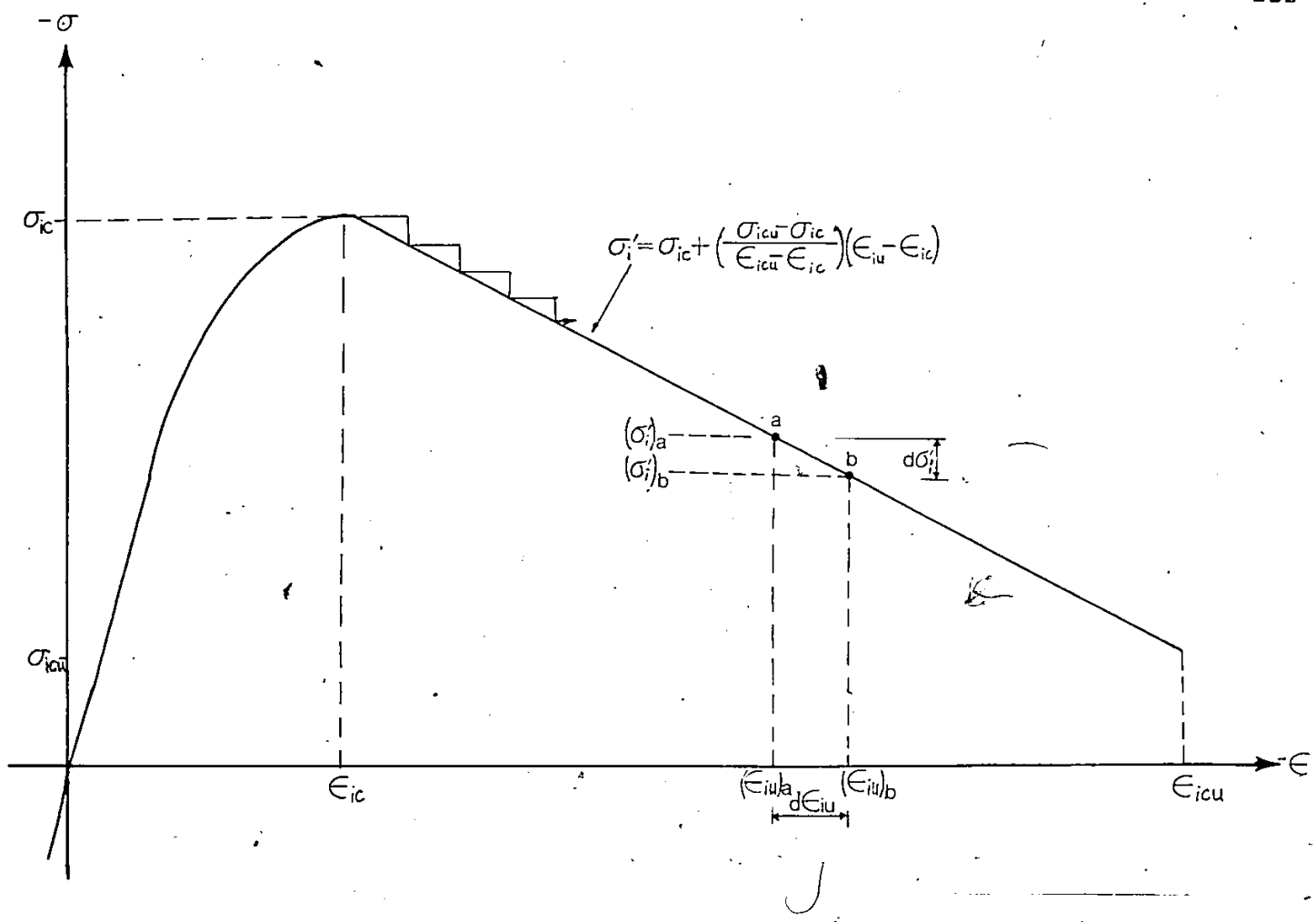

FIG.2.12 Strain Softening Beyond Maximum Compressive Stress

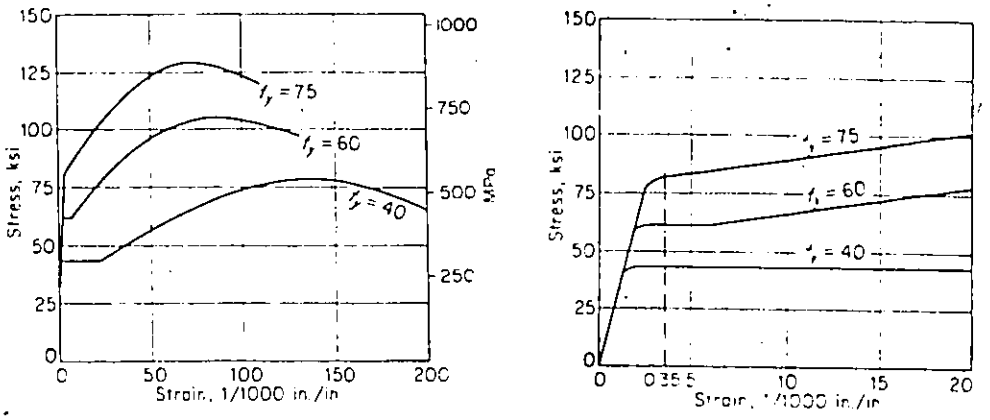

(a) Non-Tensioned Mild Steel

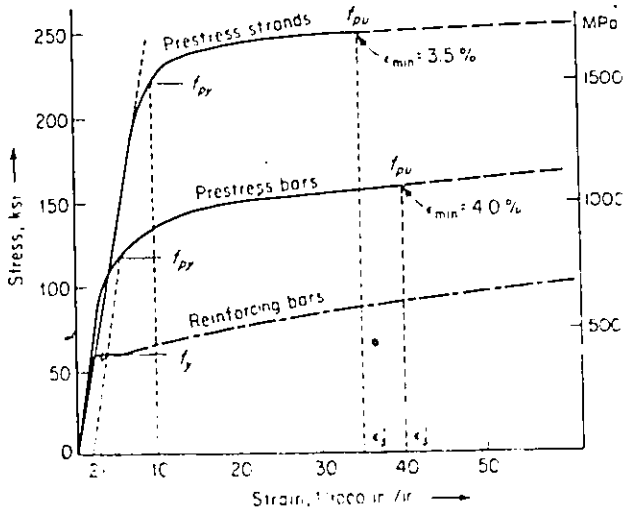

(b) Prestressing Steel

FIG.3.1 Typical Stress-Strain Curves for Reinforcing Steel (Winter and Nilson, 1979)

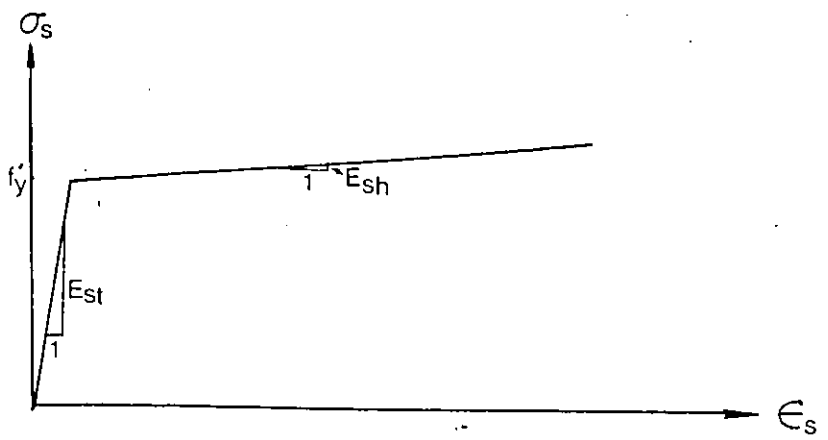

(a) Bilinear Approximation (Elastoplastic)

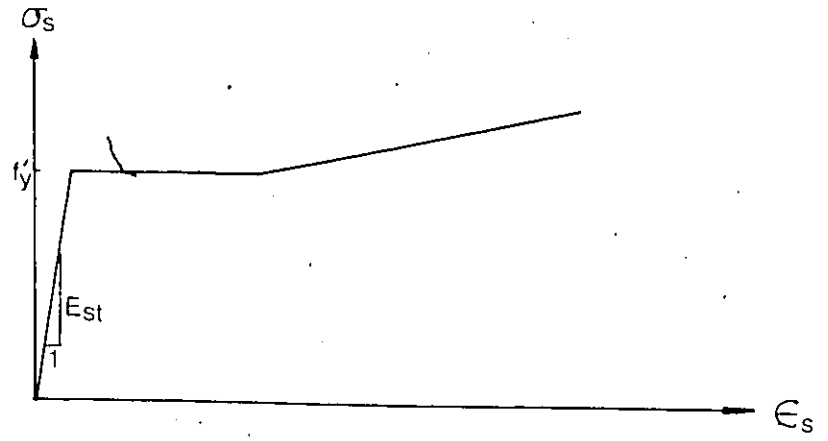

(b) Trilinear Approximation

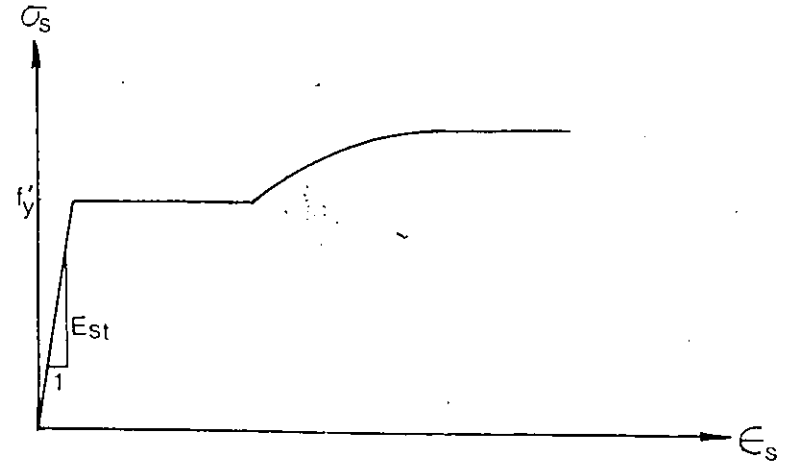

(c) Complete Curve

FIG.3.2 Idealizations of the Stress-Strain Curve for Steel in Tension or Compression

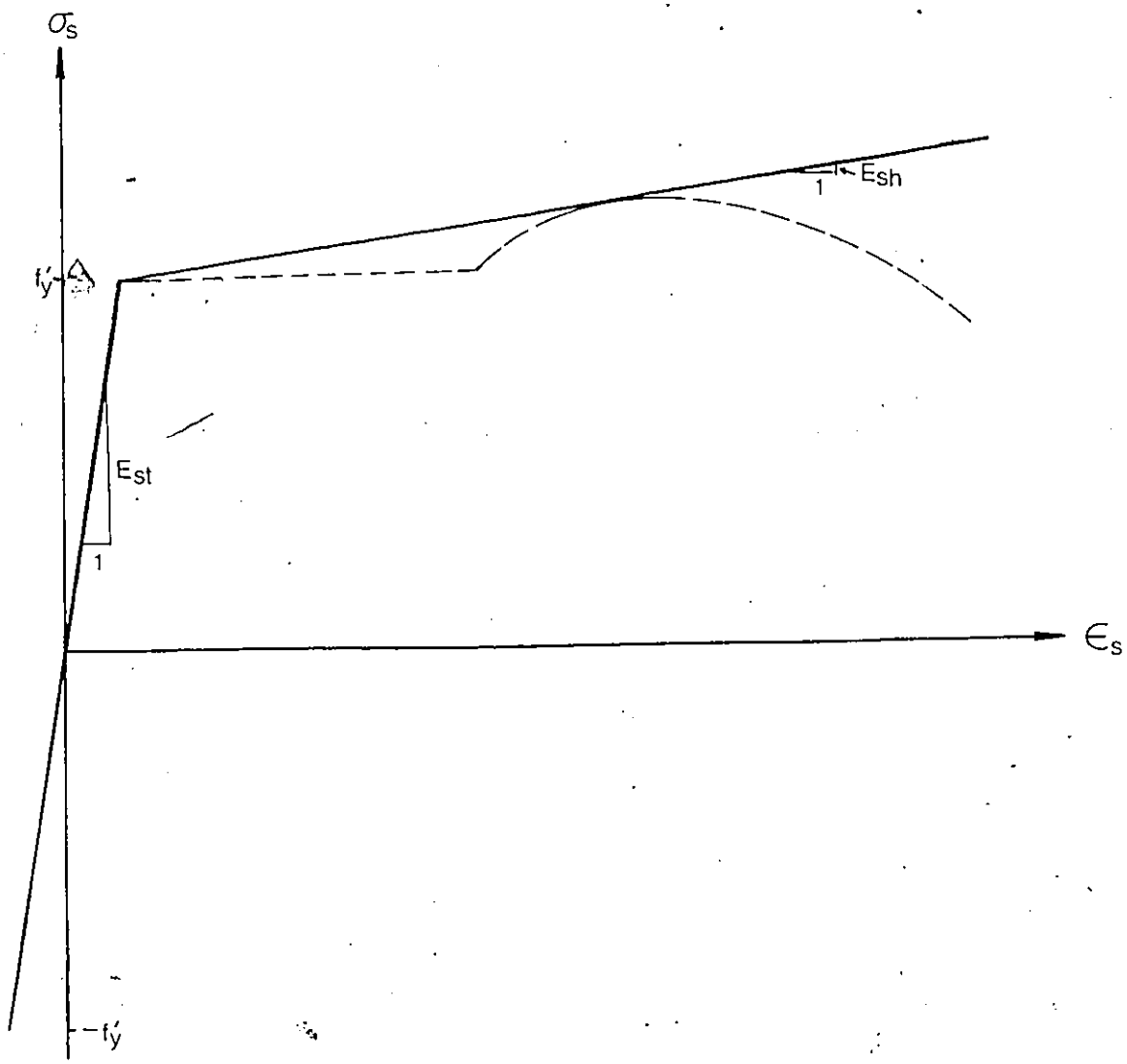

FIG.3.3 Bilinear Stress-Strain Curve Used in the Present Study

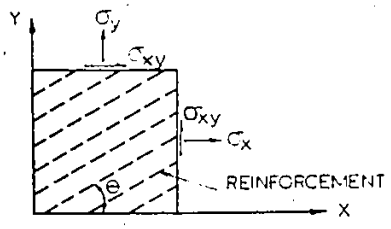

(a) Distributed Approach

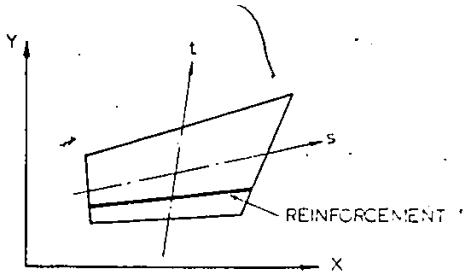

(b) Embedded Approach

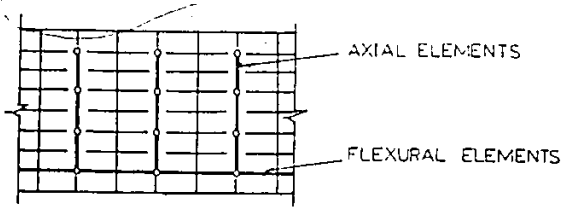

(c) Discrete Approach

FIG.3.4 Alternate Representations of Steel

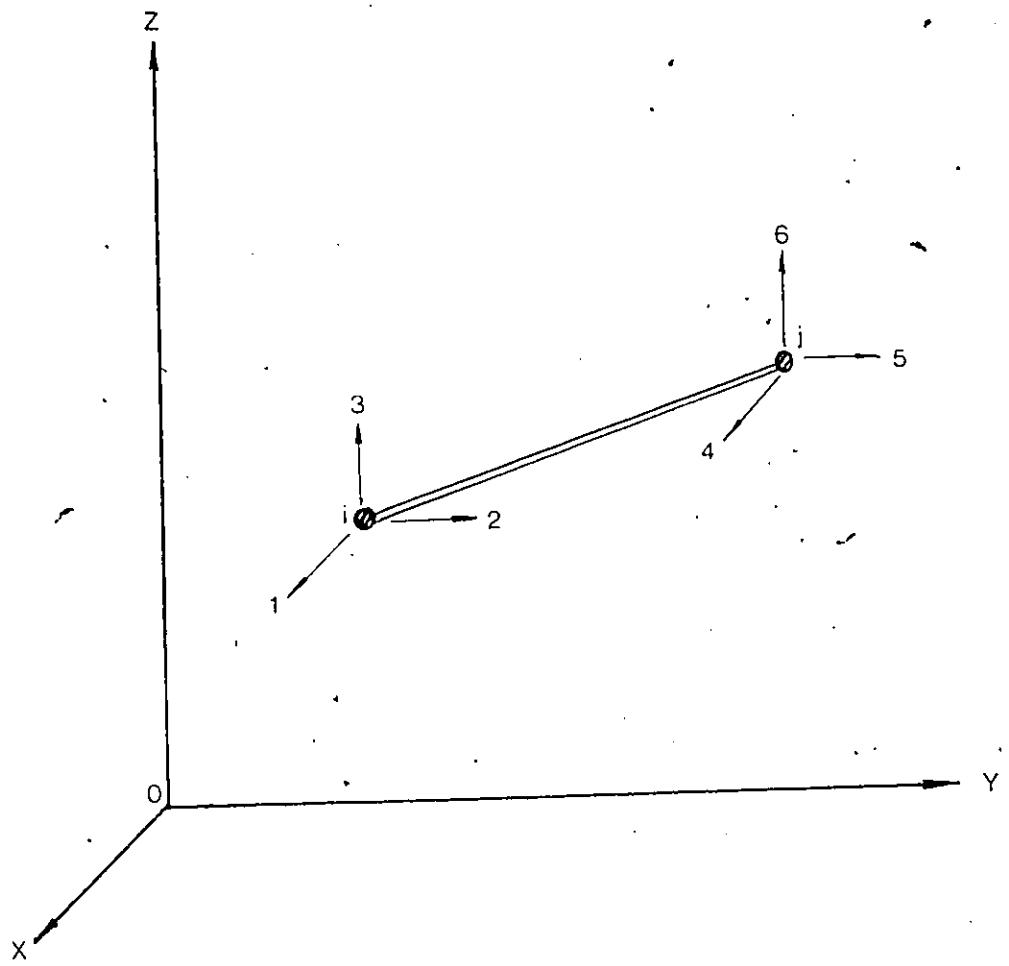

FIG.3.5 3D Truss Element for Reinforcement Idealization

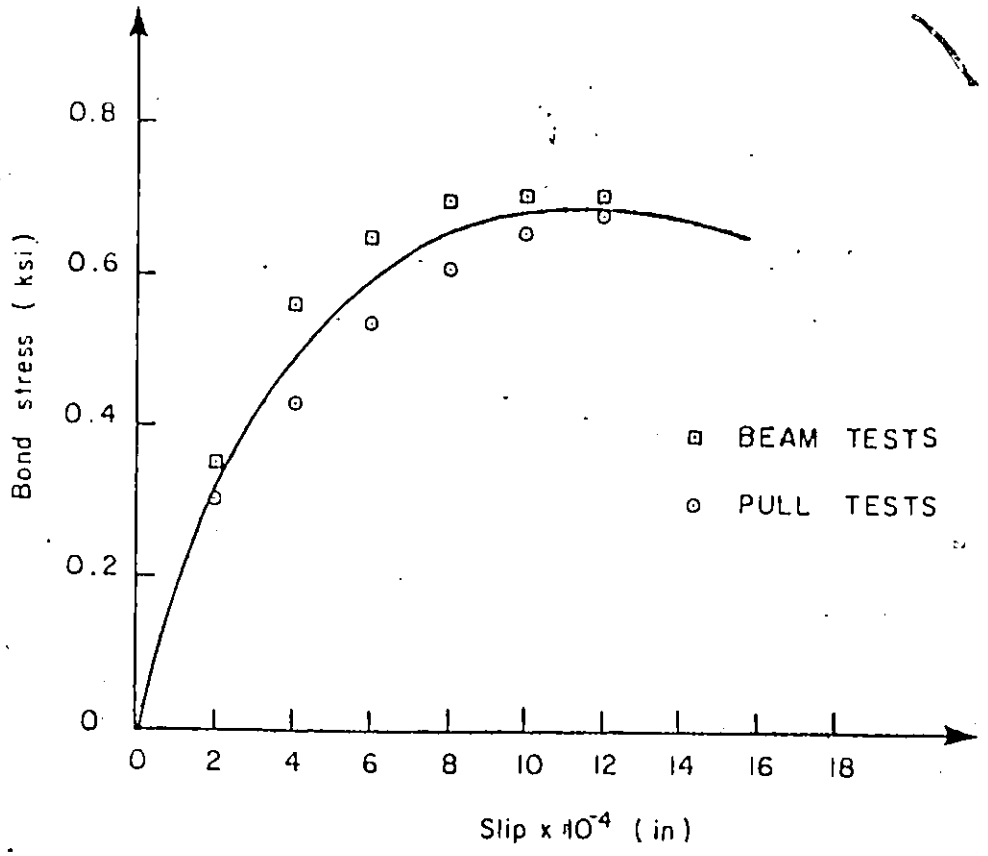

FIG.3.6 Bond Stress -- Slip Relationship Used in the Present Study (Houde, 1973)

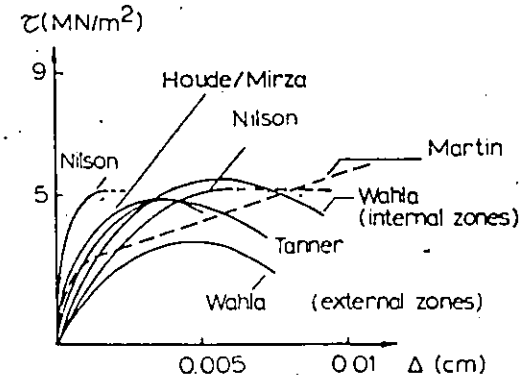

FIG.3.7 Comparison of Houde's Bond Stress-Slip Relationship with the Others of Different Researchers

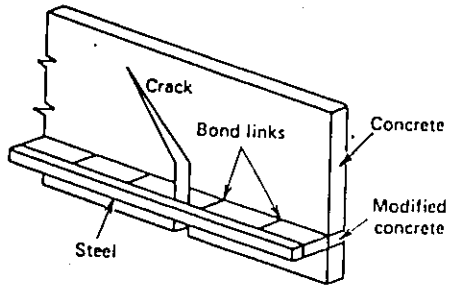

(a) Analytical Model

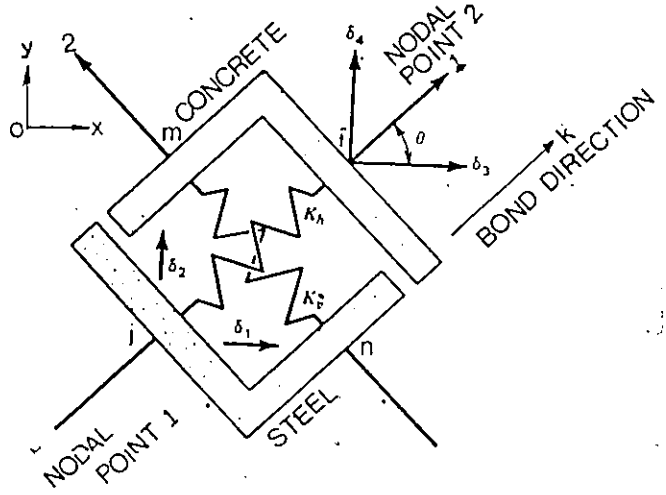

(b) 2D Linkage Element

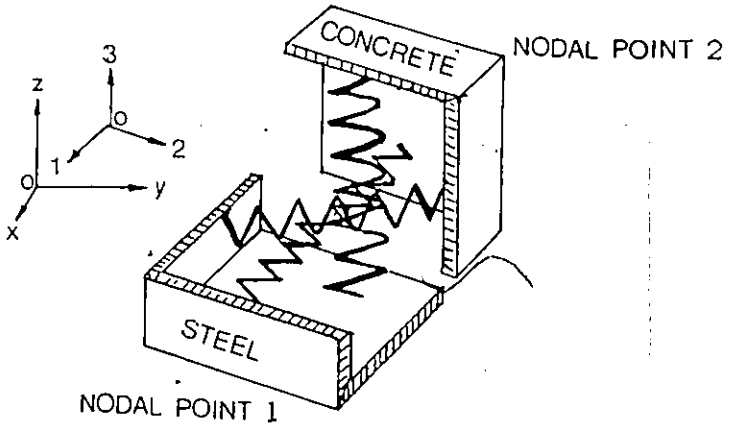

(c) 3D Linkage Element

FIG.3.8 Bond -- Dowel Action Idealization

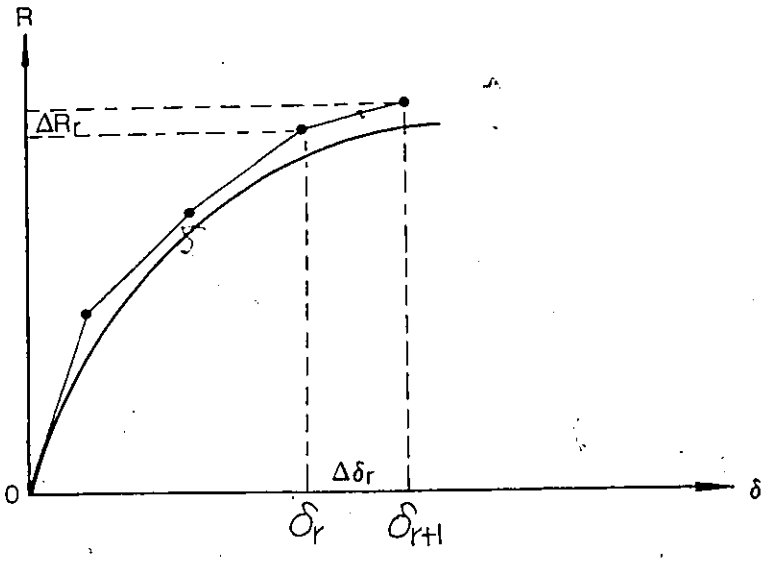

(a) Simple Step-by-Step Method

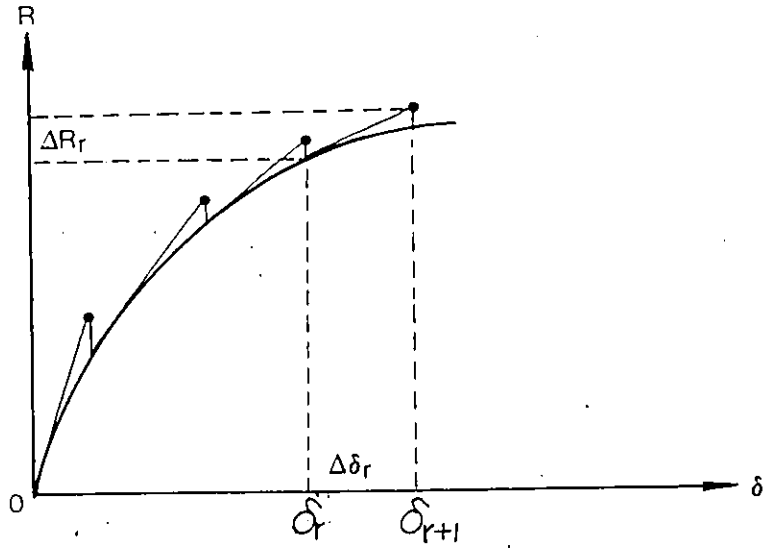

(b) Improved Step-by-Step Method

FIG.4.1 Schematics of the Solution Procedure by Step-by-Step Methods in a Nonlinear Problem

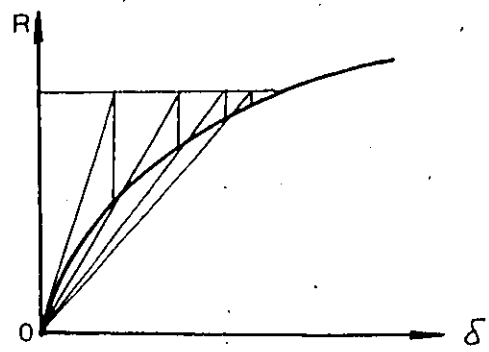

(a) Direct Iteration

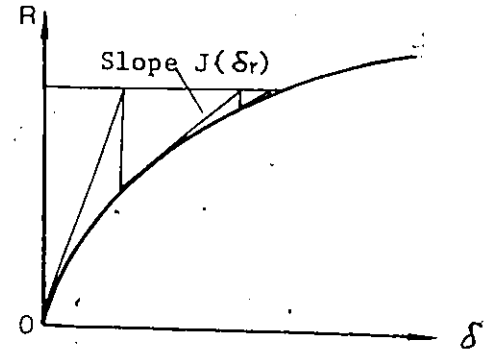

(b) Newton-Raphson Method

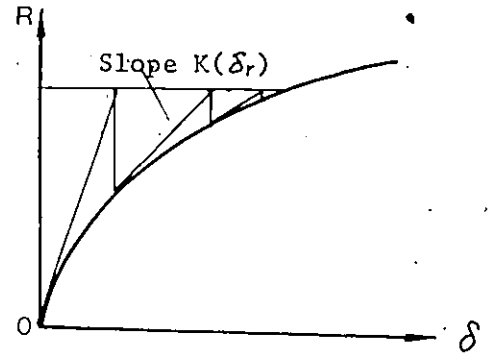

(c) The Tangential Stiffness Method

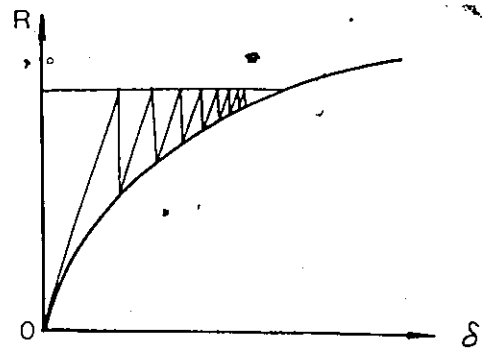

(d) The Initial Stiffness Method

FIG.4.2 Schematics of the Solution Procedure by Iteration Methods in a Nonlinear Problem

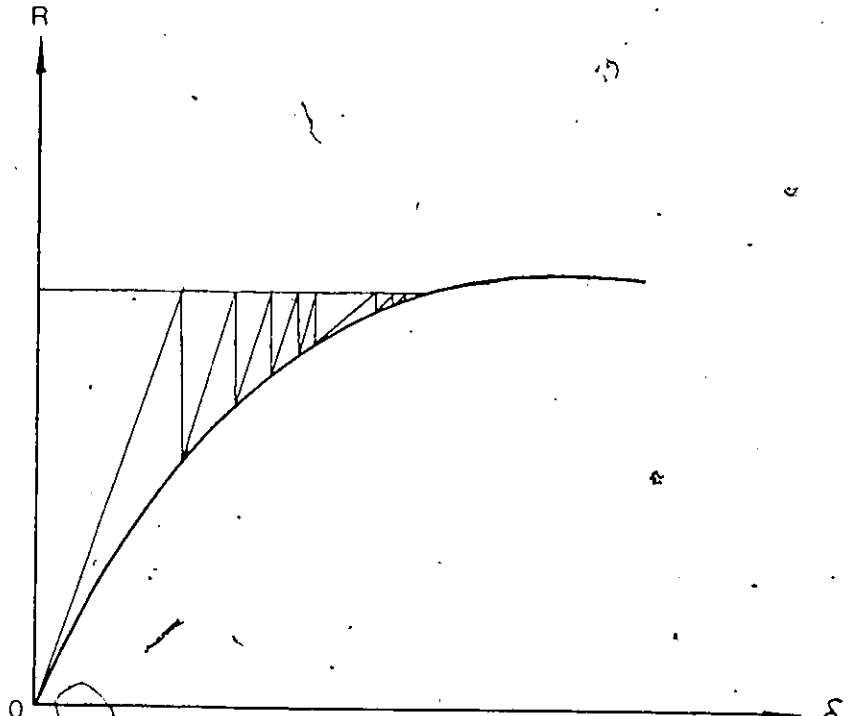

FIG.4.3 The Combined Iteration Method Used in the Present Study (the Tangential Stiffness Method with the Initial Stiffness Method)

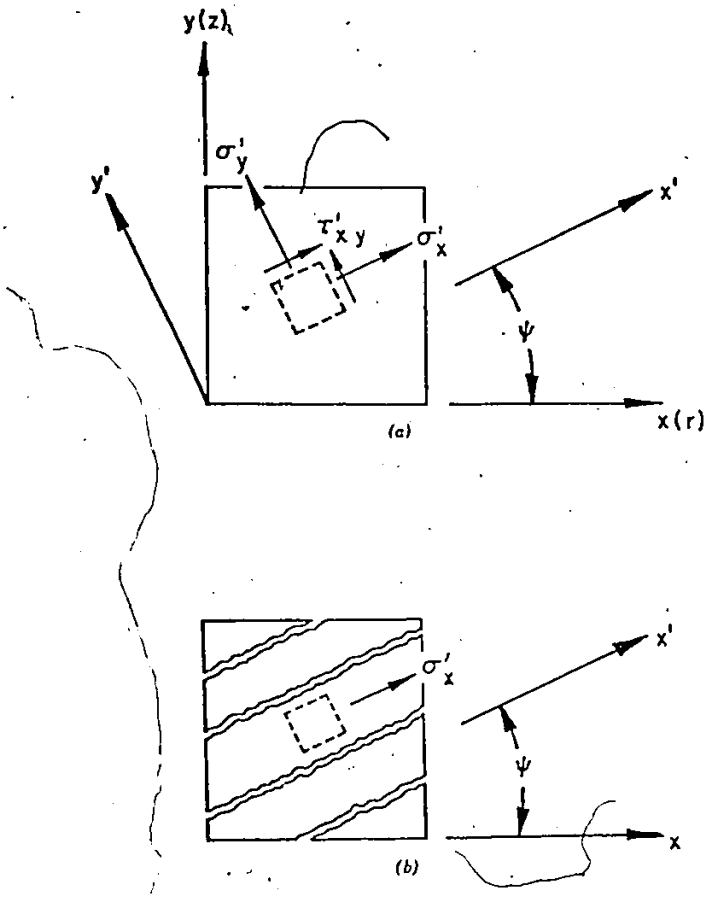

FIG.4.4 Modelling of Cracks by Smeared Approach in a Cracked Concrete Element

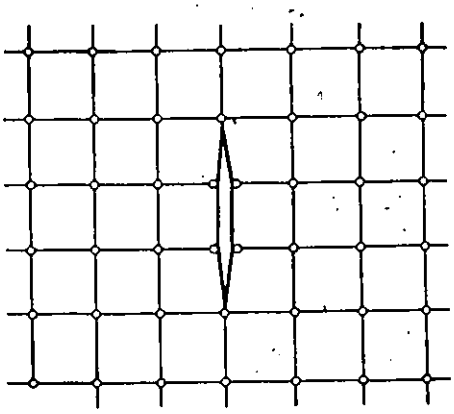

(a) One-Dimensional Cracking

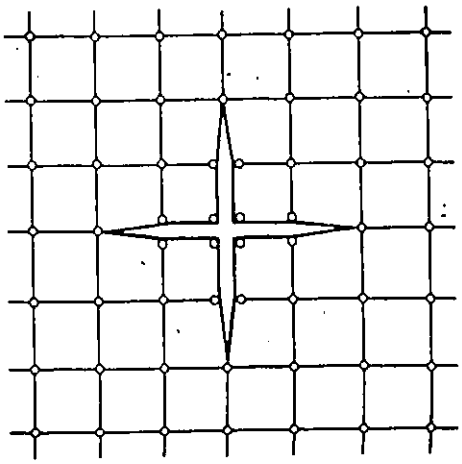

(b) Two-Dimensional Cracking

FIG.4.5 Cracking Representation in Discrete Cracking Modelling Approach

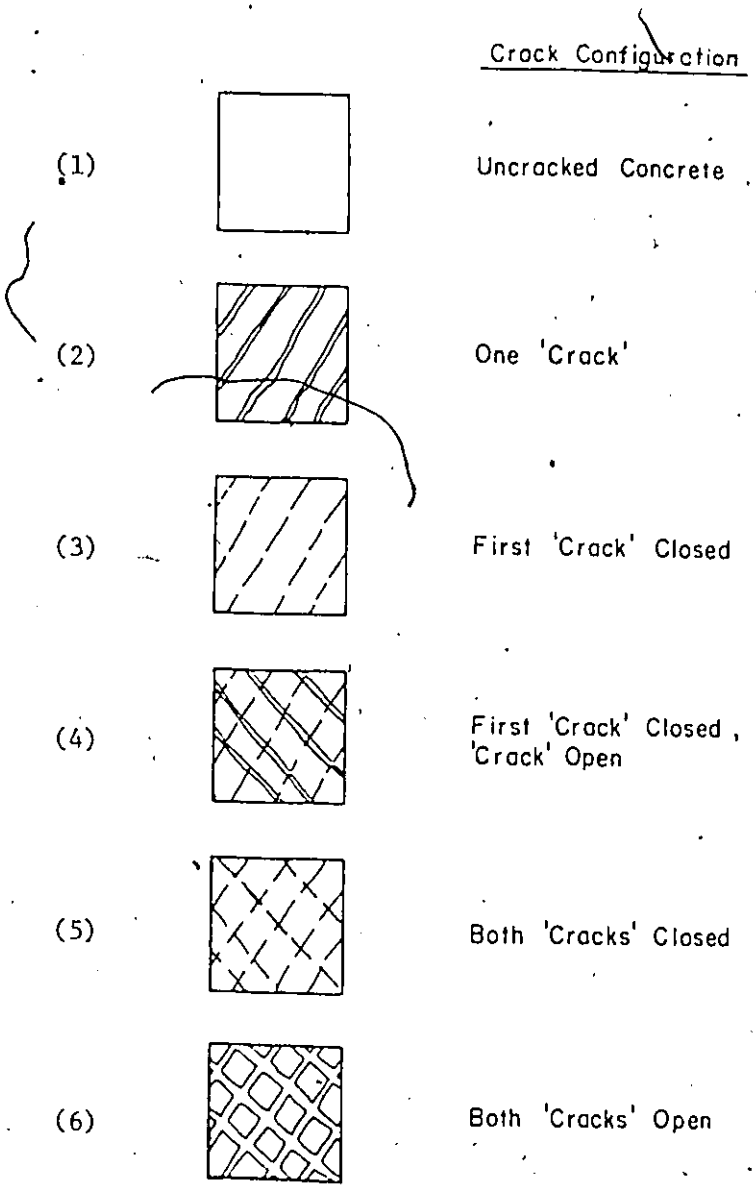

FIG.4.6 Possible Crack Configurations for Multiple Cracking Modes

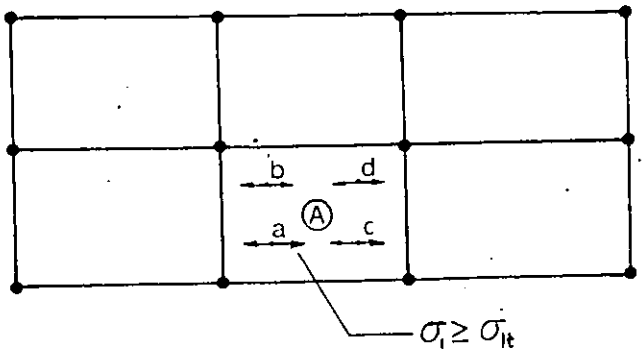

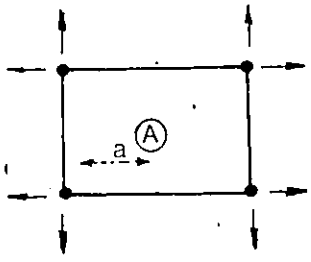

Element (A) Nodal Unbalanced Forces
due to Concrete Cracking at Integration Point a

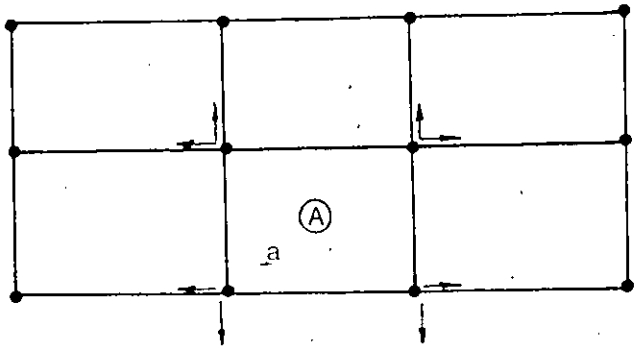

FIG.4.7 Redistribution of Element Nodal Unbalanced Forces after Concrete Cracking

AXIALLY LOADED TENSILE SPECIMEN
ELEMENT MESH

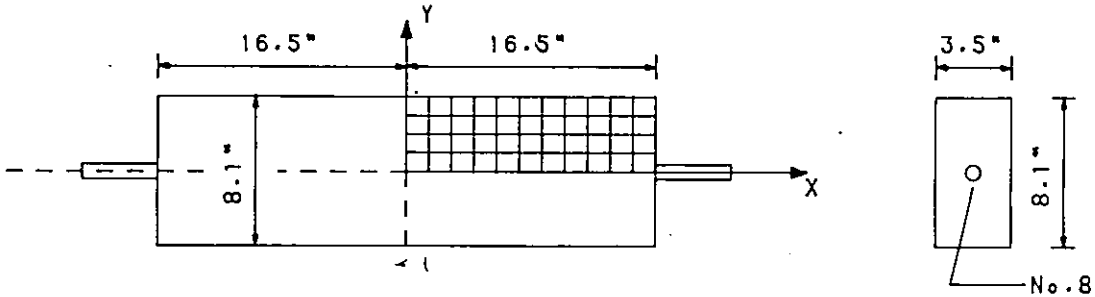

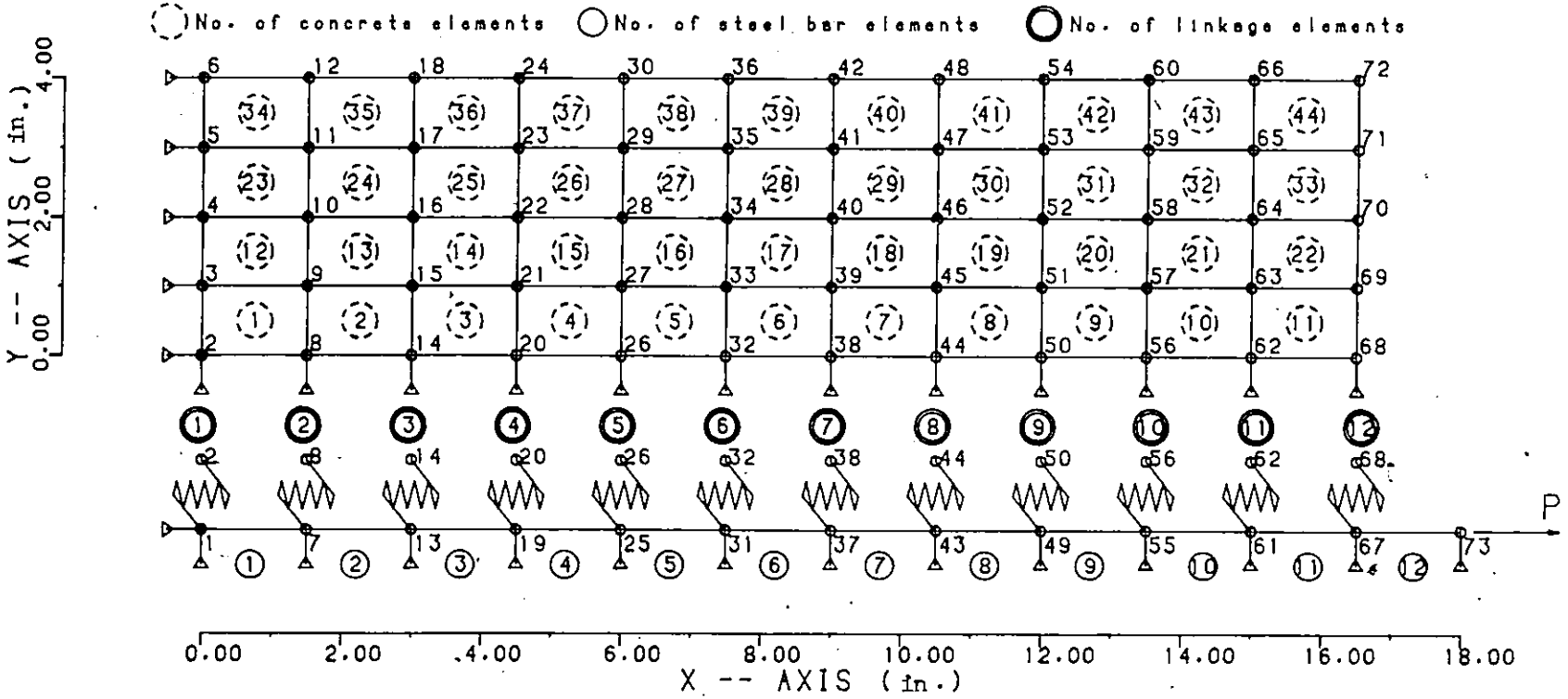

FIG.5.1 : Axially Loaded Tensile Specimen Idealization

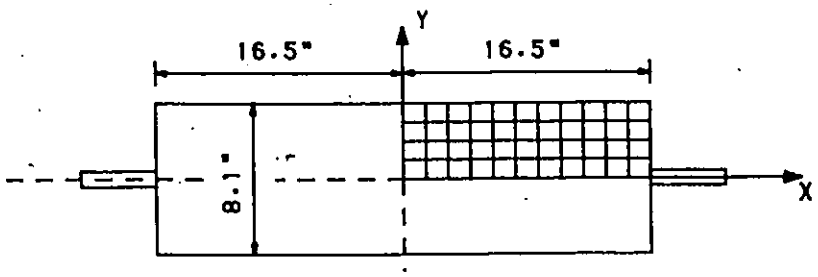

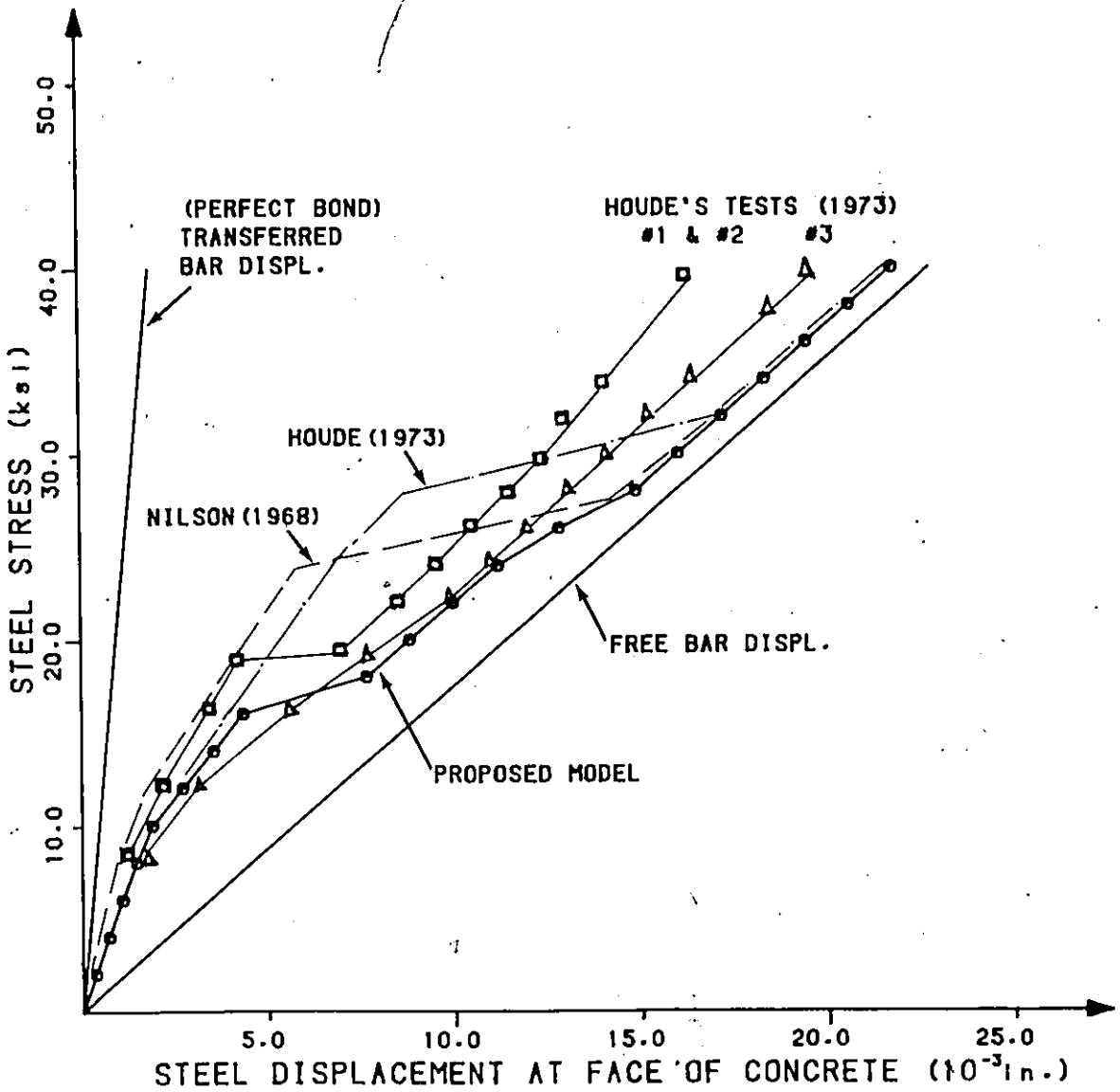

FIG.5.2 : Comparison of Force Displacement Relationship fo
Axially Loaded Tensile Specimen (Houde, 1973)

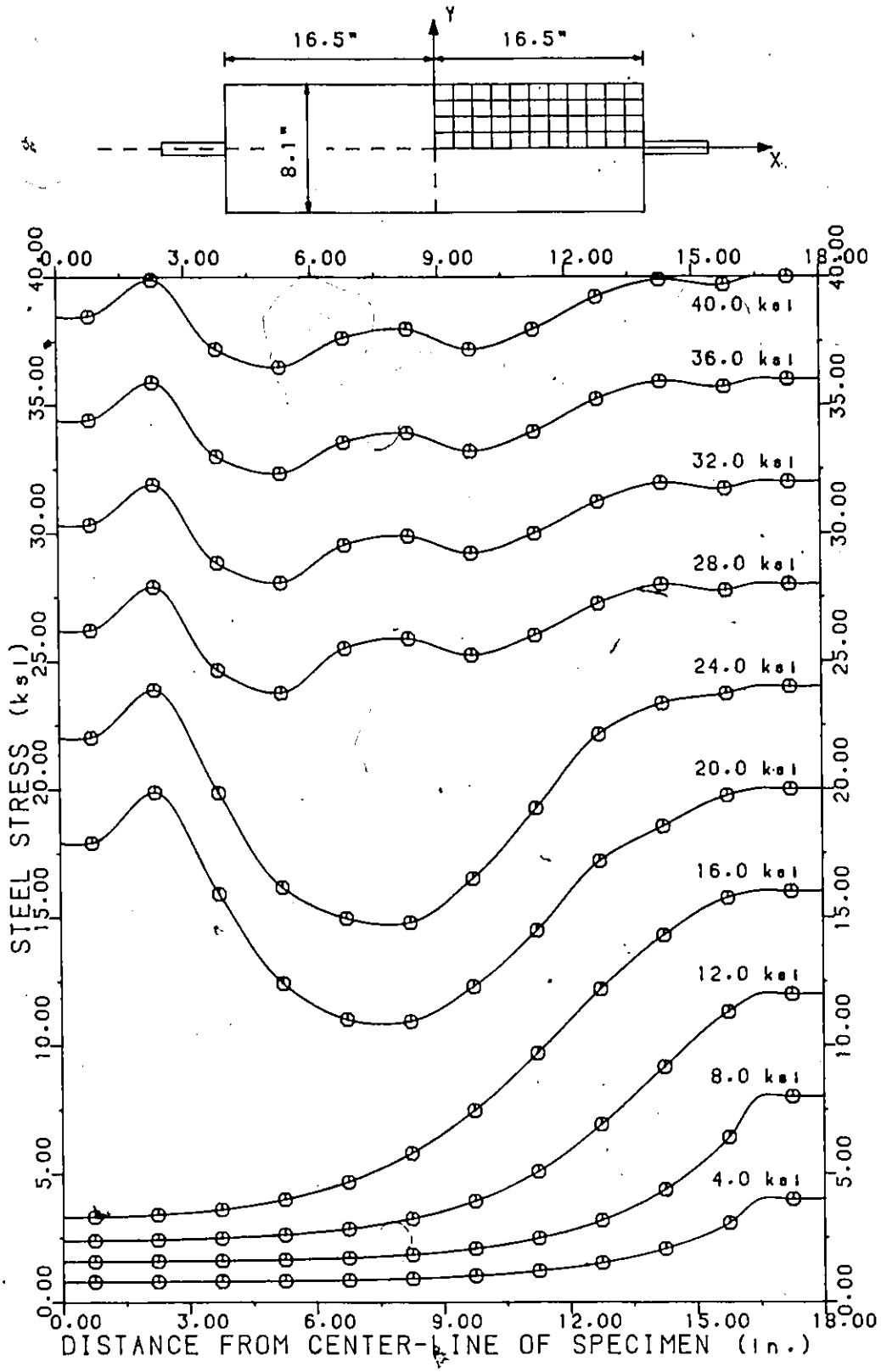

FIG.5.3 : Steel Stress Variation for Axially Loaded Specimen

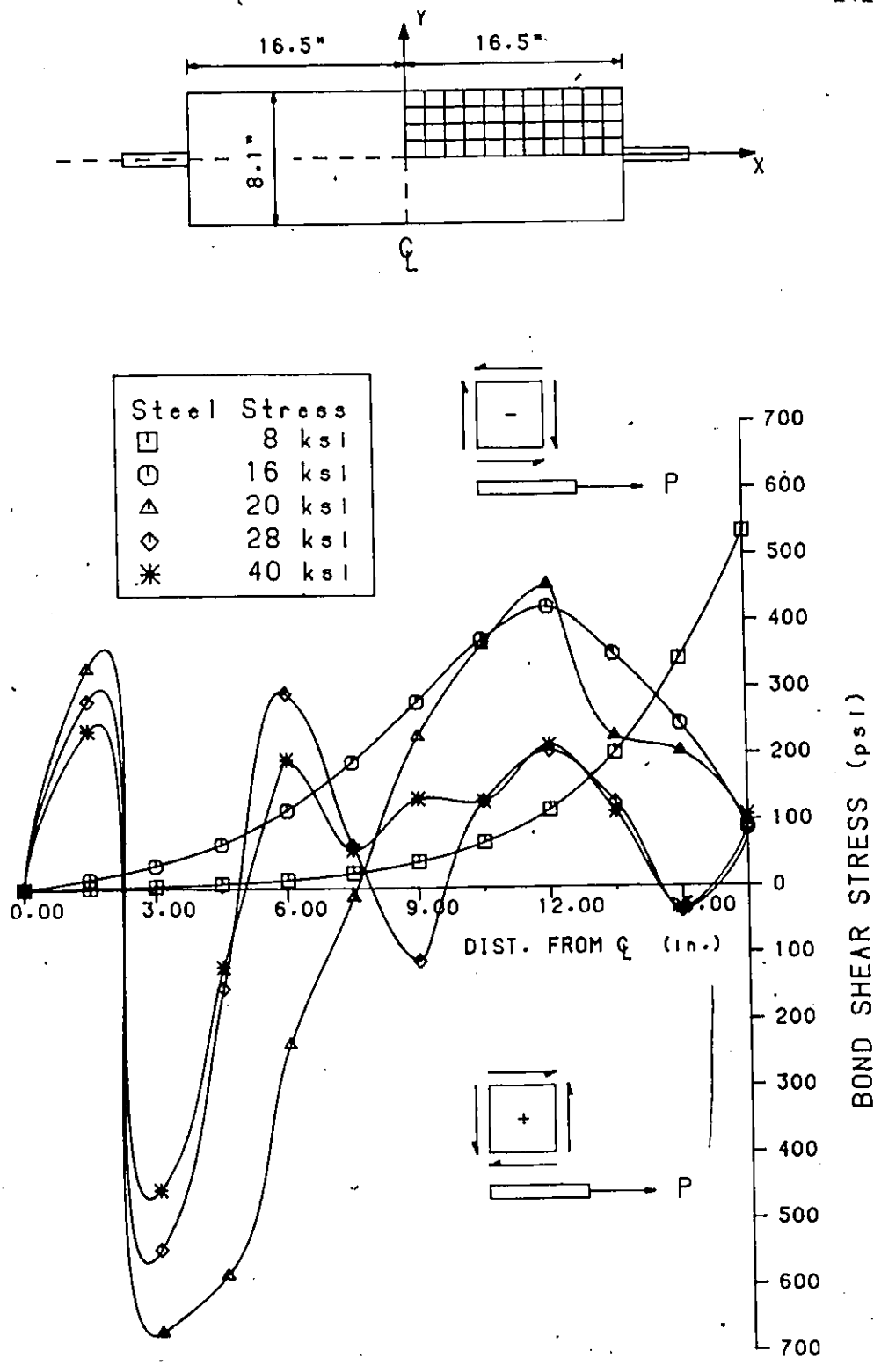

FIG.5.4 : Bond Shear Stress Variation for Axially Loaded Tensile Specimen

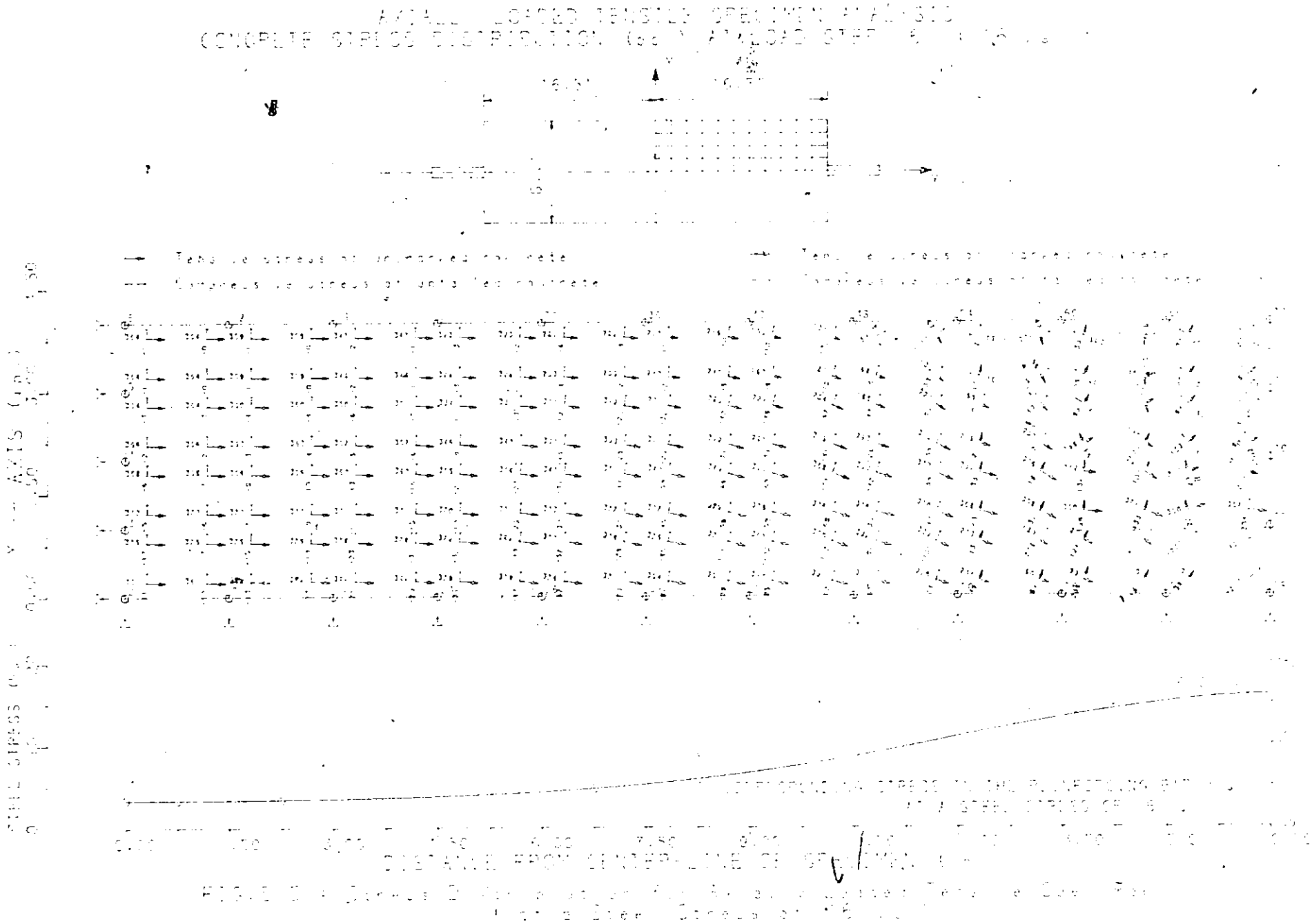

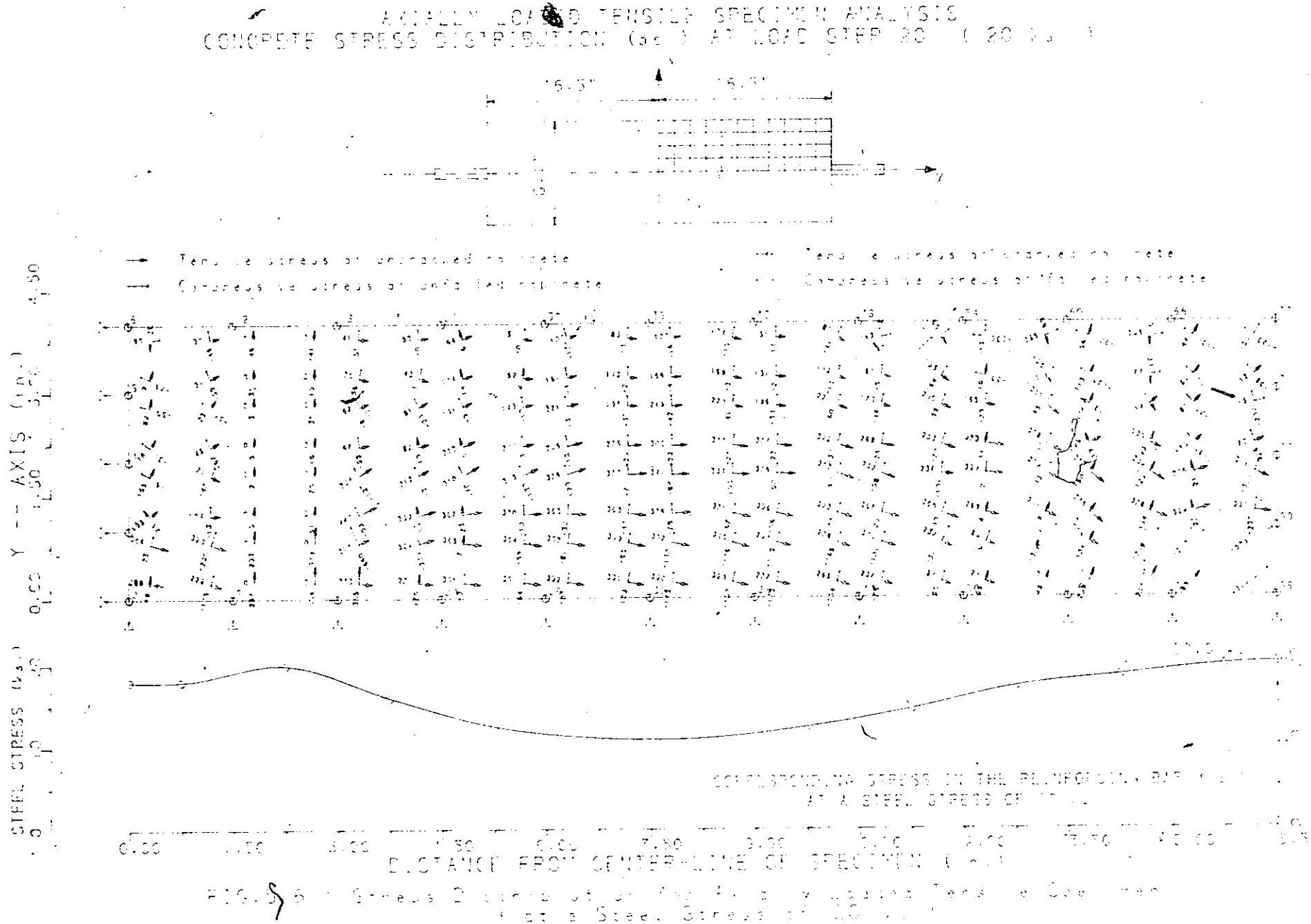

CONCRETE STRESS IN THE REINFORCING BAR (psi)
AT A STEEL STRESS OF

FIG. 5 Stress Distribution of the Axially Loaded Tensile Specimen
at a Steel Stress of

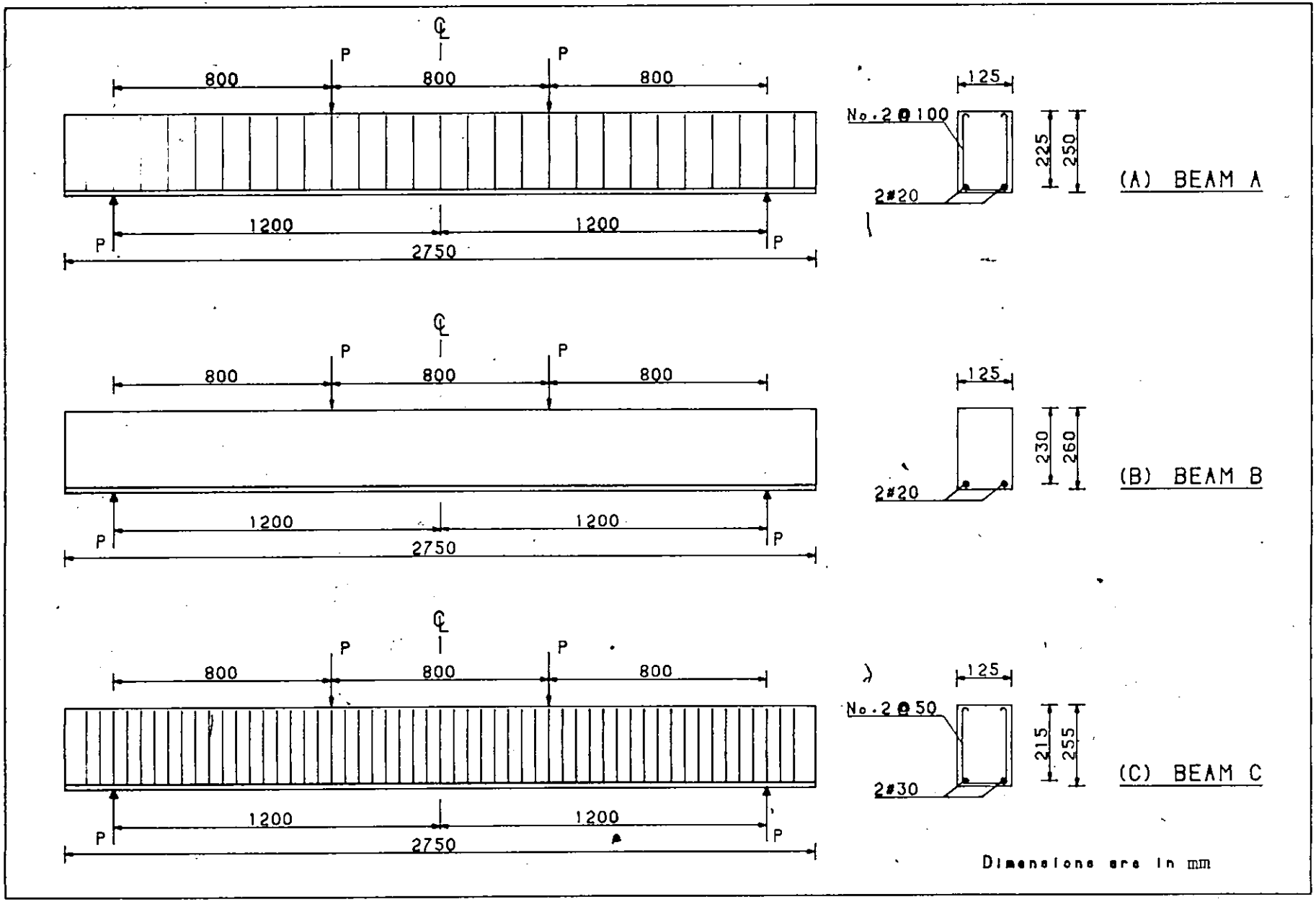

FIG.5.7 : Simply Supported Beam Test Series at the University of Ottawa (Pillete, 1984)

SIMPLE REINFORCED CONCRETE BEAM A. C
ELEMENT MESH

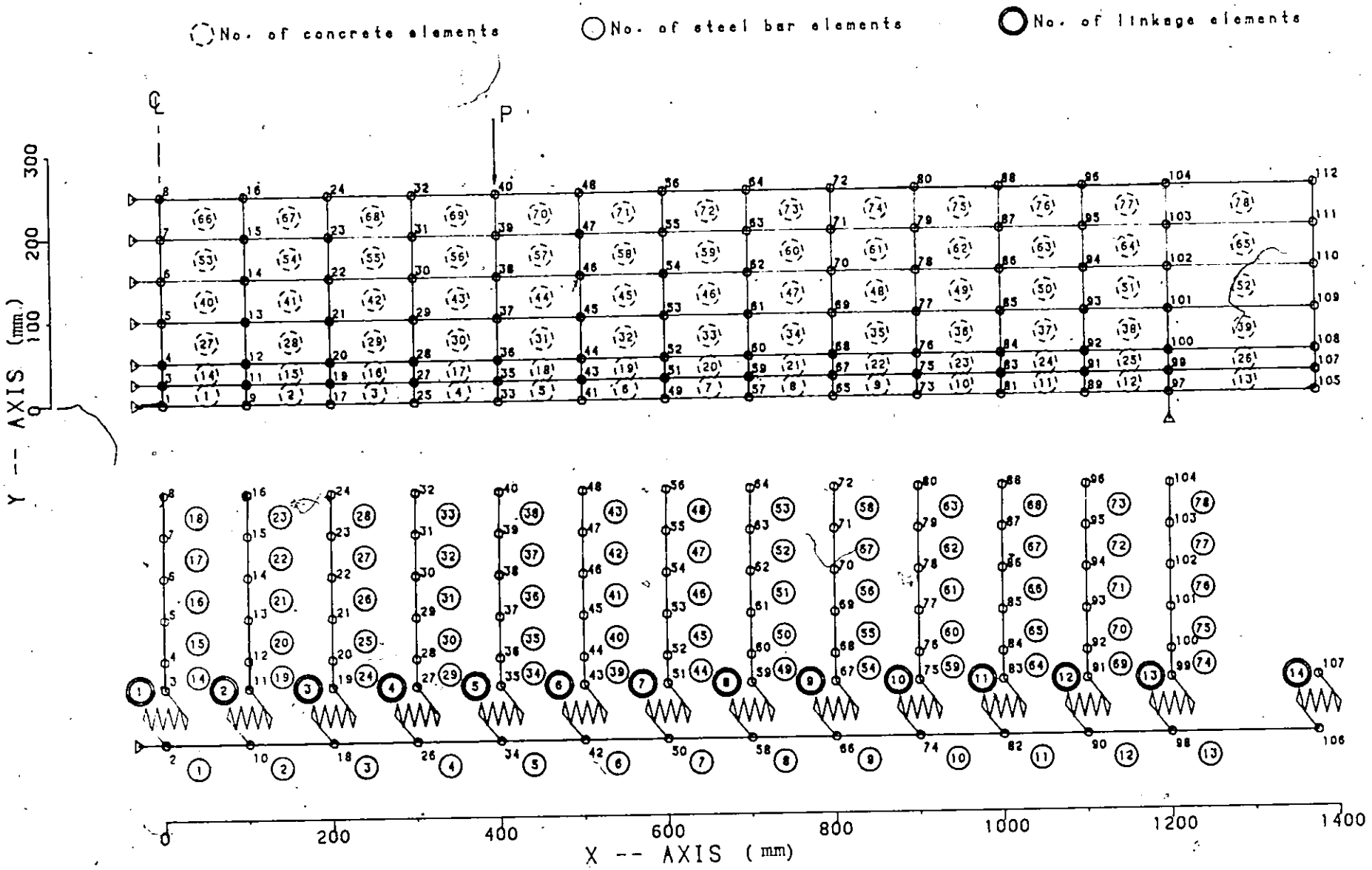

FIG.5.8 : Finite Element Idealization for Beam A. C

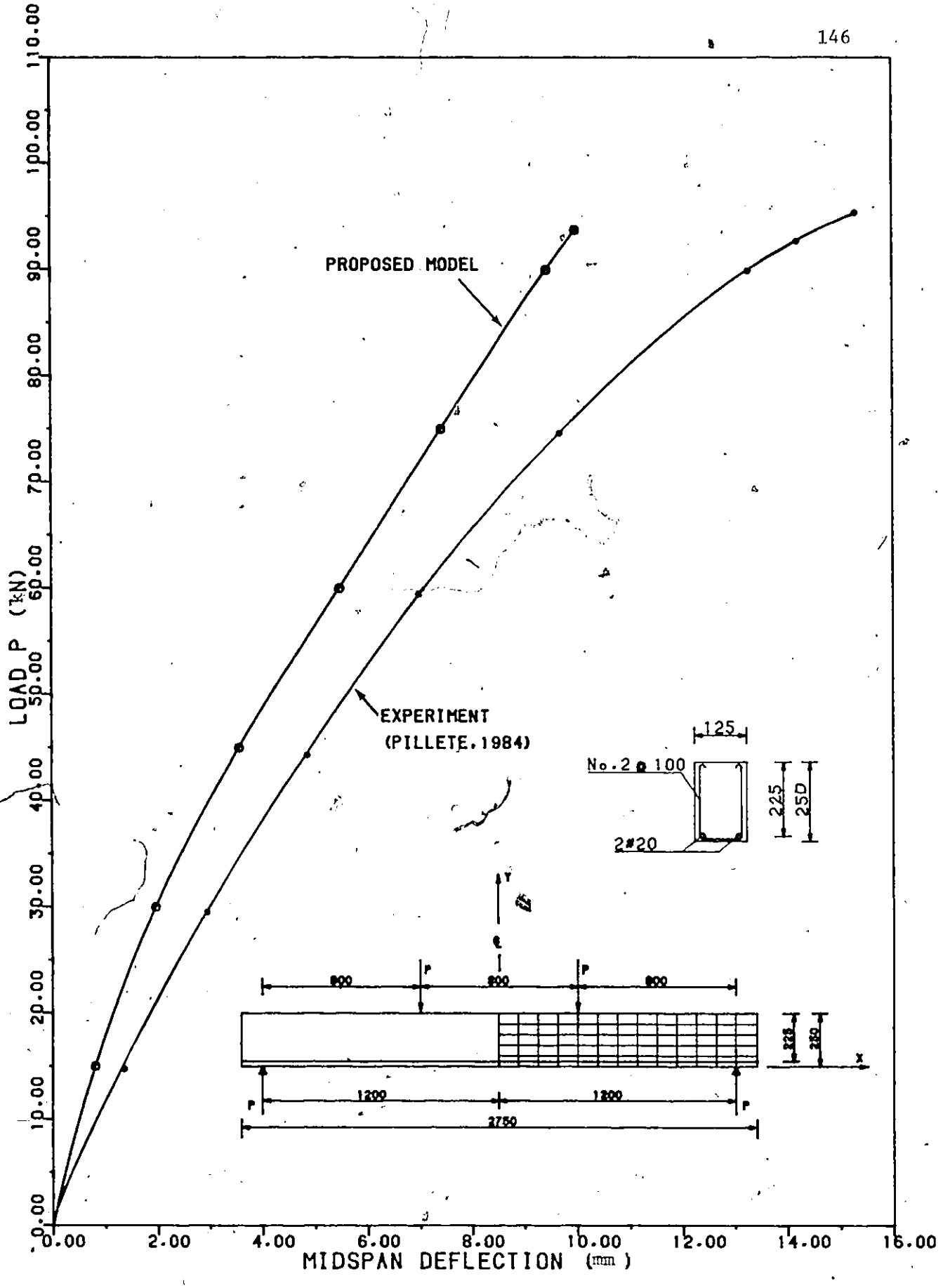

FIG.5.9 : Load-Deflection Curves for Beam A (Pillete, 1984)

SIMPLE REINFORCED CONCRETE BEAM B
ELEMENT MESH

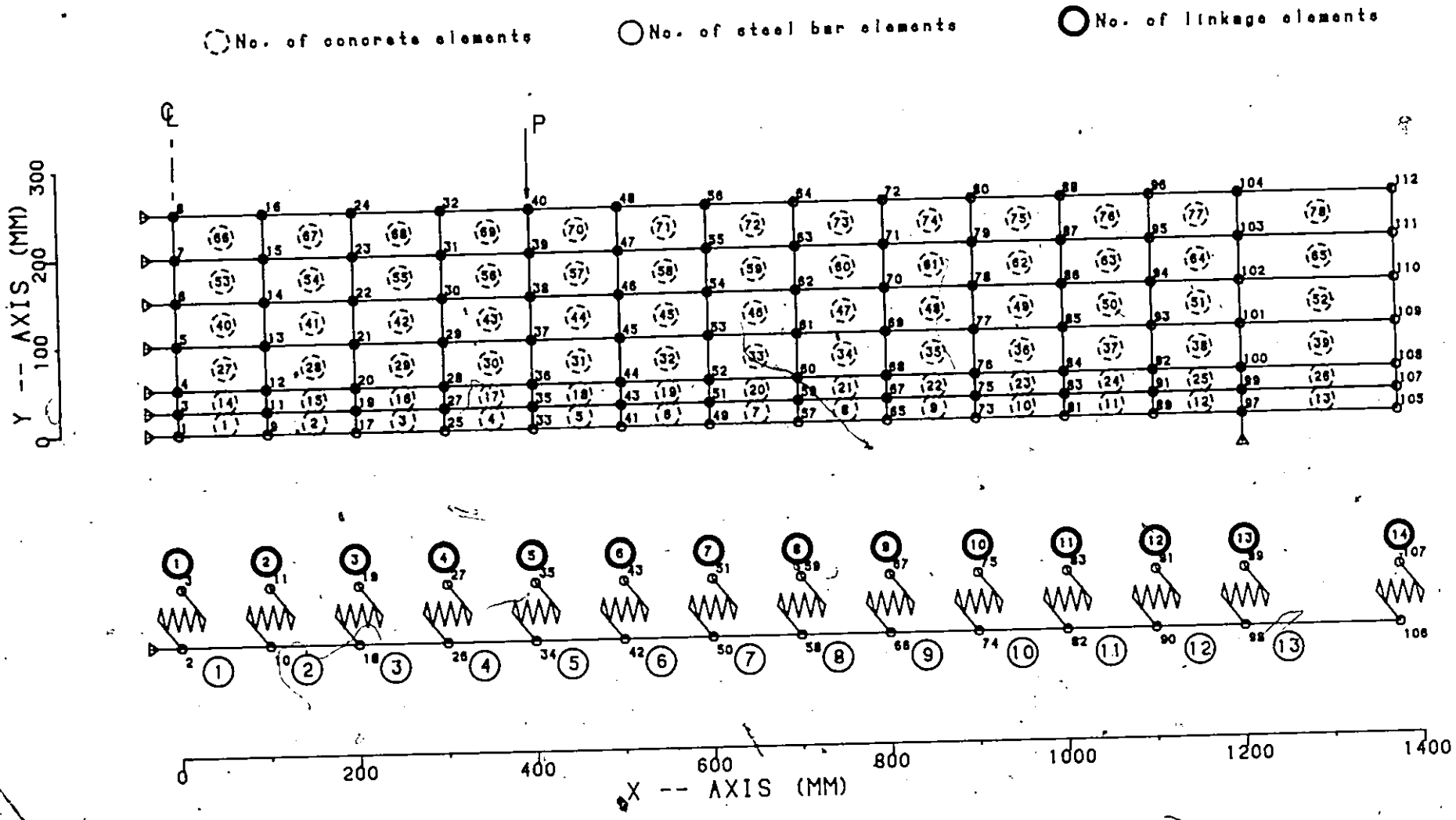

FIG.5.10 : Finite Element Idealization for Beam B

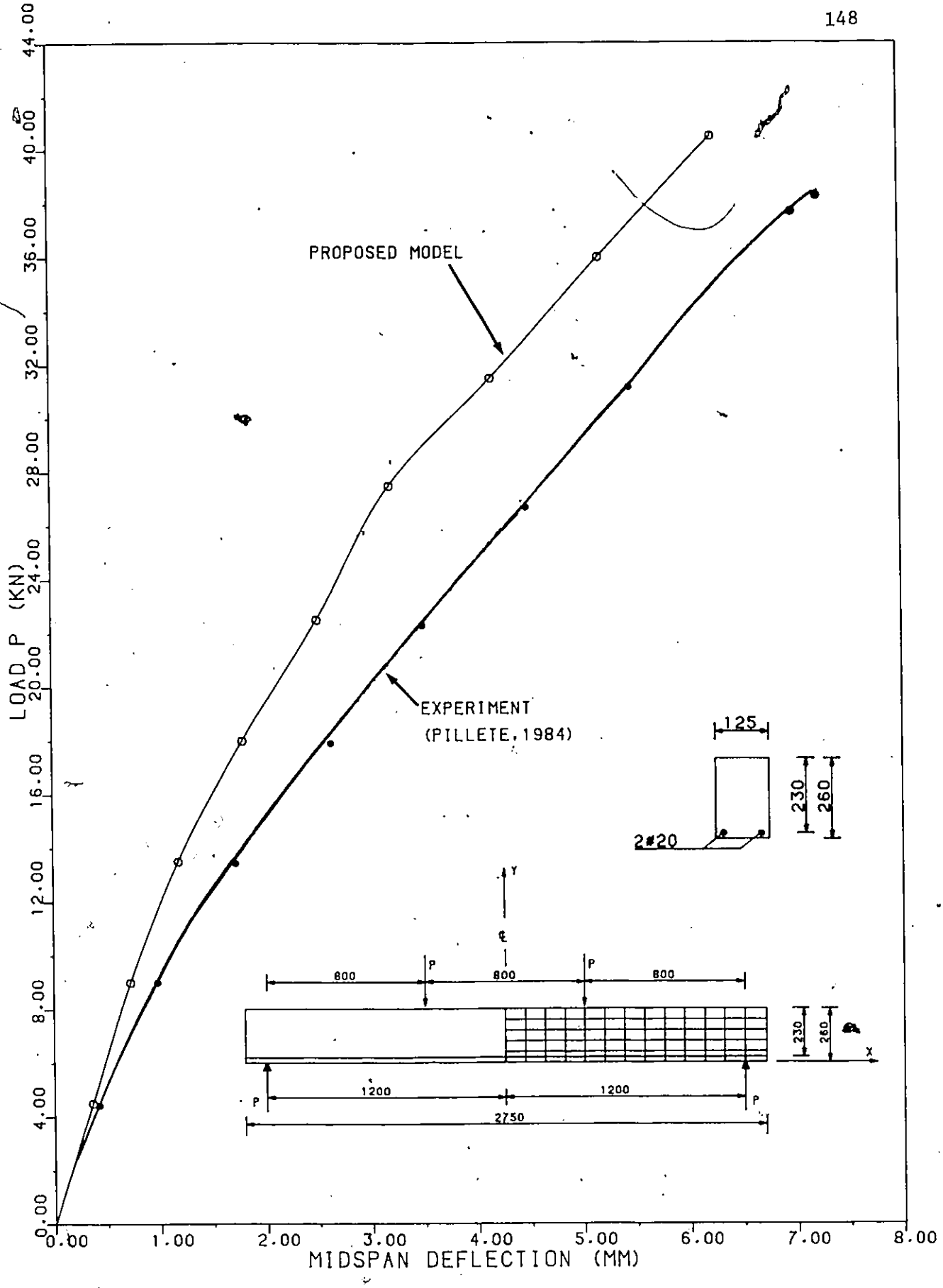

FIG 5.11 : Load-Deflection Curves for Beam B (Pillete, 1984)

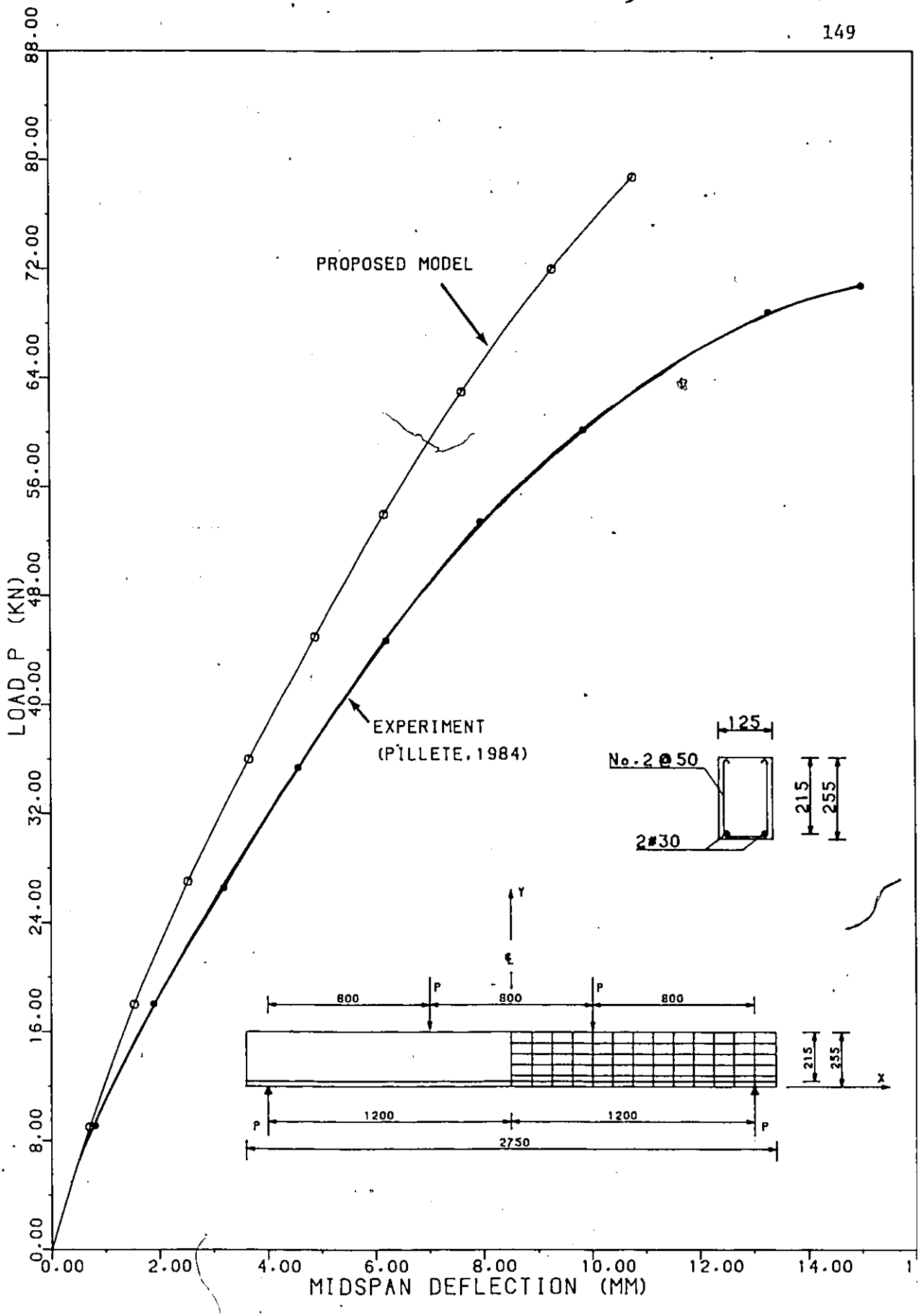

FIG.5.12 : Load-Deflection Curves for Beam C (Pillete, 198

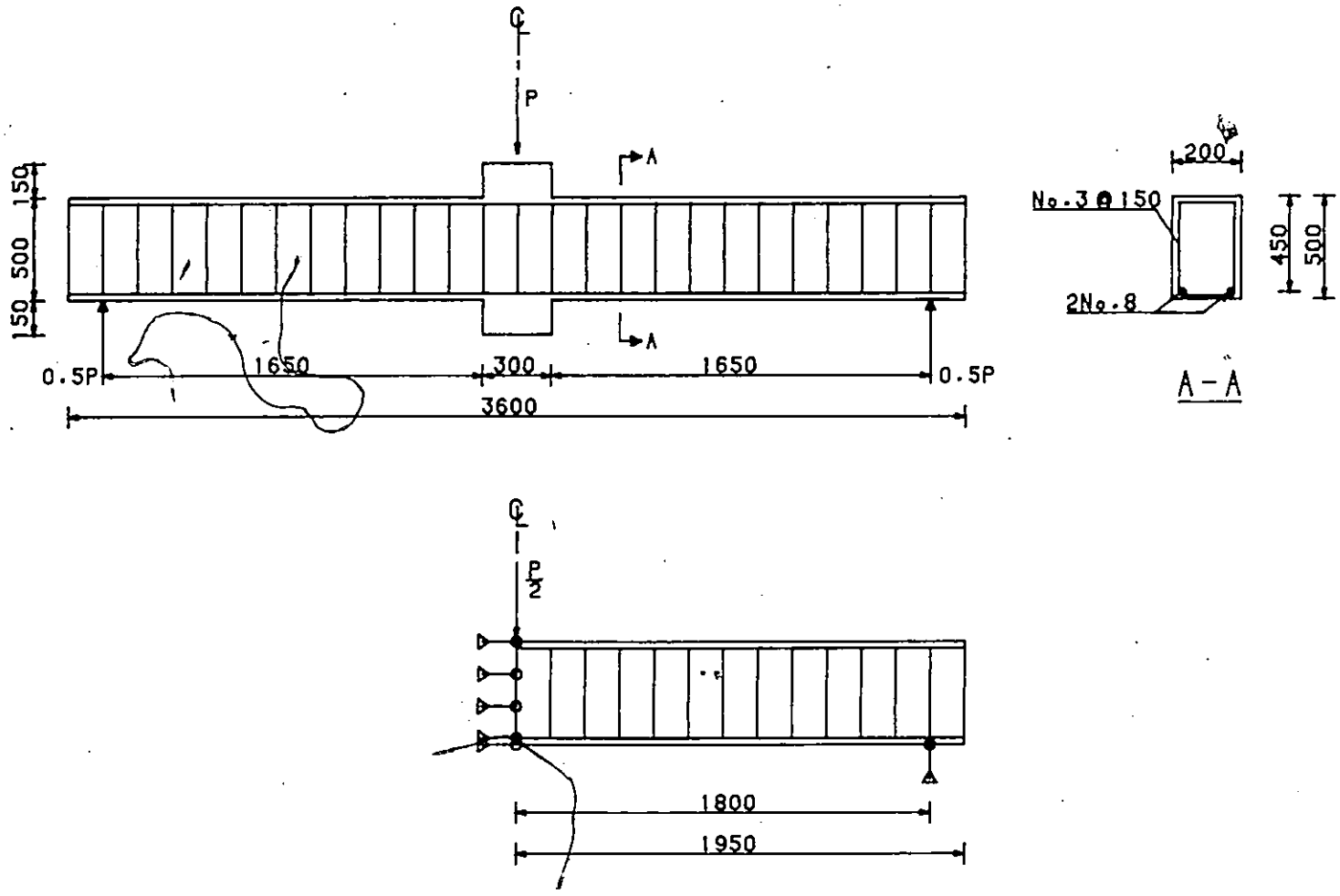

FIG.5.13 : Simply Supported Beam Specimen, BEAM J-4, (Burns and Seiss, 1962)

SIMPLE REINFORCED CONCRETE BEAM J-4
ELEMENT MESH

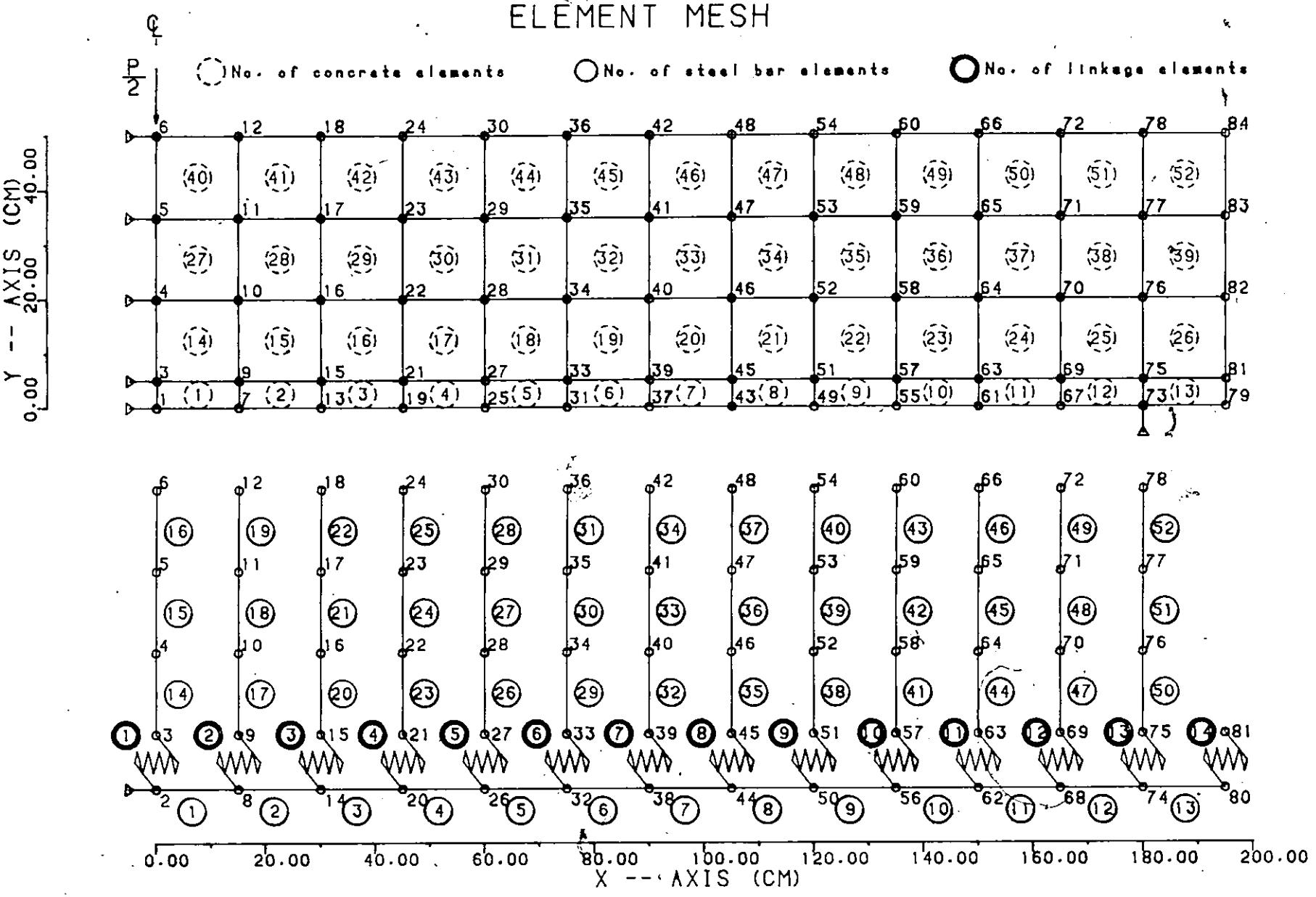

FIG.5.14 : Finite Element Idealization for Beam J-4

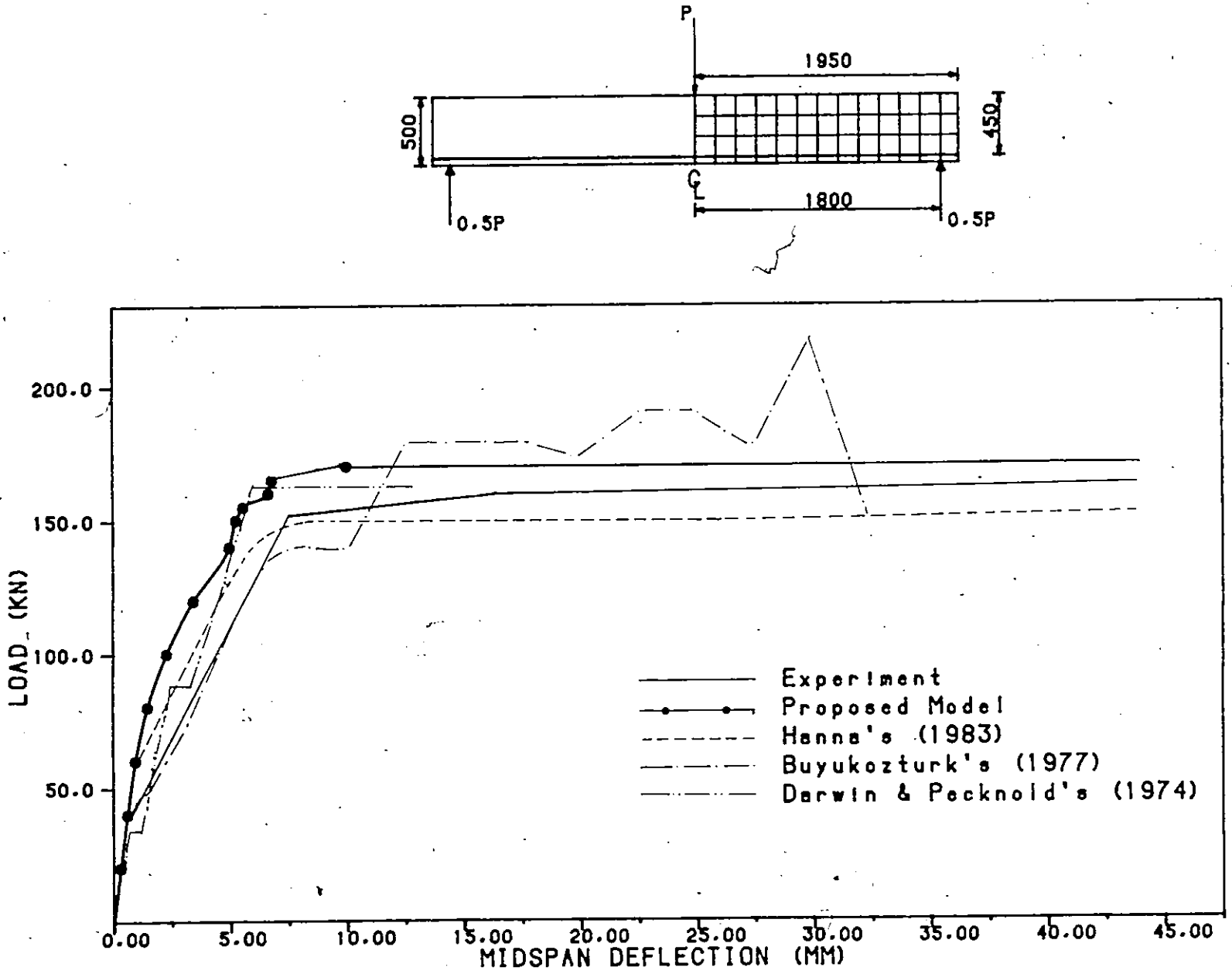

FIG.5.15 : Load-Deflection Curves for Beam J-4 (Burns, et al. 1962)

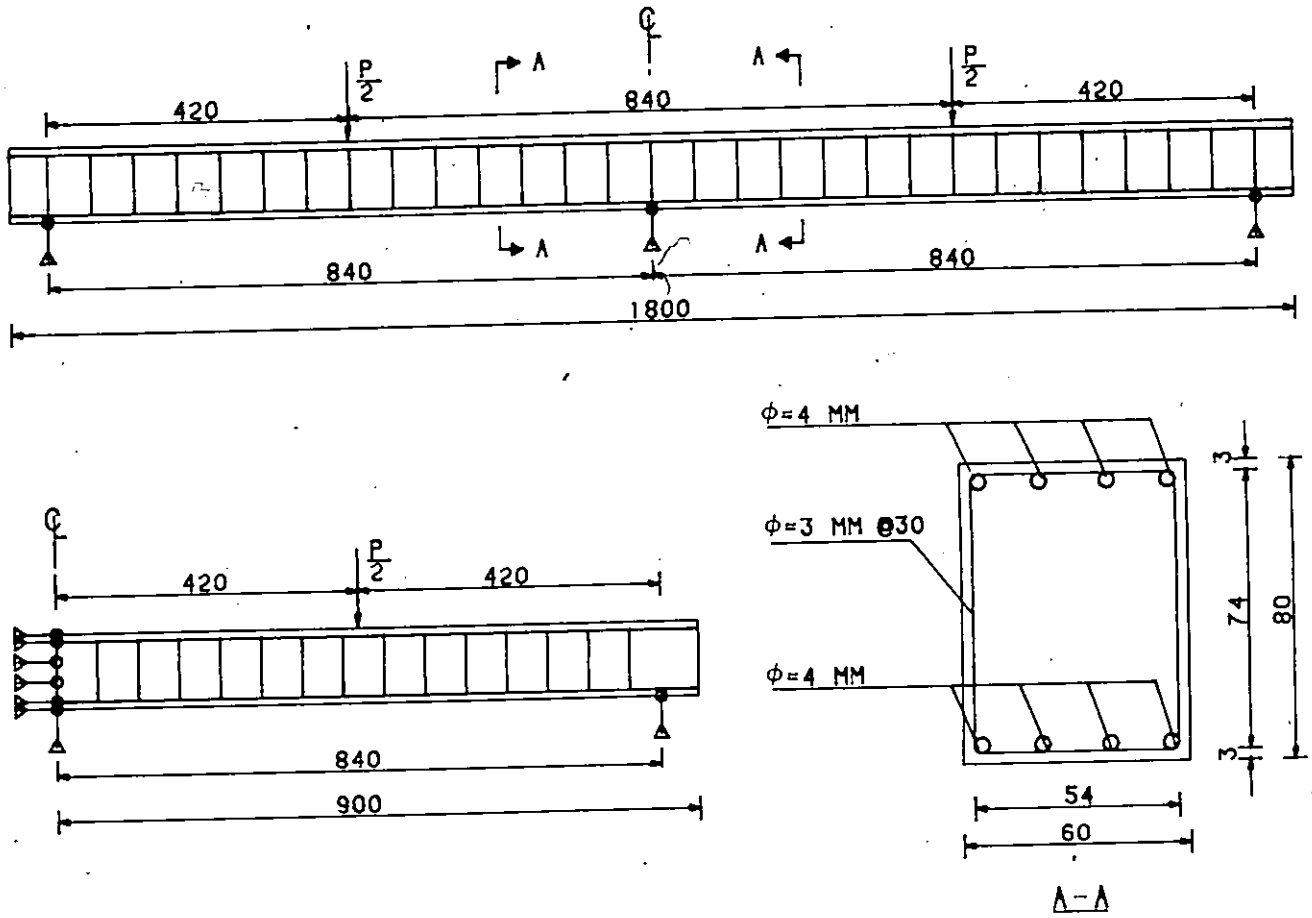

FIG.5.16 : Continuous Beam Test Specimen, BEAM 23100, (Duddeck, et al., 1962)

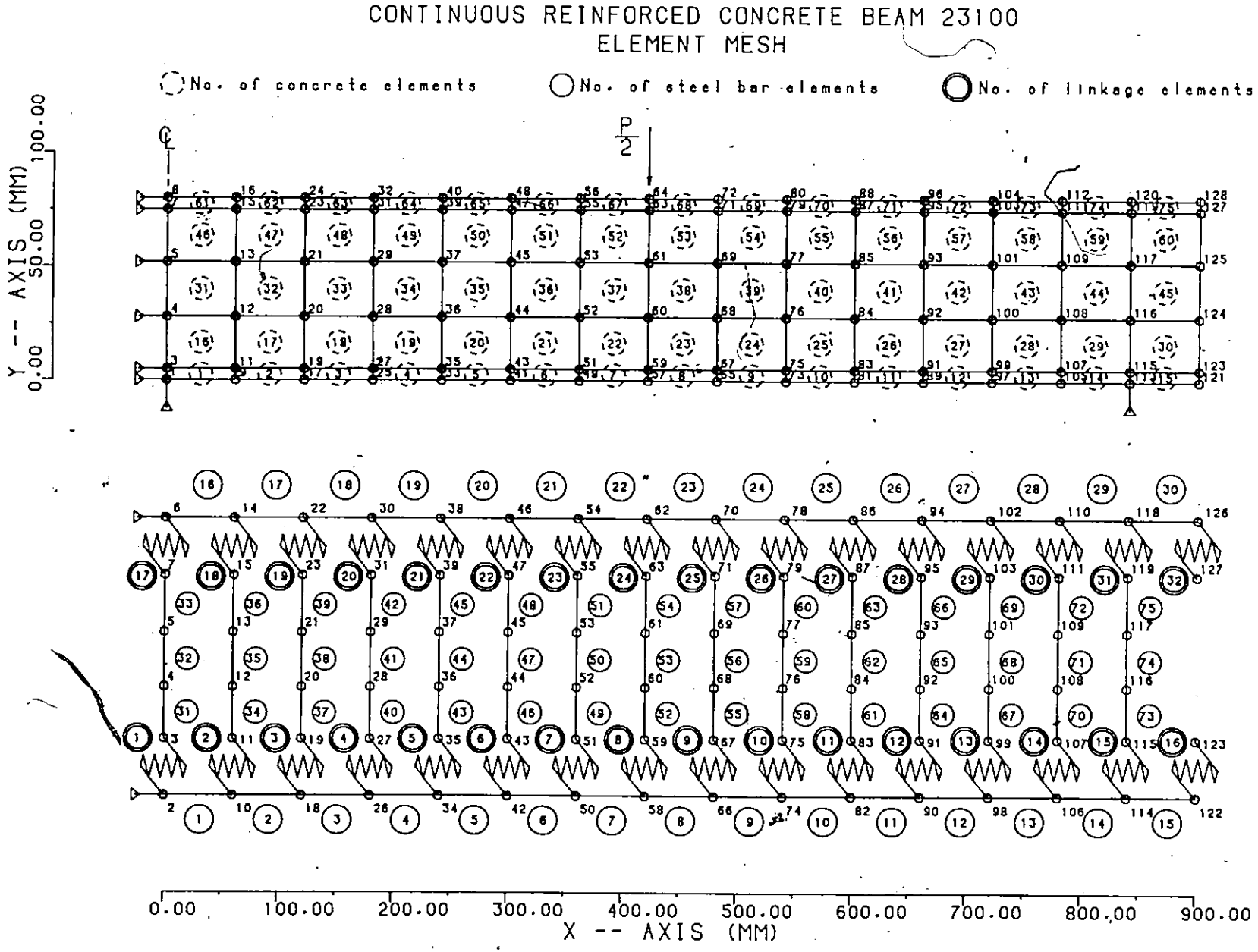

FIG.5.17 : Finite Element Idealization for Beam 23100

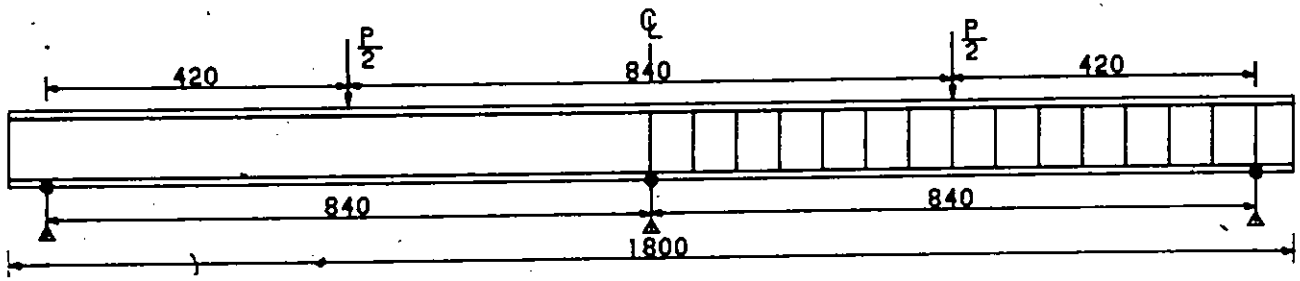

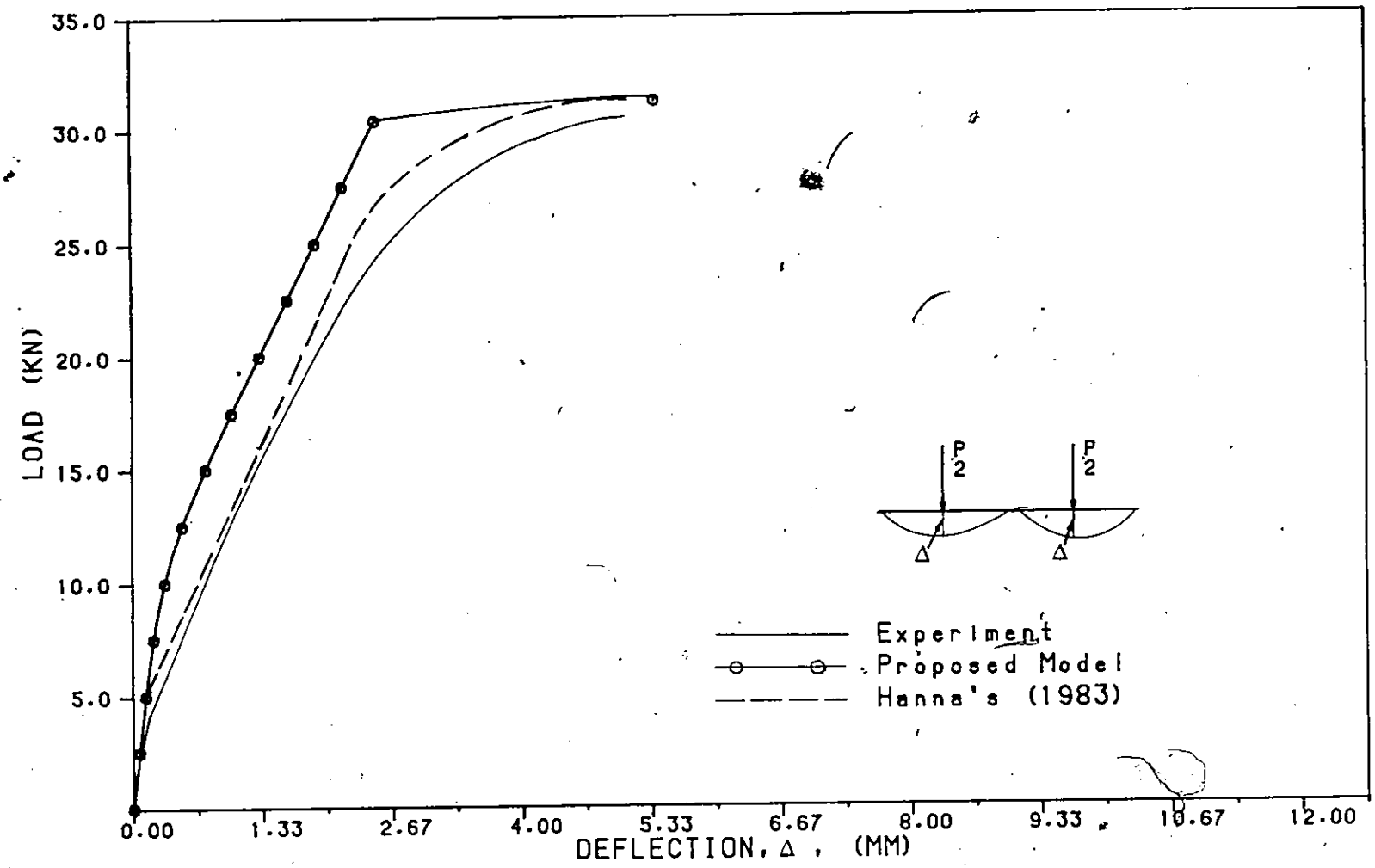

FIG.5.18 : Load-Deflection Curves for Beam 23100 (Duddeck, et al. 1976)

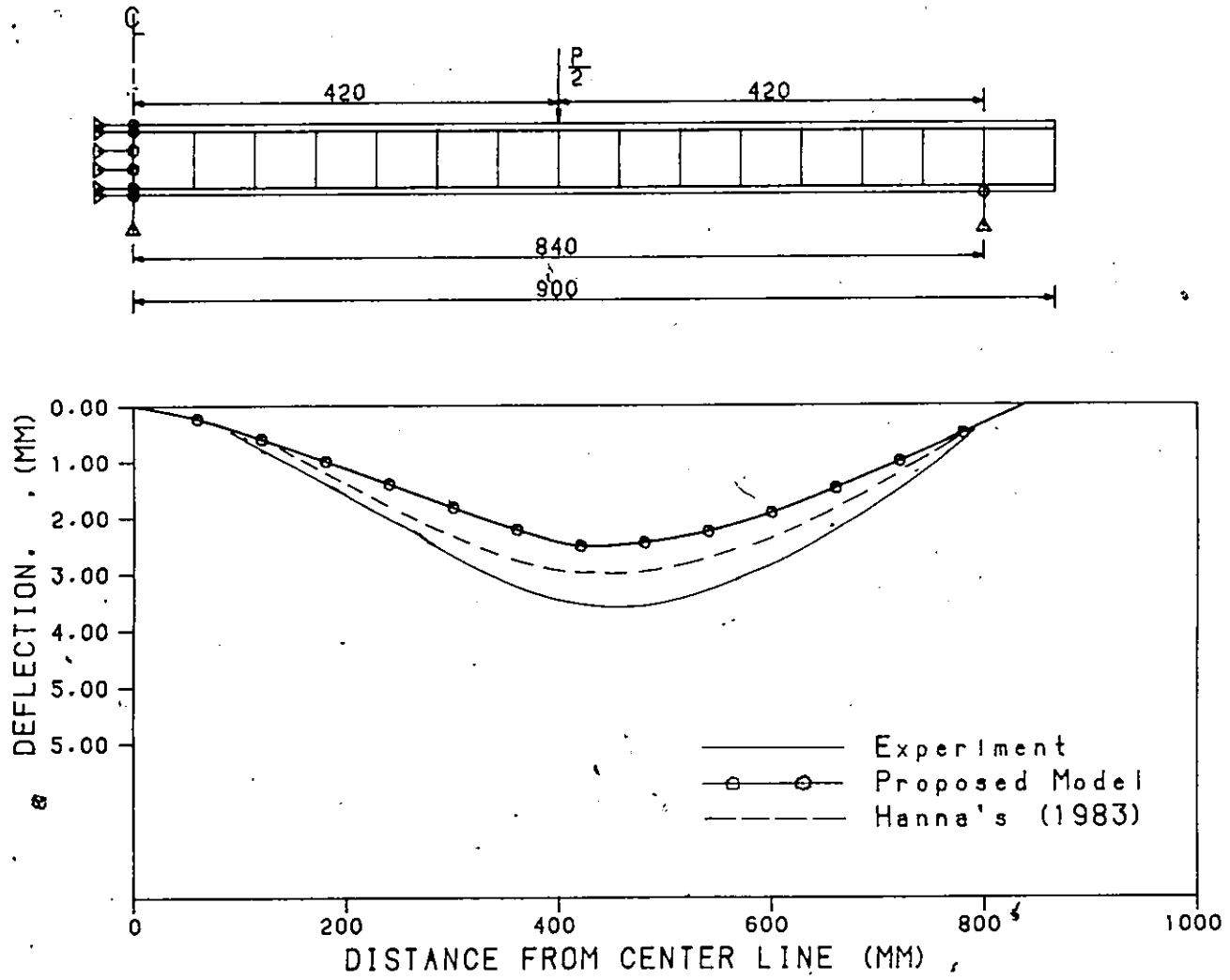

FIG.5.19 : Deflection Profile for Beam 23100 at a Load P = 30.42 KN.

Appendix B

COMPUTER PROGRAMING FLOW CHARTS

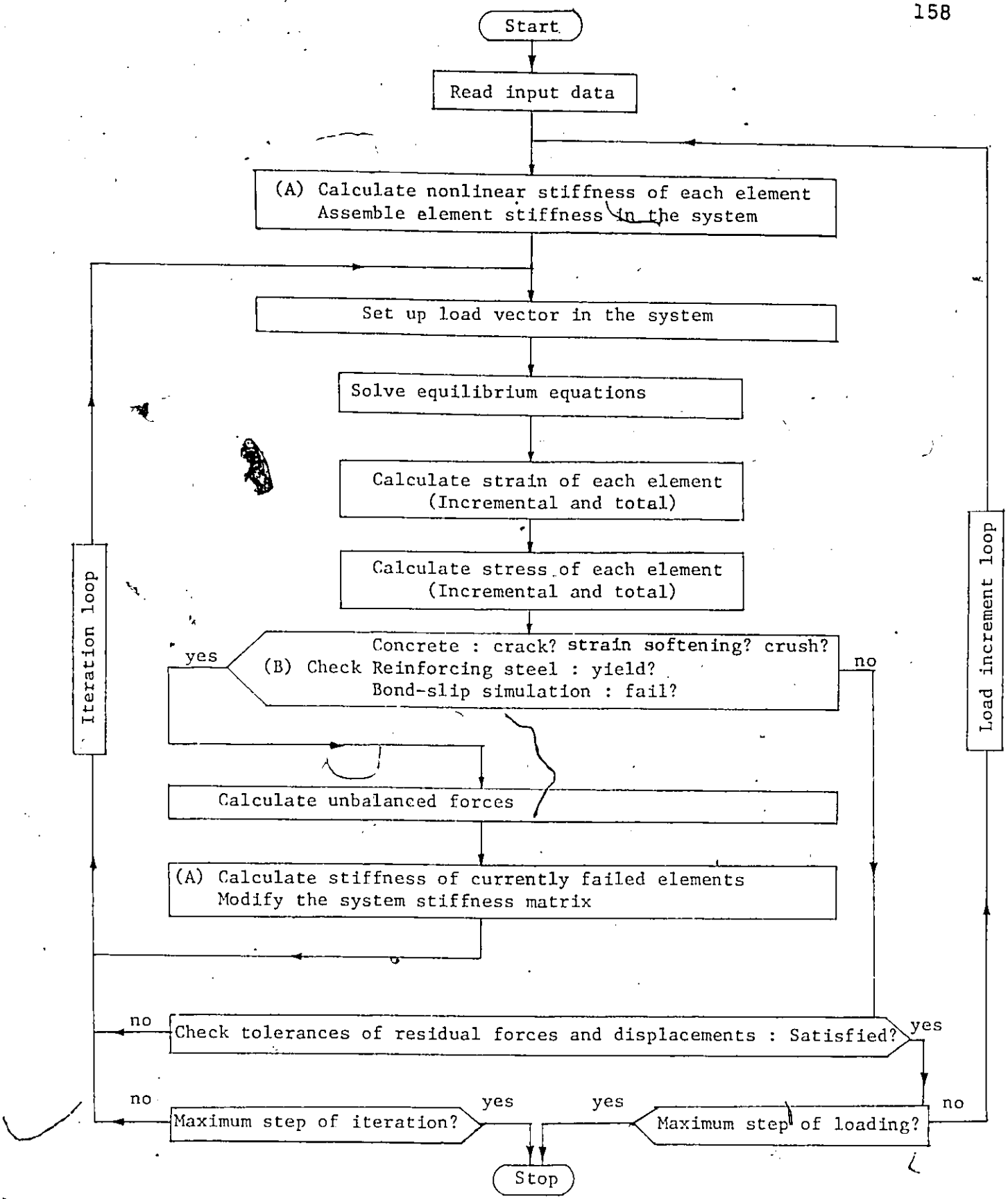

CHART 1 : Computer Program Flow Chart

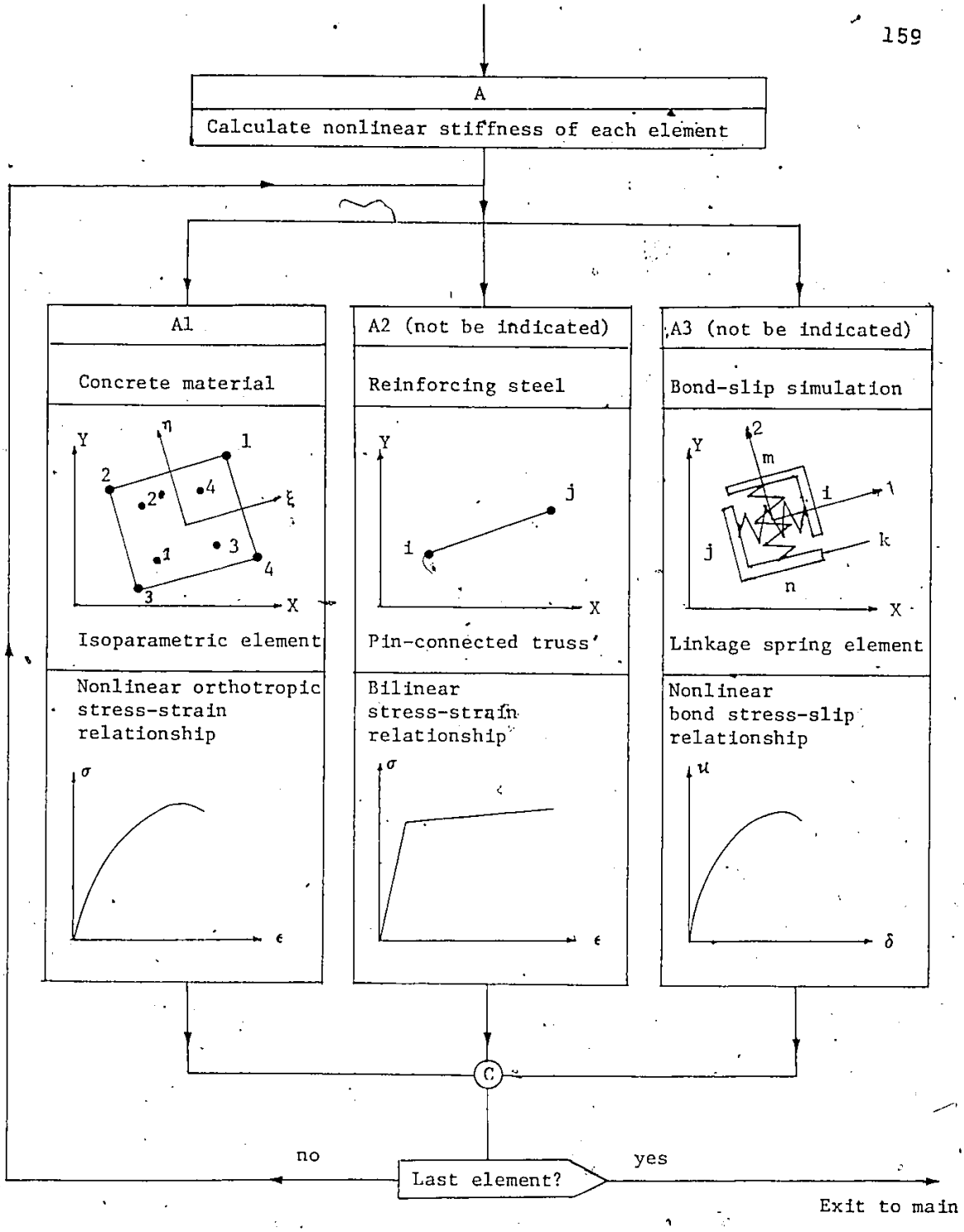

CHART 2 : Flow Chart A -- Calculate Nonlinear Stiffness of Each Element

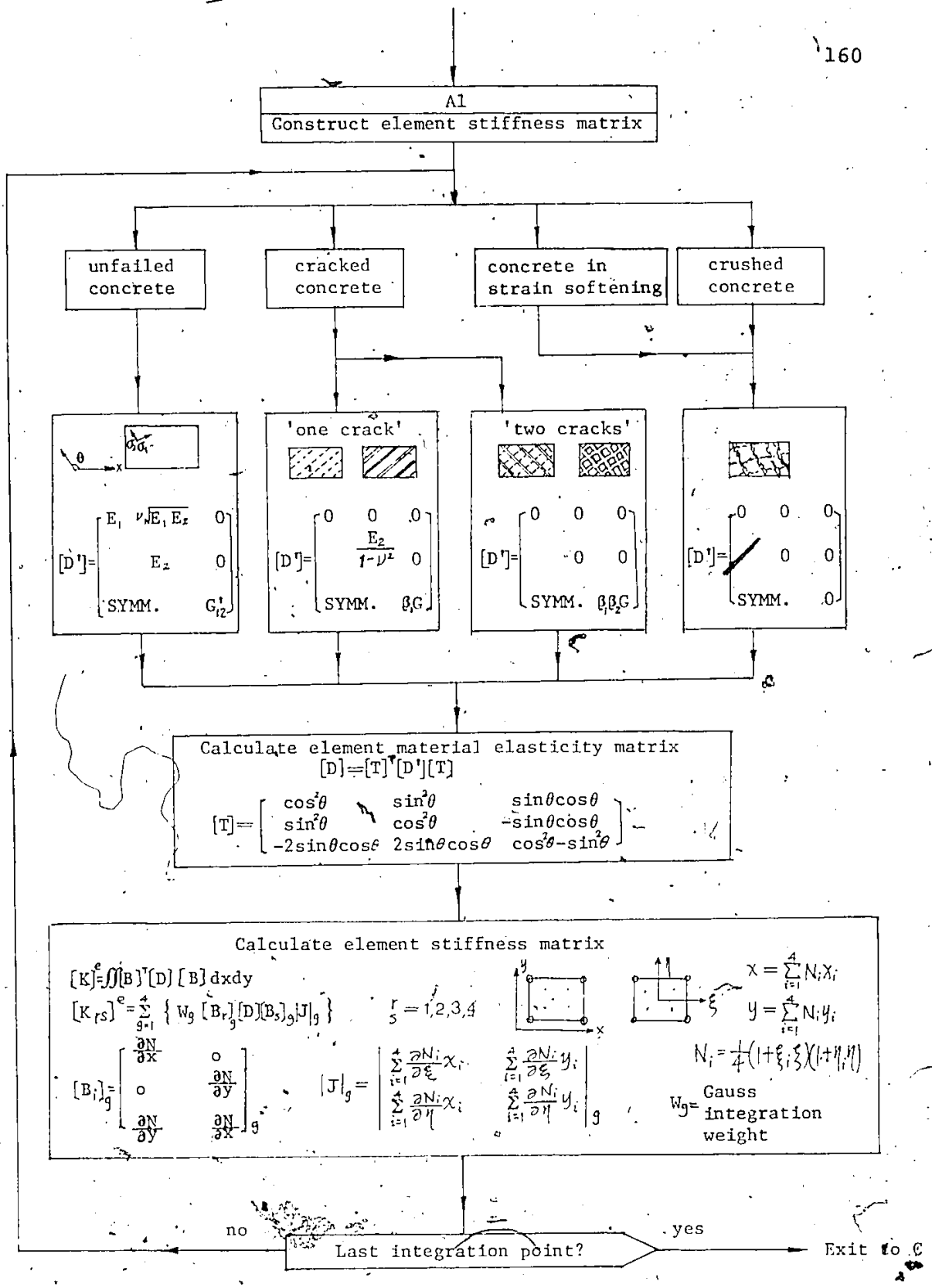

CHART 3 : Flow Chart A1 -- Construct Concrete Element Stiffness Matrix

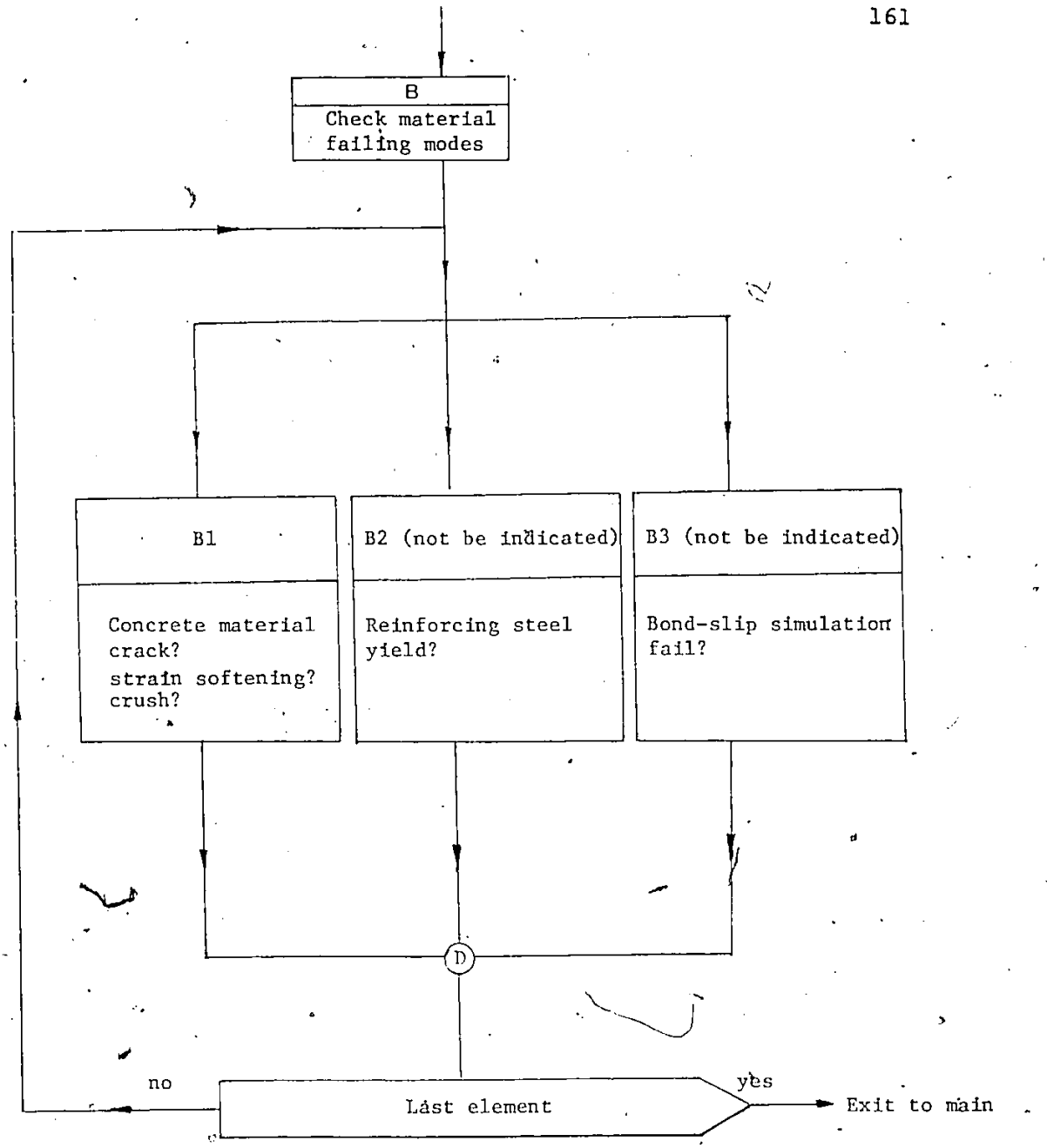

CHART 4 : Flow Chart B -- Check Material Failing Modes

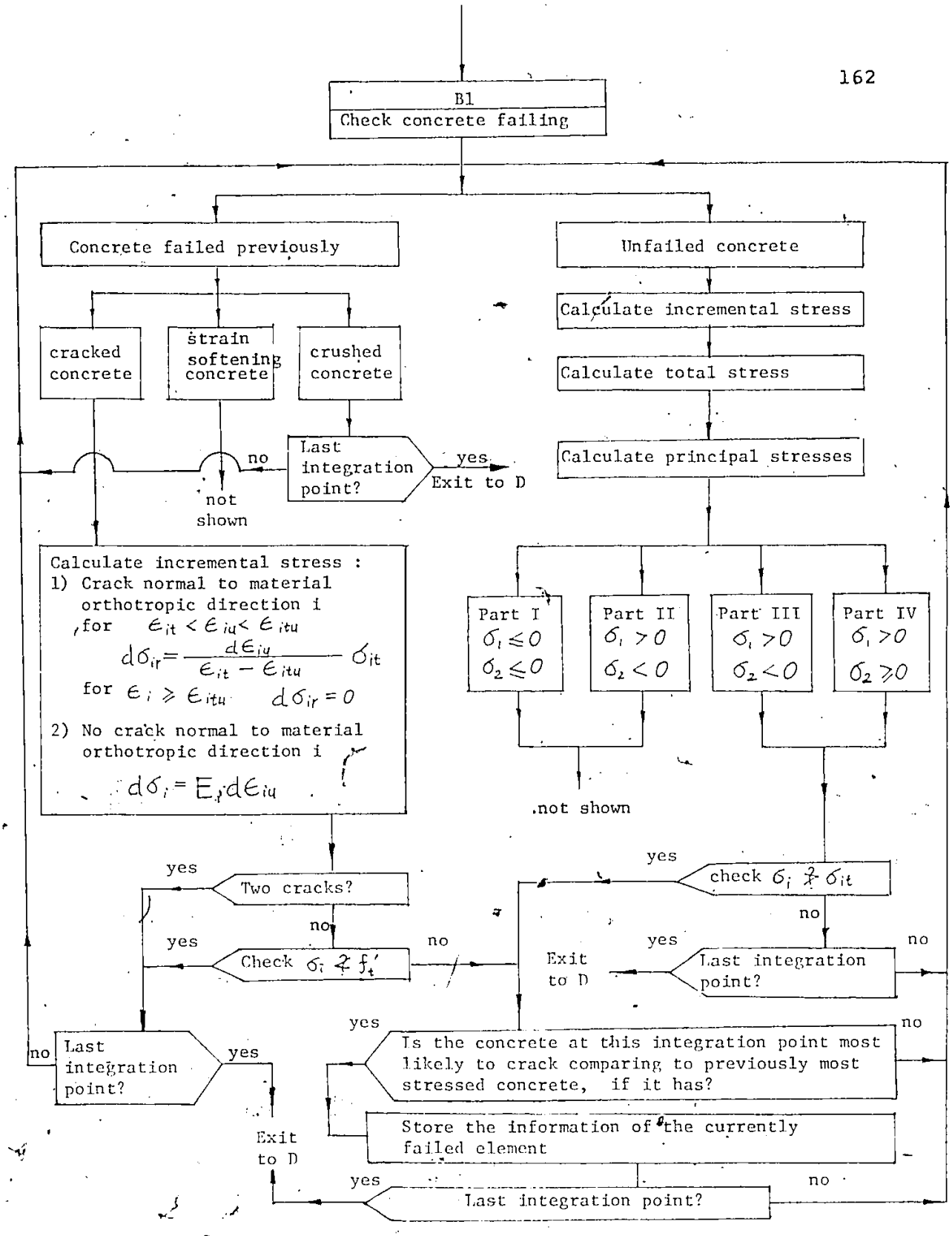

CHART 5 : Flow Chart B1 -- Check Concrete Failing Modes

REFERENCES

1. ACI Standard 318, Building Code Requirements for Reinforced Concrete, American Concrete Institute, U.S.A., 1983.

2. Adham, S., Bhaumik, A., and Isenberg, J., 'Reinforced Concrete Constitutive Relations', Air Force Weapons Laboratory Report, AFWL-TR-74-72, February 1975.

3. Al-Mahaidi, Riadh, S. H., and Nilson, A. H., 'Non-linear Finite Element Analysis of Reinforced Concrete Deep Member', Research Report No. 79-1, Dept. of Structural Engineering, Cornell University, Ithaca, New York 14853, U.S.A. January 1979.

4. Anderson, C. A., Smith, P. D., and Carruthers, L. M., 'NONSAP-C: A Nonlinear Stress Analysis Program for Concrete Containment under Static, Dynamic, and Long-Term Loadings', Los Alamos National Laboratory Report, LA-7496-MS, Rev. 1, January 1982.

5. Aoyama, H., and Noguchi, H., 'Mechanical Properties of Steel and Concrete under Load Cycles Idealizing Seismic Actions. Studies on Bond between Concrete and Steel: b) Concrete', AICAP-CEB symposium, Rome, May 1979.

6. Argyris, J. H., Faust, G., Szimmat, J., Warnke, E. P., and Willam, K. J., 'Recent Developments in the Finite Element Analysis of Prestressed Concrete Reactor Vessels', Nuclear Engineering ang Design, Vol. 28, 1974, pp. 42-75.

7. Bathe, K. J., Ozdemir, H., and Wilson, E. L., 'Static and Dynamic Geometric and Material Nonlinear Analysis', Report No. UCSESM 74-4, Department of Civil Engineering, Structural Engineering Laboratory, University of California, Berkeley, February 1974a.

8. Bathe, K. J., and Ramaswamy, S., 'On Three-Dimensional Nonlinear Analysis of Concrete Structures', Nuclear Engineering and Design, 52, 1979, pp. 385-409.

9. Bathe, K. J., Wilson, E. L., and Iding, R. H., 'NONSAP - A Structural Analysis Program for Static and Dynamic Response of Nonlinear System', Report No. UCSESM 74-3, Department of Civil Engineering, Structural Engineering Laboratory, University of California, Berkeley, February 1974b.

10. Bazant, Z. P., and Bhat, P. D., 'Endochronic Theory of Inelasticity and Failure of Concrete', Journal of the Engineering Mechanics Division, ASCE, Vol. 102, No. EM4, Proceedings Paper 12360, August 1976, pp. 701-721.

11. Bazant, Z. P., Bhat, P. D., Shieh, C. L., 'Endochronic Theory for Inelasticity and Failure of Concrete Structures', Structural Engineering Report No. 76-12/259 , Northwestern University Evanston, Ill., December 1976.

12. Bazant, Z. P., and Cedolin, L., 'Blunt Crack Band Propagation in Finite Element Analysis', Journal of the Engineering Mechanics Division, ASCE, Vol. 105, No. EM2, Proceedings Paper 14529, April 1979, pp. 279-315.

13. Bazant, Z. P., and Cedolin, L., 'Fracture Mechanics of Reinforced Concrete', Journal of the Engineering Mechanics Division, ASCE, Vol. 106, No. EM6, December 1980, pp. 1287-1306.

14. Bazant, Z. P., and Kim, S. S., 'Plastic-Fracturing Theory of Concrete', Journal of the Engineering Mechanics Division, ASCE, Vol. 105, No. EM3, Proceedings Paper 14653, June 1979, pp. 407-428.

15. Bazant, Z. P., and Shieh, C. L., 'Hysteretic Fracturing Endochronic Theory for Concrete', Journal of the Engineering Mechanics Division, ASCE, Vol. 106, No. EM5, Proceedings Paper 15781, October 1980, pp. 929-950, and Aug. 1981, p728.

16. Bazant, Z. P., and Tsubaki, T., 'Total strain Theory and Path-Dependence of Concrete', Journal of the Engineering Mechanics Division, ASCE, Vol. 106, No. EM6, Proceedings Paper 15911, December 1980, pp. 1151-1173.

17. Bresler, B., and Bertero, V., 'Behaviour of Reinforced Concrete Under Repeated Loads', Journal of the Structural Division, ASCE, Vol. 94, No. ST6, June 1968, pp. 1576-1590.

18. Bresler, B., and Pister, K. S., 'Strength of Concrete under Combined Stresses', ACI Journal, September 1958, pp. 321-345.

19. Burns, N. H., and Seiss, C. P., 'Load-Deformation Characteristics of Beam Column Connections in Reinforced Concrete', SRS. No. 234, Civil Engineering Studies, University of Illinois, Urbana-Champaign, Illinois, U. S. A., January, 1962.

20. Broms, B. B., 'Technique for Investigation of Internal Cracks in Reinforced Concrete Members', ACI Journal, Proceedings, Vol. 62, No. 1, January 1965, pp. 35-44.

21. Buyukozturk, O., 'Nonlinear Analysis of Reinforced Concrete Structures', Computers and Structures, Vol. 7, 1977.

22. CAN3 A23.3-M77, Code for the Design of Concrete Structures for Building, National Standard of Canada, Canada, 1977.

23. Cedolin, L., Crutzen, Y. R. J., and Poli, S. D., 'Triaxial Stress-Strain Relationship for Concrete', Journal of the Engineering Mechanics Division, ASCE, Vol. 103, No. EM3, June 1977, pp. 423-439.

24. Cervenka, V., and Gerstle, K. H., 'Inelastic Analysis of Reinforced Concrete Panels', IABSE Publications, V. 31-11, Zurich, 1971.

25. Chan, E. C., 'Nonlinear Geometric, Material and Time Dependent Analysis of Reinforced Concrete Shells with Edge Beams', Ph.D. Thesis, University of California, Berkeley, December 1982.

26. Chen, A. C. T., and Chen, W. F., 'Constitutive Relations for Concrete', ASCE, Journal of the Engineering Mechanics Division, Vol. 101, No. EM4, August 1975, pp. 465-481.

27. Chen, W. F., and Saleeb, A. F., 'Constitutive Equations for Engineering Materials, Vol. 1: Elasticity and Modeling', CISTI TA653.C48, John Wiley and Son, 1982.

28. Coon, M. D., and Evans, R. J., 'Incremental Constitutive Laws and Their Associated Failure Criteria with Application to Plain Concrete', International Journal of Solid and Structures, Vol. 8, Pergamon Press, 1972, pp. 1169-1183.

29. Cowan, H. J., 'The Strength of Plain, Reinforced and Prestressed Concrete under Action of Combined Stresses, with Particular References to the Combined Bending and Torsion of Rectangular Sections', Magazine of Concrete Research, Vol. 5, No. 14, December 1953, pp. 75-86.

30. Darwin, D., and Pecknold, D.A.W., 'Inelastic Model for Cyclic Biaxial Loading of Reinforced Concrete', Civil Engineering Studies, STS No.409, University of Illinois, Urbana, Illinois, U.S.A., July 1974.

31. Darwin, D., and Pecknold, D. A. W., 'Analysis of RC Shear Panels under Cyclic Loading', Journal of the Structural Division, ASCE, Vol. 102, No. ST2, February 1976, pp. 355-369.

32. Darwin, D., and Pecknold, D. A., 'Nonlinear Biaxial Stress-Strain Law for Concrete', Journal of the Engineering Mechanics Division, ASCE, Vol. 103, No. EM2, April 1977, pp. 623-641.

33. Darwin, D., and Pecknold, D. A. W., 'Analysis of Cyclic loading of Plane R/C Structures', Computers and Structures, Vol. 7, Pergamon Press, 1979, pp. 137-147.

34. Drucker, D. C., and Prager, W., 'Soil Mechanics and Plastic Analysis of Limit Design', Quarterly of Applied Mathematics, Vol. X, No. 2, 1952, pp. 157-165.

35. Duddeck, H., Griebenow, G., and Schaper, G., 'Auszuge aus dem Sechsten Arbeitsbericht zum Forschungsvorhaben Stahlbetonplatten mit Nichtlinearen Stoffgesetzen', Arbeitsbericht Institut fur Statik, TU Braunschweig, 1976.

36. Elwi, A. A., and Murray, D. W., ' A 3-D Hypoelastic Concrete Constitutive Relationship', Journal of the Engineering Mechanics Division, ASCE, Vol. 105, No. EM4, August 1979, pp. 623-641.

37. Epstein, M., Rijub, K., and Murray, D. W., 'A Two-Parameter Concrete Constitutive Law for Axisymmetric Shell Analysis', Proceedings, Symposium on Applications of Computer Methods in Engineering, University of Southern California, August 1977.

38. Filippou, F. C., Popov, E. P., and Bertero, V. V., 'Modeling of R/C Joints under Cyclic Excitations', Journal of the Structural Division, ASCE, Vol. 109, No. 11, November 1983, pp. 2666-2684.

39. Franklin, H. A., 'Nonlinear Analysis of Reinforced Concrete Frames and Panels', Ph.D. Thesis, Unversity of California, Berkeley, California, March 1970.

40. Gardner, N. J., 'Triaxial Behaviour of Concrete', ACI Journal, Proceedings, V.66, No. 2, February 1969, pp. 136-146.

41. Gerstle, K. H., 'Simple Formulation of Biaxial Concrete Behaviour', ACI Journal, Vol. 78, No. 1, 1981, pp. 62-68.

42. Gilbert, R. I., and Warner, R. F., 'Nonlinear Analysis of Reinforced Concrete Slabs with Tension Stiffening', UNICIV Report No. R-167, University of New South Wales, Kensington, N. S. W., Australia, January 1977.

43. Gilbert, R. I., and Warner, R. F., 'Tension Stiffening in Reinforced Concrete Slebs', Journal of the Structural Division, ASCE, Vol. 104, No. ST12, December 1978, pp. 1885-1900.

44. Hanna, Y. G., 'Finite Element Modelling of Reinforced Concrete Structures', Ph.D. Thesis, McGill University, Montreal, February 1983.

45. Houde, J., 'Study of Force-Displacement Relationships for the Finite Element Analysis of Reinforced Concrete', Ph.D. Thesis, McGill University, Montreal, December 1973.

46. Hughes, B. P., and Champman, G. P., 'The Complete Stress-Strain Curve for Concrete in Direct Tension', RILEM Bulletin 30, 1966.

47. Hsieh, S. S., Ting, E. C., and Chen, W. F., 'An Elastic-Fracture Model for Concrete,Proceedings of the Third Engineering Mechanics Division Speciality Conference, ASCE, the University of Texas at Austin, Texas, September 1979, pp. 437-440.

48. Kang, Y. J., 'Nonlinear Geometic, Material and Time Dependent Analysis of Reinforced and Prestressed Concrete Frames', Ph.D. Dissertation, Division of Structural Engineering and Structural Mechanics, University of California, Berkeley, US-SESM Report No. 77-1, January 1977.

49. Karsan, I. D., and Jirsa, J. O., 'Behaviour of Concrete under Compressive Loadings', Journal of the Structural Division, ASCE, Vol. 95, No. ST12, December 1969.

50. Khouzam, M., 'A Finite Element Investigation of Reinforced Concrete Beams', M. Eng. Thesis, McGill University, Montreal, October 1976.

51. Kotsovos, M. D., and Newman, J. B., 'Generalized Stress-Strain Relations for Concrete', ASCE, Journal of the Engineering Mechanics Division, Vol. 99, No. EM4, August 1978, pp. 852-866.

52. Kupfer, H. B., and Gerstle, K. H., 'Behaviour of Concrete under Biaxial Stresses', ASCE, Journal of the Engineering Mechanics Division, Vol. 99, No. EM4, August 1973, pp. 852-866.

53. Kupfer, H., Hilsdorf, H. K., and Rusch, H., 'Behaviour of Concrete under Biaxial Stresses', ACI Journal, V. 66, No. 8, August 1969, pp. 656-666.

54. Lamb, R. S., and Davies, G., 'Discussion on 'Nonlinear Stress Analysis of Reinforced Concrete' by Valliappan, S. and Doolan, T. F.', Journal of the Structural Division, ASCE, Vol. 99, No. ST3, March 1973, pp. 583-585.

55. Lin, C. S., 'Nonlinear Analysis of Reinforced Concrete Slabs and Shells', Ph.D. Thesis, Division of Structural Engineering and Structural Mechanics, University of California, Berkeley, UC-SESM Report No. 73-7, April 1973.

56. Lin, C. S., and Scordelis, A., 'Nonlinear Analysis of RC Shell of General Form', Journal of the Structural Division, ASCE, No.513, Proceedings Paper 11164, March 1975, pp. 523-538.

57. Liu, T. C. Y., Nilson, A.H., and Slate, F. O., 'Stress-Strain Response and Fracture of Concrete in Uniaxial and Biaxial Compression', ACI Journal, Vol. 69, No. 5, May 1972. pp. 291-295.

58. Liu, T. C. Y., Nilson, A. H., and Slate, F. O., 'Biaxial Stress-strain Relations for Concrete', Journal of the Structural Division, ASCE, Vol. 98, No. ST5, 1972, pp. 1025-1034.

59. Mirza, M. S., and Houde, J., 'Study of Bond Stress-Slip Relationship in Reinforced Concrete', ACI Journal, Proceedings, Vol. 76, No. 1, January 1979, pp. 19-46.

60. Murray, D. W., 'Octahedral Based Incremental Stress-Strain Matrices', Journal of the Engineering Mechanics Division, ASCE, Vol. 103, No. EM3, June 1977, pp. 377-393.

61. Murray, D. W., Chitnuyanondh, L., Rijub-Agha, K. Y., and Wong, C., 'Concrete Plasticity Theory for Biaxial Stress Analysis', Journal of the Engineering Mechanics Division, ASCE, Vol. 105, No. EM6, December 1979.

62. Nam, C. H., and Salmon, C. G., 'Finite Element Analysis of Concrete Beams', Journal of the Structural Division, ASCE, Vol. 100, No. ST12, December 1974, pp. 2419-2432.

63. Nelissen, L. J. M., 'Biaxial Testing of Normal Concrete', HERON, Vol. 18, No. 1, Delft, 1972.

64. Ngo, D., Franklin, H. A., and Scordelis, A. C., 'Finite Element Study of Reinforced Concrete Beams with Diagonal Tension Cracks', Report No. UC-SESM 70-19, College of Engineering Office of Research Services, University of California, Berkeley, December 1970.

65. Ngo, D., and Scordelis, A. C., 'Finite Element Analysis of Reinforced Concrete Beams', ACI Journal, Vol. 64, No. 3, March 1967, pp. 152-163.

66. Nilson, A. H., 'Finite Element Analysis of Reinforced Concrete', Ph.D. Thesis, University of California at Berkeley, U. S. A., 1968.

67. Nilson, A. H., 'Nonlinear Analysis of Reinforced Concrete by the Finite Element Method', ACI Journal, Vol. 65, No. 9, Sept. 1968, pp. 757-766.

68. Nilson, A. H., 'Internal Measurement of Bond Slip', ACI Journal, Vol. 69, No. 7, July 1972, pp. 439-441.

69. Ottosen, N. S., 'A Failure Criterion for Concrete', Journal of the Engineering Mechanics Division, ASCE, Vol. 103, No. EM4, August 1977, pp. 527-535.

70. Ottosen, N. S., 'Constitutive Model for Short-Time Loading of Concrete', Journal of the Engineering Mechanics Division Division, ASCE, Vol. 105, No. , February 1979, pp.127-141.

71. Owen, D. R. J., and Hinton, E., 'Finite Elements in Plasticity', ISBN 0-906674-05-2, CISTI (AERO) TA418 097, Prineridge Press Limited, Swansea, U. K., 1980.

72. Pilette, C.,'Reinforced Concrete Design-----Laboratory Report for CVG3045', Department of Civil Engineering, University of Ottawa, Ottawa, Canada, July 1984.

73. Rashid, Y. R., 'Analysis of Prestressed Concrete Pressure Vessels', Nuclear Engineering and Design, Vol. 7, No. 4, April 1968, pp. 334-344.

74. Rejagopal, K. R., 'Nonlinear Analysis of Reinforced Concrete Beams, Beam-Columns and Slabs by Finite Elements', Ph.D. Thesis, Iowa State University, Ames, Iowa, 1976.

75. Saenz, I. P., 'Discussion of 'Equation for the Stress-Strain Curve of Concrete' by Desayi and Krishnan', ACI Journal, Proceedings, Vol. 61, No. 9, September 1964, pp. 1229-1235.

76. Scanlon, A., 'Time Dependent Deflections of Reinforced Concrete Slabs', Ph.D. Thesis, Dept. of Civil Engineering, University of Alberta, Edmonton, December 1971.

77. Scordelis, A. C., 'Finite Element Analysis of Reinforced Concrete Structures', 'Proceedings of the Speciality Conference on Finite Element Method in Civil Engineering', Montreal, 1972, pp. 71-96.

78. Scordelis, A. C., 'Finite Element Modelling of Reinforced Concrete Structures', Seminar on the Finite Element Analysis of Reinforced Concrete Structures, University of Milan, Italy, June 1978.

79. Suidan, M., and Schnobrich, W.C., 'Finite Element Analysis of Reinforced Concrete', Journal of the Structural Division, ASCE, Vol. 99, No. ST10, October 1973, pp. 2109-2122.

80. Tasuji, M. E., Slate, F. O., and Nilson, A. H., 'Stress-strain Response and Fracture of Concrete in Biaxial Loading', ACI Journal, Proceedings, Vol. 75, No. 7, July 1978, pp. 306-312.

81. Tokes, S. I., 'Non-Linear Finite Element Analysis of Reinforced Concrete Members', M. Eng. Thesis, McGill University , Montreal, October 1976.

82. Valliappan, S., and Doolan, T. F., 'Nonlinear Stress Analysis of Reinforced Concrete', Journal of the Structural Division, ASCE, Vol. 98, No. ST4, April 1972, pp. 885-898.

83. William, R. J., and Warnke, E. P., 'Constitutive Model for the Triaxial Behaviour of Concrete', IABSE Seminar on Concrete Structures Subjected to Triaxial Stresses, Paper III-1, Instituto Sperimentali Modelli e Structure, Bergamo, Italy, May 1974.

84. Winter, G., and Nilson, A. H., 'Design of Concrete Structures', McGraw-Hill, TA683.2.W48, New York, 1979.

85. Wu, H. C., 'Dual Failure Criterion for Plain Concrete', Journal of the Engineering Mechanics Division, ASCE, Vol. 100, No. EM6, December 1974, pp. 1167-1181.